NASA CR-72480

LAMINAR MIXING OF HETEROGENEOUS AXISYMMETRIC COAXIAL CONFINED JETS

by

Kirti N. Ghia, T. Paul Torda, and Zalman Lavan

prepared for

NATIONAL AERONAUTICS AND SPACE ADMINISTRATION
CONTRACT NsG-694

November 1968

Illinois Institute of Technology
Department of
Mechanical and Aerospace Engineering
Chicago, Illinois

NASA CR-72480

FINAL REPORT

LAMINAR MIXING OF HETEROGENEOUS AXISYMMETRIC COAXIAL CONFINED JETS

by

Kirti N. Ghia, T. Paul Torda, and Zalman Lavan

prepared for

NATIONAL AERONAUTICS AND SPACE ADMINISTRATION

November 1968

CONTRACT NsG-694

Technical Management
NASA Lewis Research Center
Cleveland, Ohio
Nuclear Systems Division
Maynard F. Taylor

ILLINOIS INSTITUTE OF TECHNOLOGY
Chicago, Illinois

FOREWORD

Research related to advanced nuclear rocket propulsion is described herein. This work was performed under NASA Grant NsG-694 with Mr. Maynard F. Taylor, Nuclear Systems Division, NASA Lewis Research Center as Technical Manager.

ABSTRACT

Confined laminar mixing of dissimilar circular axisymmetric jets was studied. A binary isothermal system of non-reacting gases was considered. The central jet consisted of a slow moving heavy gas and the coflowing annular stream was a fast moving light gas. This investigation provides valuable information about the hydrodynamics of the coaxial flow gas-core nuclear reactor.

The boundary layer equations in cylindrical coordinates were used to formulate the mathematical model. These equations were transformed to the von Mises plane for numerical stability, and further to the φ-z plane to obtain a better representation of the flow problem in the central region. The solution was obtained by an explicit finite difference scheme. Karplus' as well as von Neumann's methods were used to determine the numerical stability conditions for the finite difference equations. Typical running time on the IBM 360/40 computer was about 10 minutes for obtaining results for the complete entrance region. The numerical method developed was also used to generate the solution for the classical entrance flow problem and the agreement of this solution with the available solutions provided a verification of the method. For the results of the confined jet mixing problem, partial check was also obtained by comparing the numerical values of the fully developed flow parameters with the corresponding

asymptotic values computed independently from simple theoretical considerations.

A detailed parametric investigation of the present problem was carried out and consisted of studying the effects of the parameters - velocity ratio $\frac{U_2}{U_1}$, density ratio $\frac{\rho_1}{\rho_2}$, radius ratio $\frac{R_1}{R}$, Reynolds number $N_{Re,2}$ of outer stream, Schmidt number $N_{Sc,2}$ based on outer stream and viscosity ratio $\frac{\mu_2}{\mu_1}$ - on the length of the mass fraction potential core L_{ω_1}, length of the velocity potential core L_v, the centerline velocity $v_{z,1}$, the wall mas fraction $\omega_{1,w}$ and the index of the effect of mixing η. The numerical method permitted large initial variations of $\frac{U_2}{U_1}$, $\frac{\rho_1}{\rho_2}$ and $\frac{R_1}{R}$. Results were obtained in the form of velocity and mass fraction fields and are valid in the near jet region as well as in the developing region downstream. Of the 57 cases investigated, the results of some selected runs are presented in order to show only typical effects of the parameters of the problem. (These 57 cases are tabulated in Appendix D.)

The principal results of the parametric study show that, for confined jet mixing, as $\frac{U_2}{U_1}$ increases, L_{ω_1} decreases but L_v increases, and as $\frac{\rho_1}{\rho_2}$ increases, L_{ω_1} increases but L_v decreases. This behavior of L_v is in direct contrast to the results available for unconfined mixing where L_v decreases as $\frac{U_2}{U_1}$ increases and L_v increases as $\frac{\rho_1}{\rho_2}$ increases. The present study shows also that an increase in $\frac{U_2}{U_1}$ results in rapid change of the centerline values, i.e., rapid mixing, and a narrower jet as well as a shorter developing length.

Further, an increase in $\frac{\rho_1}{\rho_2}$ reduces the centerline velocity in the mixing region and increases the developing length. Finally, η decreases as $\frac{U_2}{U_1}$ increases and η increases as $\frac{\rho_1}{\rho_2}$ increases, thus showing rapid mixing.

The effects of $\frac{U_2}{U_1}$ and $\frac{\rho_1}{\rho_2}$ on the laminar mixing compare with those available for turbulent jet mixing. Hence, the present study provides trends which are useful in understanding turbulent jet mixing.

At high velocity ratios, increase in $\frac{\rho_1}{\rho_2}$ and reduction of $\frac{R_1}{R}$ were found to be the main factors for stabilizing the numerical solutions. For some of the cases investigated, a positive pressure gradient or an oscillatory negative pressure gradient was observed; a suitable explanation for this behavior was not found.

The analysis presented gives useful insight into the complex problem of incompressible laminar confined jet mixing.

TABLE OF CONTENTS

Table of Contents (Cont'd)

LIST OF ILLUSTRATIONS

NOMENCLATURE

Symbol	Definition
Latin Letter	
D_{12}	Diffusion coefficient for binary system
G	Amplification matrix
J	Jacobian of von Mises transformation, $J = \frac{\partial(\psi,z)}{\partial(r,z)}$
J'	Jacobian of φ-transformation, $J' = \frac{\partial(\varphi,z)}{\partial(\psi,z)}$
k	Wave number
M	Total number of grid steps in transverse direction, $M = \frac{\Phi}{\Delta\varphi}$
M_i	Molecular weight of component i
$\dot{m}$	Mass flow rate
m	Subscript in transverse direction for discretized problem
n	Subscript in axial direction for discretized problem
N_{Re}	Reynolds Number of overall flow, $N_{Re} = \frac{2RU}{\nu}$
$N_{Re,1}$	Reynolds Number of inner stream, $N_{Re,1} = \frac{2R_1U_1}{\nu_1}$
$N_{Re,2}$	Reynolds Number of outer stream, $N_{Re,2} = \frac{2(R-R_1)U_2}{\nu_2}$

Nomenclature (Cont'd)

N_{Sc}	Schmidt Number of overall flow, $N_{Sc} = \frac{\nu}{D_{12}}$
$N_{Sc,2}$	Schmidt Number based on outer stream, $N_{Sc,2} = \frac{\nu_2}{D_{12}}$
p	Static pressure
P	Static pressure in atm.
r	Radial coordinate
R	Radius of confining pipe
R_1	Radius of inner jet tube
T	Temperature
U	Average axial velocity of overall flow
U_1	Average axial velocity of inner stream
U_2	Average axial velocity of outer stream
v_r	Mass average radial velocity
v_z	Mass average axial velocity; non-dimensional axial velocity
$v_{z,1}$	Non-dimensional centerline axial velocity
$w^{(1)}_{(1)}$	Collision integral for mass diffusivity

x_i	Mole fraction of species i
z	Axial coordinate

Greek Letter

Δ	Correction factor in expression for D_{12}
Δr	Step size in r-direction
Δz	Step size in z-direction
$\Delta\varphi$	Step size in φ-direction
$\Delta\psi$	Step size in ψ-direction
η	Index of mixing as defined in Equation (120)
λ_i	Boundary values at z = 0, as defined in Equations (17), (46), and (78)
μ	Dynamic viscosity
ν	Kinematic viscosity
π	Constant, = 3.1415927
ρ	Mass average density
σ	Collision diameter

φ	Transverse coordinate in φ-z plane
Φ	Value of φ at confining pipe wall
ψ	Stokes' stream function; transverse coordinate in von Mises plane
Ψ	Value of ψ at confining pipe wall
ω_i	Mass fraction of species i
$\omega_{1,w}$	Wall mass fraction
Ω_μ	Collision integral for viscosity

Subscripts

r	Denotes radial direction
z	Denotes axial direction
1	Refers to inner stream, i.e., species 1
2	Refers to outer stream, i.e., species 2
12	Refers to binary mixture
avg	Average value
i	Species i

max	Maximum value
min	Minimum value
mix	Mixture
p	Pure component

Abbreviations

FDA	Finite difference approximation
FDE	Finite difference equation
PDE	Partial differential equation

CHAPTER 1

INTRODUCTION

Circular confined jet mixing takes place between two streams in concentric ducts, downstream of the position where the inner duct is discontinued, allowing the jet stream from the inner duct to mix with the confined outer stream. Mixing and diffusion take place in the entrance region which is composed of an initial mixing region directly downstream from the jet exit, followed by a developing region. The jet and the annulus streams mix primarily in the initial mixing region. In the developing region, the velocity profiles become more and more of a "similar" shape as the flow becomes fully developed.

In several practical applications, jet mixing occurs in a confined outer stream as in the case of jet pumps, ejectors, jet engine combustion chambers and also in gaseous core reactors for nuclear rocket engines. The feasibility of the last application has been studied in detail by Ragsdale and his associates[1,2,3*] The present study has also been motivated by the recent interest in the gas-core rocket engines where a low velocity fissionable gas is ejected coaxially into a high velocity hydrogen propellant stream. The primary goal of such an advanced nuclear rocket engine is to produce a substantially higher specific impulse than the 850 seconds available from a solid core reactor. It is also necessary to reduce the loss of uranium to a minimum; such loss results from the mixing of the

---

* Superscript numerals refer to similarly numbered references at end of report.

fluid streams. Hence, for optimum performance, it is desired to make both the specific impulse and the hydrogen to uranium flow rate ratio a maximum. For this reason it is necessary to understand the behavior of a confined fluid jet system. The work presented is carried out to promote such understanding. Though only the initial mixing region is of interest for the gas-core nuclear rocket studies, the entire mixing and developing regions are investigated so that the results may be checked against the known behavior of the fully developed flow. Also, the complete study has applications beyond gas-core reactor problems.

Several investigations by the Nuclear Systems Division, NASA Lewis Research Center, show that the flow in a gas-core nuclear reactor is turbulent and that compressibility effects are negligible. However, as an intermediate step to the turbulent mixing problem, the corresponding laminar problem is analyzed; this study provides useful information about the confined mixing of coaxial jets. A literature survey of pertinent studies was carried out and it shows that laminar jet mixing has been investigated for both incompressible and compressible cases but that most of the work is limited to the unconfined, i.e., free jet mixing; the more complex confined jet mixing has not been studied in sufficient detail.

1.1 Literature Survey

1.1.1 Unconfined Jet Mixing

Free jet mixing of fluids has been extensively studied by several investigators, experimentally as well as analytically. The case of laminar incompressible jet mixing was first analyzed by Schlichting[4] in 1933. Schlichting solved the problems of the plane as well as the circular jet issuing into a medium at rest. Schlichting's analyses were confirmed experimentally by Andrade and Tsien[5] in 1937, and were found not to hold in the near jet region. In 1951, Squire[6] obtained exact solution of the Navier Stokes equations; this turned out to be the solution for an axially symmetric laminar jet which had been earlier analyzed by Schlichting.

In 1949, Pai[7] studied the flow of a two-dimensional jet of compressible fluid issuing from a finite opening, exhausting into a uniform stream, and further investigated the mixing of two uniform streams of a compressible fluid. This investigation was for laminar as well as turbulent flows. In 1952, Pai[8] extended the previous analysis to the case of an axially symmetric jet. The von Mises transformation was applied to the flow equations and numerical integration was used for computing the velocity and the temperature fields.

In 1953, Torda[9] used the von Karman integral principle to analyze the laminar incompressible mixing of two parallel streams having equal velocities. This case was referred to as "symmetric mixing". In 1955, Torda et al[10] analyzed the laminar incompressible

mixing of two-dimensional and axisymmetric jets. The analyses were for the region downstream of the potential core and indicated that the boundaries of the mixing region are curved, a fact which had been observed experimentally but not confirmed analytically by previous investigators. Further, in 1956 Torda and Stillwell[11] presented a comprehensive report of their analytical and experimental investigations of laminar as well as turbulent mixing of jets for incompressible and compressible cases.

In 1962, Kleinstein[12] investigated the mixing of an axisymmetric laminar jet of a conpressible fluid with a constant external flow. The von Mises transformation was used for the flow equations with a subsequent linearization of the viscous term. This facilitated the determination of the velocity field in the von Mises plane without use of the energy equation. The results obtained indicate close agreement with the exact numerical calculations of Pai[8].

In 1963, Weinstein and Todd[13] studied the problem of mixing of laminar isothermal coaxial streams of greatly different densities. The analysis is based on the boundary layer assumptions with constant pressure in the entire flow field and the solution was obtained by numerical techniques. It was shown that the velocity potential core length increases with increasing ratio of densities of inner to outer streams and decreases with increasing ratio of velocities of outer to inner streams. The influence of the initial boundary layers in the velocity profiles considerably increases the length of the velocity potential core.

In 1964, Sherman and Grey[14] carried out analytical as well as experimental investigations of the laminar mixing of a high temperature partially ionized subsonic argon plasma jet with a surrounding helium atmosphere. The boundary layer approximations were used in the analysis which involved the simultaneous solution of three nonlinear parabolic partial differential equations by finite difference techniques. The transport properties were computed by an improved version of the Chapman-Enskog method. The results indicated a rapid diffusion of the helium into the argon jet; diffusion of the helium upstream of the jet exit section was also shown by the experiment. The axial gradients of the temperatures and the velocities were small.

1.1.2 Confined Jet Mixing

Laminar mixing of confined jets has been experimentally shown to occur for suitable inlet conditions. In 1964, Wood[15] conducted experiments for the confined mixing of jets of air containing tracer quantities of HCl or NH_3 and determined the extent of the region of laminar flow for various entrance conditions. However, only little analytical or experimental work has been done on the fluid mechanics of confined laminar jet mixing.

Mass transfer in confined laminar jet mixing has been investigated to some extent during the last several years. Two recent studies pertinent to the present work are discussed here. The range of applicability of the model used by Burke and Schumann[16] (1928) was extended by Savage[17] in 1962. Enclosed laminar diffusion flames were

studied and the flame shape was predicted with surprising success in spite of several assumptions such as spontaneous combustion, plug flow throughout the entrance region, constant diffusion coefficient, and absence of all forms of mixing other than radial diffusion. Diffusion in a laminar, circular, confined jet reactor was studied by Wood[15] experimentally as well as analytically. In his experimental studies, Wood used ethylene and nitrogen for the primary and the secondary streams, respectively. The concentration of ethylene in nitrogen was measured for the entire field for this non-reacting system. In the mathematical model for mass transfer, Wood assumed the existence of either plug flow or parabolic flow in the mixing region. Another major assumption was that no radial convection exist, implying a diffusion controlled process. For nearly equal entrance velocities, the calculated concentration profiles compared well with the experimental data. The agreement deteriorated for velocity ratios largely different from unity when the effect of radial convection was no longer negligible.

In 1966, Seider[18] performed analytical studies of laminar, incompressible homogeneous jet mixing with chemical reaction. Seider transformed the Navier Stokes equations to the vorticity and the stream function equations which were solved numerically to determine the velocity profiles. The implicit alternating directions scheme was used to obtain the numerical solution. The specific solutions obtained provide a quantitative description of the mixing region of the laminar confined jet. These results were confirmed semi-

quantitatively by his dye-tracer experiments. The concentration profiles were obtained by solving the coupled partial differential equations describing mass transfer with chemical reaction in the entrance region. Negligible axial diffusion was assumed and a modified Crank Nicholson method was used for these calculations. Although these computational schemes are claimed to yield unconditionally stable numerical solutions, large instabilities were encountered in the near jet region for entrance flow conditions which are known to yield laminar flow. The instability was attributed mainly to the discontinuity in the flow at the jet boundary. Similar instabilities were encountered also in the present investigation and will be discussed later. For the non-reacting case, the results obtained by Seider are in good agreement with the concentration measurements of Wood.

Confined jet mixing has been investigated at Illinois Institute of Technology also. Fejer et al[19] carried out experimental as well as analytical studies of the confined mixing of coaxial streams. In their analytical study, it was pointed out that the results obtained by using the boundary layer equations show good agreement with Wood's[15] results for wall concentration. Unsteady as well as steady homogeneous mixing of confined laminar jets were studied by Agarwal and Torda[20]. In these studies, comparisons were also obtained for solutions of the boundary layer equations with solutions of the Navier Stokes equations for the steady flow configurations of Seider; the agreement with Seider's results was satisfactory. Also, Mehta and Lavan[21] have obtained results

for laminar incompressible homogeneous jet mixing using the Navier Stokes equations for ratio of velocities of outer to inner streams as high as 30. These results have not yet been verified.

1.2 Present Study

The literature survey presented shows that the confined laminar mixing of streams of highly differing fluid properties has not been studied thus far. In view of this, the present investigation of mixing of laminar axisymmetric confined circular jets of dissimilar fluids was undertaken. In this study, an isothermal and non-reacting flow field is considered. The flow problem is formulated as a boundary value problem and is solved numerically by an explicit finite difference scheme. The flow equations are approximated by their finite difference forms such that flow parameters at any point may be expressed explicitly in terms of known parameters only. Numerical stability is ensured by satisfying Karplus'[22] stability criterion. Numerical stability conditions for these equations were obtained also be using von Neumann's method, first given by O'Brien, Hyman and Kaplan, and were found to be similar to Karplus' conditions. Whereas for the linear problem, convergence of the obtained numerical solution to the exact solution of the boundary value problem is established under the hypothesis due to Lax,[24] for the nonlinear problem, convergence can be proved by a method due to Strang[25]. The flow equations are programmed in Fortran IV and are solved using the IBM 360/40 computer.

The three main contributions of this investigation are:

1. The study enables an initial assessment of the gas-core nuclear reactor and predicts mixing for confined jet flow configurations which are difficult to investigate experimentally.

2. The results provide detailed information of laminar, incompressible, coaxial confined jet mixing for most of the parameters of practical interest. The range of these parameters over which the boundary layer equations are unquestionably valid is established.

3. A finite difference method is developed for the solution of the coupled nonlinear parabolic partial differential equations. This method can be extended to study the effects of compressibility and turbulence.

CHAPTER 2

ANALYSIS

2.1 Objective

The laminar coaxial confined heterogeneous mixing of incompressible jets is studied analytically in the present work. The aims of the investigation are:

1. to obtain the velocity and concentration fields in the entire mixing and developing regions,
2. to determine the parameters of importance and to study their effects on mixing, and
3. to find the range of applicability of the numerical method developed for the jet mixing problem using the boundary layer equations.

2.2 Mathematical Model

The jet mixing problem to be studied is represented mathematically by the boundary layer equations with appropriate boundary conditions. Auxiliary expressions are used to determine the thermodynamic and transport properties of the fluid medium. The use of boundary layer equations may be supported by the success with which they have been applied in investigations of unconfined mixing (References 8, 12, 13, 14 and 26). Their application to the confined jet problem is further justified in Chapter 4. Also, the effects of compressibility and turbulence can be more easily studied with the use of the boundary layer equations than with the Navier Stokes equations. Thus, the present mathematical model is based on the following assumptions:

1. The boundary layer assumptions.
2. Steady state, isothermal flow without body forces and chemical reaction.
3. Cylindrical duct of constant cross-section.
4. Incompressible component fluids.
5. Invariance of binary diffusivity D_{12} with concentration.

A typical geometry of the problem is shown in Figure 1.

The mathematical model is designed to predict the mixing of two streams as it progresses in the entrance region of the outer pipe. The solution is obtained by a finite difference method which will be discussed in Chapter 3. Any types of entrance velocity and density profiles can be used with only minor modification of the numerical scheme developed. The equations and boundary conditions describing the mathematical model in the physical plane can now be written.

2.3 Formulation of Problem in Physical Plane (r,z)

2.3.1 Governing Differential Equations

Continuity Equation

$$\frac{\partial}{\partial r}(\rho r v_r) + \frac{\partial}{\partial z}(\rho r v_z) = 0 \qquad (1)$$

Momentum Equation

$$\rho v_r \frac{\partial v_z}{\partial r} + \rho v_z \frac{\partial v_z}{\partial z} = -\frac{dp}{dz} + \frac{1}{r}\frac{\partial}{\partial r}\left(\mu r \frac{\partial v_z}{\partial r}\right) \qquad (2)$$

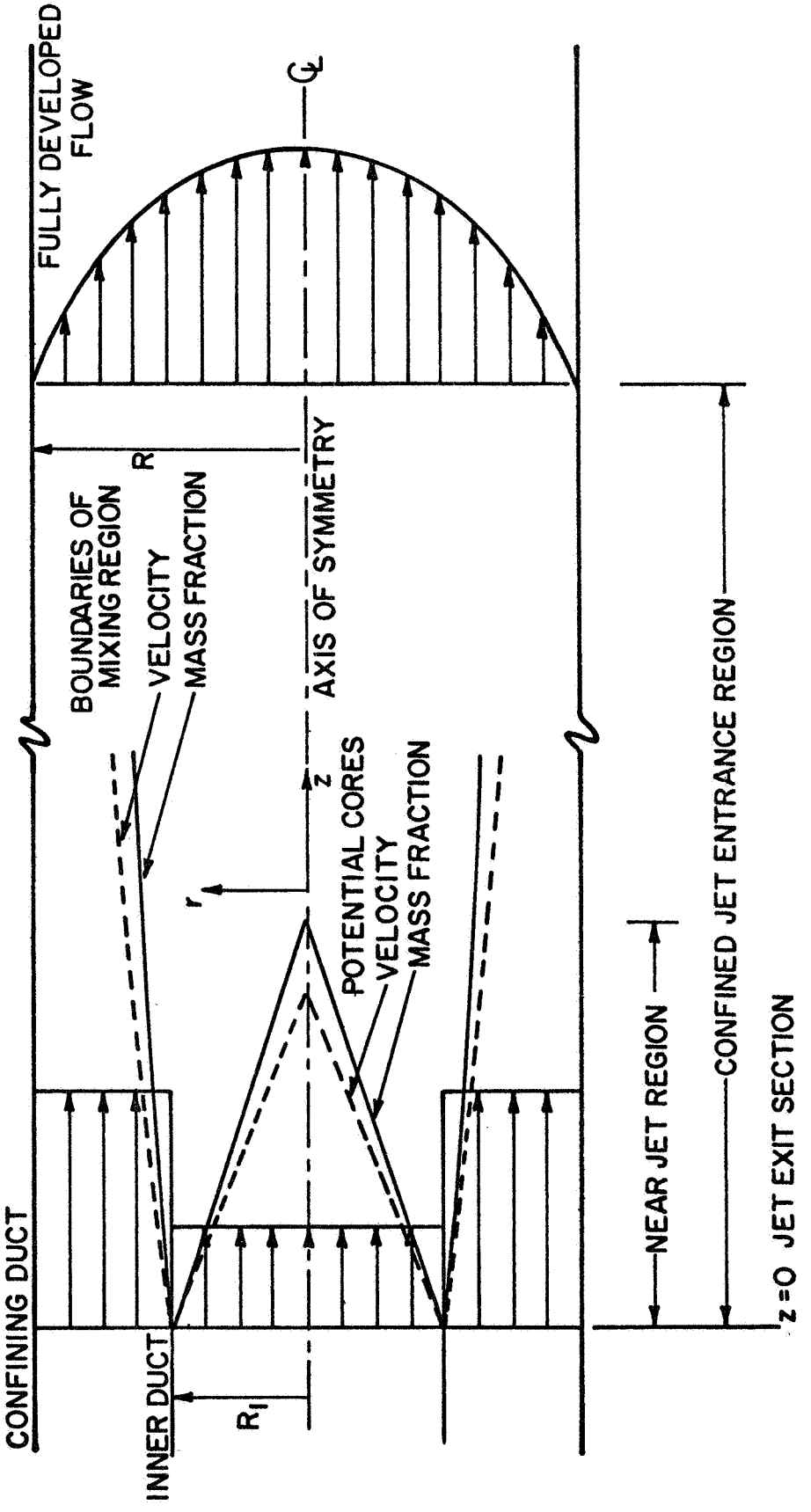

FIGURE 1. TYPICAL CONFINED JET ENTRANCE REGION AND COORDINATE SYSTEM.

Diffusion Equation

$$\rho v_r \frac{\partial \omega_1}{\partial r} + \rho v_z \frac{\partial \omega_1}{\partial z} = \frac{1}{r} \frac{\partial}{\partial r} \left[r \rho D_{12} \frac{\partial \omega_1}{\partial r} \right] \tag{3}$$

where

D_{12}	binary diffusivity for gas mixture
p	static pressure
v_r	mass average radial velocity
v_z	mass average axial velocity
r	radial space coordinate
z	axial space coordinate
μ	viscosity of mixture
ρ	mass average density
ω_1	mass fraction of species 1

2.3.2 Auxiliary Expressions

The auxiliary expressions relating thermodynamic and transport properties namely density, viscosity and binary diffusivity are given below. Except for the expression for density, the other two equations may be found in References 27,28 and 29.

Expression for Density

The expression for density is derived in Appendix A.

$$\rho = \frac{\frac{\omega_1}{M_1}}{\frac{\omega_1}{M_1} + \frac{\omega_2}{M_2}} \left[\rho_{p,1} - \rho_{p,2} \right] + \rho_{p,2} \tag{4}$$

where

M_i molecular weight of fluid component i

ρ_p density of pure fluid

Expression for Viscosity

Viscosities of monatomic or polyatomic non-polar gases and gas mixtures at low density can be computed from the following formulas.

For a monatomic or polyatomic gas,

$$\mu_p = \frac{2.6693 \times 10^{-5} \sqrt{MT}}{\sigma^2 \Omega_\mu} \tag{5}$$

where

μ_p viscosity of pure component

T temperature

σ collision diameter

Ω_μ collision integral for viscosity

For a binary gaseous mixture,

$$\mu = \sum_{i=1}^{2} \frac{x_i \mu_{p,i}}{\sum_{j=1}^{2} x_j \Phi_{ij}} \tag{6}$$

where

$\mu_{p,i}$ viscosity of component i

$$\Phi_{ij} = \frac{1}{\sqrt{8}} \left[1 + \frac{M_i}{M_j} \right]^{-1/2} \left[1 + \left(\frac{\mu_i}{\mu_j} \right)^{1/2} \left(\frac{M_j}{M_i} \right)^{1/4} \right]^2 \tag{7}$$

Expression for Binary Diffusivity

$$D_{12} = \frac{BT^{3/2}\left[\frac{M_1 + M_2}{M_1 M_2}\right]^{1/2}}{P\sigma_{12}^2\, w_{(1)}^{(1)}\,(1-\Delta)} \tag{8}$$

where

$$\sigma_{12}^2 = \left[\frac{\sigma_1 + \sigma_2}{2}\right]^2 \tag{9}$$

$$B = \left\{10.7 - 2.46\left[\frac{M_1 + M_2}{M_1 M_2}\right]^{1/2}\right\} \times 10^{-4} \tag{10}$$

P static pressure of mixture in atm.

$w_{(1)}^{(1)}$ collision integral for mass diffusivity

x_i mole fraction of species i

Δ correction factor

Equations (1), (2), (3), (4), (6) and (8) involve the seven unknowns $v_r(r,z)$, $v_z(r,z)$, $\frac{dp}{dz}(z)$, $\omega_1(r,z)$, $\rho(\omega_1)$, $\mu(\omega_1)$ and $D_{12}(\omega_1)$. For a unique solution, the pressure gradient $\frac{dp}{dz}$ must be either prescribed or computed for any flow problem governed by the boundary layer equations. In the present study, $\frac{dp}{dz}$ is calculated by imposing a valid and a unique constraint on the problem. The constraint essential to make the equation set complete is the conservation of mass flow rate across any cross section in the flow region. Expressed mathematically, this leads to the integral continuity equation; further mathematical operations on this gives the equation which will be hereafter referred to as the "Equation of

Constraint". It should be noted here that for the isothermal flow under study, D_{12} is assumed to be independent of concentration and, hence, is a constant. However, for the sake of generality, D_{12} is retained in the functional form.

2.3.3 Equation of Constraint

The mass rate of flow is conserved across every axial cross section of a confined jet mixing flow. Thus

$$\int_0^R 2\pi r \rho v_z dr = \dot{m} \quad \text{for any } z \tag{11}$$

where

R outer radius of the confining pipe

$\dot{m}$ mass rate of flow

Differentiating with respect to z, Equation (11) becomes

$$\frac{\partial}{\partial z} \int_0^R 2\pi r \rho v_z dr = 0 \tag{12}$$

It is assumed that the integrand of the above equation is an integrable function of r for each value of z, and that the partial derivative $\frac{\partial(\rho v_z)}{\partial z}$ exists and is a continuous function of r and z in the region of interest. Then Equation (12) can be written as

$$2\pi \int_0^R r \frac{\partial(\rho v_z)}{\partial z} dr = 0 \tag{13}$$

Substituting for $\frac{\partial(\rho v_z)}{\partial z}$ from the momentum equation (2), the axial pressure gradient $\frac{dp}{dz}$ can be written, after some simplification, as

$$\frac{dp}{dz} = \frac{\int_o^R \frac{r}{v_z}\left[v_z^2 \frac{\partial \rho}{\partial z} - \rho v_r \frac{\partial v_z}{\partial r} + \frac{1}{r}\frac{\partial}{\partial r}\left[\mu r \frac{\partial v_z}{\partial r}\right]\right] dr}{\int_o^R \frac{r}{v_z}\, dr} \qquad (14)$$

The term $\frac{\partial \rho}{\partial z}$ in the above equation can be replaced by the derivative of Equation (4).

$$\frac{\partial \rho}{\partial z} = \frac{\frac{\partial \omega_1}{\partial z}}{M_1 M_2 \left[\frac{\omega_1}{M_1} + \frac{\omega_2}{M_2}\right]^2}\left[\rho_{p,1} - \rho_{p,2}\right] \qquad (15)$$

Then Equation (14) can be written as

$$\frac{dp}{dz} = \frac{1}{\int_o^R \frac{r}{v_z}\, dr} \int_o^R \frac{r}{v_z}\left[\begin{array}{l} v_z^2\left[\frac{\frac{\partial \omega_1}{\partial z}}{M_1 M_2\left[\frac{\omega_1}{M_1} + \frac{\omega_2}{M_2}\right]^2}\right]\left[\rho_{p,1} - \rho_{p,2}\right] \\ \\ - \rho v_r \frac{\partial v_z}{\partial r} + \frac{1}{r}\frac{\partial}{\partial r}\left[\mu r \frac{\partial v_z}{\partial r}\right] \end{array}\right] dr \qquad (16)$$

Equation (16) is the required "Equation of Constraint" and a unique solution of the problem can be obtained after prescribing appropriate boundary conditions.

2.3.4 Boundary Conditions

1. At the initial section z = 0

$$v_z(r,0) = \begin{cases} \lambda_1(r) & 0 \le r \le R_1 \\ \lambda_2(r) & R_1 < r \le R \end{cases} \tag{17a}$$

$$v_r(r,0) = 0 \qquad 0 \le r \le R \tag{17b}$$

$$\omega_1(r,0) = \begin{cases} \lambda_3(r) & 0 \le r \le R_1 \\ \lambda_4(r) & 0 < r \le R \end{cases} \tag{17c}$$

In this problem $\lambda_1(r)$, $\lambda_2(r)$, $\lambda_3(r)$ and $\lambda_4(r)$ were chosen to be constants.

2. At the centerline r = 0

$$v_r(0,z) = 0 \tag{18a}$$

$$\frac{\partial v_z}{\partial r} = 0 \tag{18b}$$

$$\frac{\partial \omega_1}{\partial r} = 0 \tag{18c}$$

3. At the wall r = R

$$v_z (R,z) = 0 \tag{19a}$$

$$v_r (R,z) = 0 \tag{19b}$$

$$\frac{\partial \omega_1}{\partial r} = 0 \tag{19c}$$

Equations (1), (2), (3), (4), (6), (8) and (16), together with the boundary conditions given by the equations (17), (18) and (19) complete the formulation of the jet mixing problem.

The problem is thus governed by a system of coupled non-linear partial differential equations which are very complex to solve. Also several previous investigators have reported severe numerical instabilities while attempting to solve similar equations for free jet mixing problems. One of the means used in the past to overcome these difficulties was to transform the problem into the von Mises plane in which the independent variables are the stream function ψ and the axial distance z.

Indeed, von Mises plane is used to solve the present confined jet mixing problem. The advantages and disadvantages of this transformation will be discussed later.

2.4 Formulation of Problem in von Mises Plane (ψ,z)

2.4.1 Definitions

The stream function is defined by the following two relations.

$$\frac{\partial \psi}{\partial r} = \rho v_z r \tag{20a}$$

$$\frac{\partial \psi}{\partial z} = -\rho v_r r \tag{20b}$$

Thus,

$$\psi = \int_o^r \rho v_z r \, dr \tag{21}$$

The inverse transformation is given by

$$r^2 = 2 \int_o^{\psi} \frac{\partial \psi}{\rho v_z} \tag{22}$$

The differential operators in the transform plane become

$$\frac{\partial}{\partial r} = \rho v_z r \frac{\partial}{\partial \psi} \tag{23}$$

$$\frac{\partial}{\partial z} = -\rho v_r r \frac{\partial}{\partial \psi} + \frac{\partial}{\partial z} \tag{24}$$

The Jacobian of the transformation is given by

$$J = \frac{\partial(\psi,z)}{\partial(r,z)} = \rho v_z r \qquad (25)$$

Equation (25) shows that the Jacobian vanishes at the centerline and at the wall, i.e., the transformation is singular at these boundaries. Hence, at the centerline and at the wall, the mapping is not one-to-one, and therefore, the inverse transformation does not exist at $\psi = 0$ and $\psi = \Psi$, where Ψ is the wall stream function. However, $\psi = 0$ corresponds to $r = 0$, and $\psi = \Psi$ corresponds to $r = R$. Thus, this information makes it possible to transfer uniquely the calculated values of flow parameters from the von Mises plane to the physical plane in the entire flow field.

The equations and the boundary conditions describing the flow problem are transformed to the von Mises plane using Equations (20) through (24).

2.4.2 Governing Differential Equations

Continuity Equation

The continuity equation (1) is satisfied identically by the definition of the stream function given by Equation (20).

Momentum Equation

The transformed momentum equation corresponding to Equation (2) is obtained as

$$\frac{\partial v_z}{\partial z} = -\frac{1}{\rho v_z}\frac{dp}{dz} + \frac{\partial}{\partial \psi}\left[\mu r^2 \rho v_z \frac{\partial v_z}{\partial \psi}\right] \tag{26}$$

Diffusion Equation

The diffusion equation, Equation (3), transforms as

$$\frac{\partial \omega_1}{\partial z} = \frac{\partial}{\partial \psi}\left[r^2 \rho^2 D_{12} v_z \frac{\partial \omega_1}{\partial \psi}\right] \tag{27}$$

Equation of Constraint

$$\frac{dp}{dz} = \frac{1}{\int_o^{\Psi} \frac{1}{\rho v_z^2}\, d\psi} \int_o^{\Psi} \left[\begin{array}{l} -\rho v_r r \dfrac{\partial(\rho v_z)}{\partial \psi} + \dfrac{v_z \dfrac{\partial \omega_1}{\partial z}}{M_1 M_2 \left[\dfrac{\omega_1}{M_1} + \dfrac{\omega_2}{M_2}\right]^2} \\ \\ \left[\rho_{p,1} - \rho_{p,2}\right] + \rho \dfrac{\partial}{\partial \psi}\left[\mu r^2 \rho v_z \dfrac{\partial v_z}{\partial \psi}\right] \end{array}\right] \frac{d\psi}{\rho v_z} \tag{28}$$

2.4.3 Auxiliary Expressions

The auxiliary expressions (4), (6) and (8) remain unchanged, but will be repeated here for the sake of completeness of the flow equation set.

Expression for Density

$$\rho = \frac{\frac{\omega_1}{M_1}}{\frac{\omega_1}{M_1} + \frac{\omega_2}{M_2}} \left[\rho_{p,1} - \rho_{p,2}\right] + \rho_{p,2} \tag{29}$$

Expression for Viscosity

$$\mu = \sum_{i=1}^{2} \frac{x_i \mu_{p,i}}{\sum_{j=1}^{2} x_j \Phi_{ij}} \tag{30}$$

Expression for Binary Diffusivity

$$D_{12} = \frac{BT^{3/2} \left[\frac{M_1 + M_2}{M_1 M_2} \right]^{1/2}}{P\sigma_{12}^2 \, w_{(1)}^{(1)} \, (1-\Delta)} \tag{31}$$

Appropriate mathematical operations on the continuity equation make it possible to obtain v_r in the ψ-z plane as follows.

2.4.4 Equation for Determining v_r

$$\frac{\partial (r v_r)}{\partial \psi} = \frac{v_r}{v_z} r \frac{\partial v_z}{\partial \psi} - \left[\frac{1}{\rho v_z} \frac{\partial v_z}{\partial z} + \frac{1}{\rho^2} \frac{\partial \rho}{\partial z} \right] \tag{32}$$

The boundary conditions given by Equations (17), (18) and (19) for the physical plane, must be transformed also to the von Mises plane.

2.4.5 Boundary Conditions

At $z = 0$, the dependent variables are prescribed as functions of r and can be directly transformed to functions of ψ.

At $r = 0$, the boundary condition given by Equation (18) shows that the first order radial derivatives of v_z and ω_1 vanish.

These are transformed as follows.

By definition

$$\frac{\partial v_z}{\partial r} = \rho v_z r \frac{\partial v_z}{\partial \psi} \tag{33}$$

or

$$\rho v_z \frac{\partial v_z}{\partial \psi} = \frac{\frac{\partial v_z}{\partial r}}{r} \tag{34}$$

In view of Equation (18), at $r = 0$, Equation (34) has the indeterminate form

$$\rho v_z \frac{\partial v_z}{\partial \psi}\bigg|_{r=0} = \frac{0}{0} \tag{35}$$

Using L'Hospital's rule, Equation (34) may be written as

$$\lim_{r\to 0} \rho v_z \frac{\partial v_z}{\partial \psi} = \lim_{r\to 0} \frac{\frac{\partial^2 v_z}{\partial r^2}}{1} \tag{36}$$

A finite $\frac{\partial^2 v_z}{\partial r^2}$ therefore implies that $\frac{\partial v_z}{\partial r}$ is bounded. Similarly it can be shown that $\frac{\partial \omega_1}{\partial \psi}$ and all other first derivatives with respect to ψ are bounded at $r = 0$.

Equations (26) and (27) show that the first order ψ derivatives always appear accompanied by the factor r^2. Hence, the boundary condition at the centerline can be written as

$$\lim_{r\to 0} r^2 \frac{\partial v_z}{\partial \psi} = \lim_{r\to 0} r^2 \frac{\partial \omega_1}{\partial \psi} = 0 \tag{37}$$

Finally, at $r = R$, only the part of the boundary condition involving the radial derivative of ω_1 needs transformation.

Again, by definition

$$\frac{\partial \omega_1}{\partial r} = \rho v_z r \frac{\partial \omega_1}{\partial \psi} \tag{38}$$

or

$$\rho r \frac{\partial \omega_1}{\partial \psi} = \frac{\dfrac{\partial \omega_1}{\partial r}}{v_z} \tag{39}$$

Using Equation (19) in the above equation shows that at $r = R$, Equation (39) has the indeterminate form

$$\rho r \frac{\partial \omega_1}{\partial \psi}\bigg|_{r=R} = \frac{0}{0} \tag{40}$$

Using L'Hospital's rule, Equation (40) can be written as

$$\lim_{r \to R} \rho r \frac{\partial \omega_1}{\partial \psi} = \lim_{r \to R} \frac{\dfrac{\partial^2 \omega_1}{\partial r^2}}{\dfrac{\partial v_z}{\partial r}} \tag{41}$$

Now, at $r = R$, $\dfrac{\partial v_z}{\partial r}$ is finite and $\dfrac{\partial^2 \omega_1}{\partial r^2}$ can be estimated as follows. The diffusion equation in the physical plane is

$$\rho v_z \frac{\partial \omega_1}{\partial r} + \rho v_z \frac{\partial \omega_1}{\partial z} = \frac{1}{r} \frac{\partial}{\partial r} \left[r \rho D_{12} \frac{\partial \omega_1}{\partial r} \right] \tag{42}$$

Substitution of Equation (19) yields

$$\left.\frac{\partial^2 \omega_1}{\partial r^2}\right|_{r=R} = 0 \tag{43}$$

Using Equation (43) in Equation (41) above gives the boundary condition at the wall as

$$\lim_{r \to R} \rho r \frac{\partial \omega_1}{\partial \psi} = 0 \tag{44}$$

or

$$\left.\frac{\partial \omega_1}{\partial \psi}\right|_{r=R} = 0 \tag{45}$$

All the boundary conditions can now be summarized as follows.

1. <u>At the Initial Section z = 0</u>

$$v_z(\psi,0) = \begin{cases} \lambda_1(\psi) & 0 \le \psi \le \Psi_1 \\ \lambda_2(\psi) & \Psi_1 < \psi \le \Psi \end{cases} \tag{46a}$$

$$v_r(\psi,0) = 0 \qquad 0 \le \psi \le \Psi \tag{46b}$$

$$\omega_1(\psi,0) = \begin{cases} \lambda_3(\psi) & 0 \le \psi \le \Psi_1 \\ \lambda_4(\psi) & \Psi_1 < \psi \le \Psi \end{cases} \tag{46c}$$

In this problem $\lambda_1(\psi)$, $\lambda_2(\psi)$, $\lambda_3(\psi)$, $\lambda_4(\psi)$ were chosen to be constant.

2. <u>At the centerline $r = 0 \rightarrow \psi = 0$</u>

$$v_r(0,z) = 0 \tag{47a}$$

$$\lim_{r\to 0} r^2 \frac{\partial v_z}{\partial \psi} = 0 \tag{47b}$$

$$\lim_{r\to 0} r^2 \frac{\partial \omega_1}{\partial \psi} = 0 \tag{47c}$$

3. <u>At the wall $r = R \rightarrow \psi = \Psi$</u>

$$v_z(\Psi,z) = 0 \tag{48a}$$

$$v_r(\Psi,z) = 0 \tag{48b}$$

$$\frac{\partial \omega_1}{\partial \psi} = 0 \tag{48c}$$

The wall boundary condition is used to determine ω_1 at the wall. But at the centerline, instead of using the boundary condition to determine the solution function, it is preferred for higher numerical accuracy to use the limiting forms of the governing differential equations. These equations may be obtained by substituting the centerline boundary conditions in the general differential equations.

2.4.6 Centerline Equations

Momentum Equation

The momentum equation was given by Equation (26) as

$$\frac{\partial v_z}{\partial z} = -\frac{1}{\rho v_z}\frac{dp}{dz} + \frac{\partial}{\partial \psi}\left[\mu r^2 \rho v_z \frac{\partial v_z}{\partial \psi}\right] \tag{49}$$

On expanding, Equation (49) gives

$$\frac{\partial v_z}{\partial z} = -\frac{1}{\rho v_z}\frac{dp}{dz} + \mu r^2 \rho v_z \frac{\partial^2 v_z}{\partial \psi^2} + \mu r^2 \rho \left[\frac{\partial v_z}{\partial \psi}\right]^2 + \mu r^2 v_z \frac{\partial \rho}{\partial \psi}\frac{\partial v_z}{\partial \psi}$$

$$+ 2\mu r \rho v_z \frac{\partial r}{\partial \psi}\frac{\partial v_z}{\partial \psi} + r^2 \rho v_z \frac{\partial \mu}{\partial \psi}\frac{\partial v_z}{\partial \psi} \tag{50}$$

From Equation (20),

$$\rho v_z r \frac{\partial r}{\partial \psi} = 1 \tag{51}$$

Using Equation (51) and the earlier derived fact that the first order derivatives with respect to ψ are bounded, Equation (50) reduces to

$$\frac{\partial v_z}{\partial z} = -\frac{1}{\rho v_z}\frac{dp}{dz} + \mu r^2 \rho v_z \frac{\partial^2 v_z}{\partial \psi^2} + 2\mu \frac{\partial v_z}{\partial \psi} \tag{52}$$

The second term on the right hand side of this equation is examined in the following manner.

$$\mu r^2 \rho v \frac{\partial^2 v_z}{\partial \psi^2} = \mu r \frac{\partial}{\partial r}\left[\frac{1}{\rho v_z r}\frac{\partial v_z}{\partial r}\right] \tag{53}$$

or

$$\mu r^2 \rho v_z \frac{\partial^2 v_z}{\partial \psi^2} = \frac{\mu}{\rho v_z}\frac{\partial^2 v_z}{\partial r^2} - \frac{\mu}{\rho v_z r}\frac{\partial v_z}{\partial r} - \frac{\mu}{\rho v_z^2}\left[\frac{\partial v_z}{\partial r}\right]^2$$

$$- \frac{\mu}{v_z \rho^2}\frac{\partial v_z}{\partial r}\frac{\partial \rho}{\partial r} \tag{54}$$

Now by L'Hospital's rule

$$\lim_{r\to 0} \frac{\frac{\partial v_z}{\partial r}}{r} = \lim_{r\to 0} \frac{\partial^2 v_z}{\partial r^2} \tag{55}$$

Using Equations (18) and (55) in Equation (54) gives

$$\mu r^2 \rho v_z \frac{\partial^2 v_z}{\partial \psi^2} = 0 \tag{56}$$

Therefore, Equation (52) reduces to

$$\frac{\partial v_z}{\partial z} = - \frac{1}{\rho v_z}\frac{dp}{dz} + 2\mu \frac{\partial v_z}{\partial \psi} \tag{57}$$

Diffusion Equation

Similarly, at the centerline, the diffusion Equation (27) reduces to

$$\frac{\partial \omega_1}{\partial z} = 2\rho D_{12} \frac{\partial \omega_1}{\partial \psi} \tag{58}$$

The flow Equations (26) through (32) along with the boundary conditions (46) through (48) and the centerline Equations (57) and (58) complete the formulation of the problem in the von Mises plane for a unique solution.

One point is of major concern at this stage, since the problem is solved by finite difference methods. The boundary condition at $z = 0$ determines the mass flux of the outer and inner streams. As the ratio of the mass fluxes of the outer to the inner streams approaches the total number of steps of uniform size along the transverse direction, the number of grid points representing the inner stream decreases. The latter number becomes undesirably small for certain cases with large mass flux ratios investigated in the present work. Hence, to obtain a proper finite difference representation of the inner stream for these large mass flux ratios without unreasonably increasing the number of steps in the ψ direction, a suitable transformation is used to stretch the ψ coordinate in the region of the inner stream. This transformation, termed the "φ transformation" and the corresponding transformed equations and boundary conditions are presented next.

2.5 Formulation of Problem in φ-Transform Plane (φ, z)*

The φ-transform is used to obtain a proper finite difference representation of the inner stream for jet mixing systems with large ratios of the mass flow rates of the outer to the inner streams. Basically, this involves a "stretching" of the ψ-coordinate in the region of the inner stream. To achieve the desired purpose, a simple transformation in the form of a square-root function is used.

2.5.1 Definition of φ-Transformation

$$\varphi = a\psi^{1/\alpha} \tag{59}$$

where $\alpha = 1$ or 2 and a is a suitably selected constant. For the cases investigated, a is chosen to be equal to unity and α is chosen to be 2. These are the values used in further discussion of the transformation. Since the z-coordinate remains unaffected by this transformation, only the ψ derivatives need to be transformed from ψ-z to the φ-z plane.

$$\frac{\partial}{\partial\psi} = \frac{\partial\varphi}{\partial\psi}\frac{\partial}{\partial\varphi} \tag{60}$$

$$\frac{\partial^2}{\partial\psi^2} = \left[\frac{\partial\varphi}{\partial\psi}\right]^2 \frac{\partial^2}{\partial\varphi^2} + \frac{\partial^2\varphi}{\partial\psi^2}\frac{\partial}{\partial\varphi} \tag{61}$$

---

* The details of this transformation were obtained by Miss Urmila Agarwal, Research Fellow in the Mechanical and Aerospace Engineering Department, Illinois Institute of Technology.

Using the definition given by Equation (59), Equations (60) and (61) may be written as

$$\frac{\partial}{\partial \psi} = \frac{1}{2\varphi} \frac{\partial}{\partial \varphi} \tag{62}$$

$$\frac{\partial^2}{\partial \psi^2} = \frac{1}{4\varphi^2} \frac{\partial^2}{\partial \varphi^2} - \frac{1}{4\varphi^3} \frac{\partial}{\partial \varphi} \tag{63}$$

The inverse φ-transformation is defined by

$$\int_{r_1}^{r_2} r\,dr = \int_{\varphi_1}^{\varphi_2} \frac{d\varphi}{\rho v_z \frac{d\varphi}{d\psi}} = \int_{\varphi_1}^{\varphi_2} \frac{2\varphi}{\rho v_z}\, d\varphi \tag{64}$$

The Jacobian of the transformation is given by

$$J' = \frac{\partial(\varphi, z)}{\partial(\psi, z)} = \frac{1}{2\varphi} \tag{65}$$

Clearly, J' becomes infinite at $\varphi = 0$, i.e., at the centerline, so that special care must be taken while using the transformation at the centerline. Essentially, this consists of using the information that $\varphi = 0$ occurs at $r = 0$; also at the centerline, L'Hospital's rule is used in evaluating the transverse derivatives.

The equations and the boundary conditions describing the problem in the ψ-z plane are next transformed to the φ-z plane.

2.5.2 Governing Differential Equations

Momentum Equation

$$\frac{\partial v_z}{\partial z} = -\frac{1}{\rho v_z}\frac{dp}{dz} + \frac{d\varphi}{d\psi}\frac{\partial}{\partial\varphi}\left[\mu r^2 \rho v_z \frac{d\varphi}{\partial\psi}\frac{\partial v_z}{\partial\varphi}\right] \tag{66}$$

Diffusion Equation

$$\frac{\partial \omega_1}{\partial z} = \frac{d\varphi}{\partial\psi}\frac{\partial}{\partial\varphi}\left[r^2\rho^2 D_{12} v_z \frac{d\varphi}{d\psi}\frac{\partial\omega_1}{\partial\varphi}\right] \tag{67}$$

Equation of Constraint

$$\frac{dp}{dz} = \frac{1}{\int_0^{\Phi}\frac{d\varphi}{\rho v_z^2\frac{d\varphi}{d\psi}}}\int_0^{\Phi}\left[\begin{array}{l} -\rho v_r r\frac{d\varphi}{d\psi}\frac{\partial}{\partial\varphi}(\rho v_z) \\ + v_z\frac{\partial\omega_1}{\partial z}\left\{\frac{\rho_{p,1}-\rho_{p,2}}{M_1M_2\left[\frac{\omega_1}{M_1}+\frac{\omega_2}{M_2}\right]^2}\right\} \\ + \rho\frac{d\varphi}{d\psi}\frac{\partial}{\partial\varphi}\left[\mu r^2\rho v_z\frac{d\varphi}{d\psi}\frac{\partial v_z}{\partial\varphi}\right] \end{array}\right]\frac{d\varphi}{\rho v_z\frac{d\varphi}{d\psi}} \tag{68}$$

Equation (68) may also be derived directly from Equation (11) of the physical plane. This derivation is shown in Appendix A.

Equation for Determining v_r

$$\frac{d\varphi}{d\psi}\frac{\partial}{\partial\varphi}(rv_r) = r\frac{v_r}{v_z}\frac{d\varphi}{d\psi}\frac{\partial v_z}{\partial\varphi} - \frac{1}{\rho v_z}\frac{\partial v_z}{\partial z} - \frac{1}{\rho^2}\frac{\partial\rho}{\partial z} \tag{69}$$

2.5.3 Auxiliary Expressions

The auxiliary expressions (28), (29) and (30) for ρ, μ, D_{12} respectively, remain unaffected by the transformation but are repeated here for the sake of completeness of the flow equation set.

Expression for Density

$$\rho = \frac{\frac{\omega_1}{M_1}}{\frac{\omega_1}{M_1} + \frac{\omega_2}{M_2}}\left[\rho_{p,1} - \rho_{p,2}\right] + \rho_{p,2} \tag{70}$$

Expression for Viscosity

$$\mu = \sum_{i=1}^{2} \frac{x_i\mu_{p,i}}{\sum_{j=1}^{2} x_j\varphi_{i,j}} \tag{71}$$

Expression for Binary Diffusivity

$$D_{12} = \frac{BT^{3/2}\left[\frac{M_1 + M_2}{M_1M_2}\right]^{1/2}}{\rho\sigma_{12}^2\, w_{(1)}^{(1)}(1-\Delta)} \tag{72}$$

2.5.4 Boundary Conditions

At $z = 0$, Equation (46) gives the boundary conditions as prescribed functions of ψ. Since the φ-transformation defines a one-to-one correspondence between ψ and φ, the variables v_z and ω_1 can be readily computed as functions of φ.

At $\varphi = 0$, the first order ψ-derivatives were shown to be bounded. The corresponding transformed boundary condition becomes

$$\left[\frac{d\varphi}{d\psi}\frac{\partial v_z}{\partial \varphi}\right]_{\varphi=0} = \text{a bounded quantity} \tag{73}$$

Equation (59) shows that $\left.\frac{d\varphi}{d\psi}\right|_{\varphi=0}$ is unbounded, hence $\left.\frac{\partial v_z}{\partial \varphi}\right|_{\varphi=0}$ must necessarily vanish, i.e.,

$$\left.\frac{\partial v_z}{d\varphi}\right|_{\varphi=0} = 0 \tag{74}$$

Similarly,

$$\left.\frac{\partial \omega_1}{\partial \varphi}\right|_{\varphi=0} = 0 \tag{75}$$

The only boundary condition that remains to be considered is $\left.\frac{\partial \omega_1}{\partial \psi}\right|_{\psi=\Psi}$ and this transforms as

$$\left[\frac{d\varphi}{d\psi}\frac{\partial \omega_1}{\partial \varphi}\right]_{\varphi=\bar{\Phi}} = 0 \tag{76}$$

Since $\left.\frac{d\varphi}{d\psi}\right|_{\varphi=\Phi}$ is finite,

$$\left.\frac{\partial \omega_1}{\partial \varphi}\right|_{\varphi=\Phi} = 0 \tag{77}$$

The boundary conditions in the φ-z plane are presented below.

1. <u>At the initial section z = 0</u>

$$v_z(\varphi,0) = \begin{cases} \lambda_1(\varphi) & 0 \le \varphi \le \Phi_1 \\ \lambda_2(\varphi) & \Phi_1 < \varphi \le \Phi \end{cases} \tag{78a}$$

$$v_r(\varphi,0) = 0 \qquad 0 \le \varphi \le \Phi \tag{78b}$$

$$\omega_1(\varphi,0) = \begin{cases} \lambda_3(\varphi) & 0 \le \varphi \le \Phi \\ \lambda_4(\varphi) & \Phi_1 < \varphi \le \Phi \end{cases} \tag{78c}$$

In this problem $\lambda_1(\varphi)$, $\lambda_2(\varphi)$, $\lambda_3(\varphi)$, $\lambda_4(\varphi)$ were chosen to be constants.

2. <u>At the centerline φ = 0</u>

$$v_r(0,z) = 0 \tag{79a}$$

$$\left.\frac{\partial v_z}{\partial \varphi}\right|_{\varphi=0} = 0 \qquad (79b)$$

$$\left.\frac{\partial \omega_1}{\partial \varphi}\right|_{\varphi=0} = 0 \qquad (79c)$$

3. At the wall $\varphi = \Phi$

$$v_z(\Phi, z) = 0 \qquad (80a)$$

$$v_r(\Phi, z) = 0 \qquad (80b)$$

$$\left.\frac{\partial \omega_1}{\partial \varphi}\right|_{\varphi=\Phi} = 0 \qquad (80c)$$

It only remains to transform the centerline equations to the corresponding equations in the φ-z plane.

2.5.5 Centerline Equations

Since the φ-transformation has an unbounded Jacobian at $\varphi = 0$, suitable mathematical operations are necessary for transforming the ψ-derivative appearing in the centerline Equations (57) and (58). By definition

$$\frac{\partial v_z}{\partial \psi} = \frac{\partial v_z}{\partial \varphi} \frac{d\varphi}{d\psi}$$

or

$$\frac{\partial v_z}{\partial \psi} = \frac{\dfrac{\partial v_z}{\partial \varphi}}{\dfrac{d\psi}{d\varphi}} \tag{81}$$

The right-hand member of the above equation has the indeterminate form $\frac{0}{0}$ at the centerline, i.e., at $\varphi = 0$. Using L'Hospital's rule

$$\lim_{\psi \to 0} \frac{\partial v_z}{\partial \psi} = \lim_{\varphi \to 0} \frac{\dfrac{\partial^2 v_z}{\partial \varphi^2}}{\dfrac{d^2 \psi}{d\varphi^2}} \tag{82}$$

Using Equation (59) with $a = 1$, Equation (82) becomes

$$\lim_{\psi \to 0} \frac{\partial v_z}{\partial \psi} = \frac{1}{2} \frac{\partial^2 v_z}{\partial \varphi^2} \bigg|_{\varphi=0} \tag{83}$$

Similarly,

$$\lim_{\psi \to 0} \frac{\partial \omega_1}{\partial \psi} = \frac{1}{2} \frac{\partial^2 v_z}{\partial \varphi^2} \bigg|_{\varphi=0} \tag{84}$$

Therefore, the centerline equations in the φ-z plane are obtained in the following form.

Momentum Equation

$$\frac{\partial v_z}{\partial z} = -\frac{1}{\rho v_z}\frac{dp}{dz} + \mu\frac{\partial^2 v_z}{\partial \varphi^2} \tag{85}$$

Diffusion Equation

$$\frac{\partial \omega_1}{\partial z} = \rho D_{12}\frac{\partial^2 \omega_1}{\partial \varphi^2} \tag{86}$$

Thus, the flow problem is completely represented by Equations (66) through (72) (together with Equations (85) and (86) for the centerline) and the boundary conditions (78) through (80). The numerical method employed for the solution of this system is presented next.

CHAPTER 3

NUMERICAL METHOD OF SOLUTION

3.1 Introduction

At present, the solution of the parabolic system of coupled non-linear partial differential equations (PDEs) which describe the confined jet mixing problem, is not possible by analytical methods. A forward marching numerical technique is used to solve the present problem governed by Equations (66) through (69), (85), (86), together with the auxiliary equations and the boundary conditions stated in the previous chapter. Similar procedures have been employed by several authors (References 13 and 30) in numerical studies of the boundary layer equations using semi-explicit methods. However, an all-explicit numerical method is used in the present study. Reasons for selection of the all-explicit method are explained in Appendix B.

In order to use finite difference techniques, first it is necessary to establish a system of grid points in the entire flow field. The discretized rectangular grid and the coordinate system used to solve the problem are shown in Fig. 2. The values of the dependent variables correspond to these discrete grid points which are designated by appropriate subscripts. The differential equations and boundary conditions of the flow problem are replaced by their corresponding finite difference forms. For the transverse derivatives, central differences are used in the interior of the duct and backward

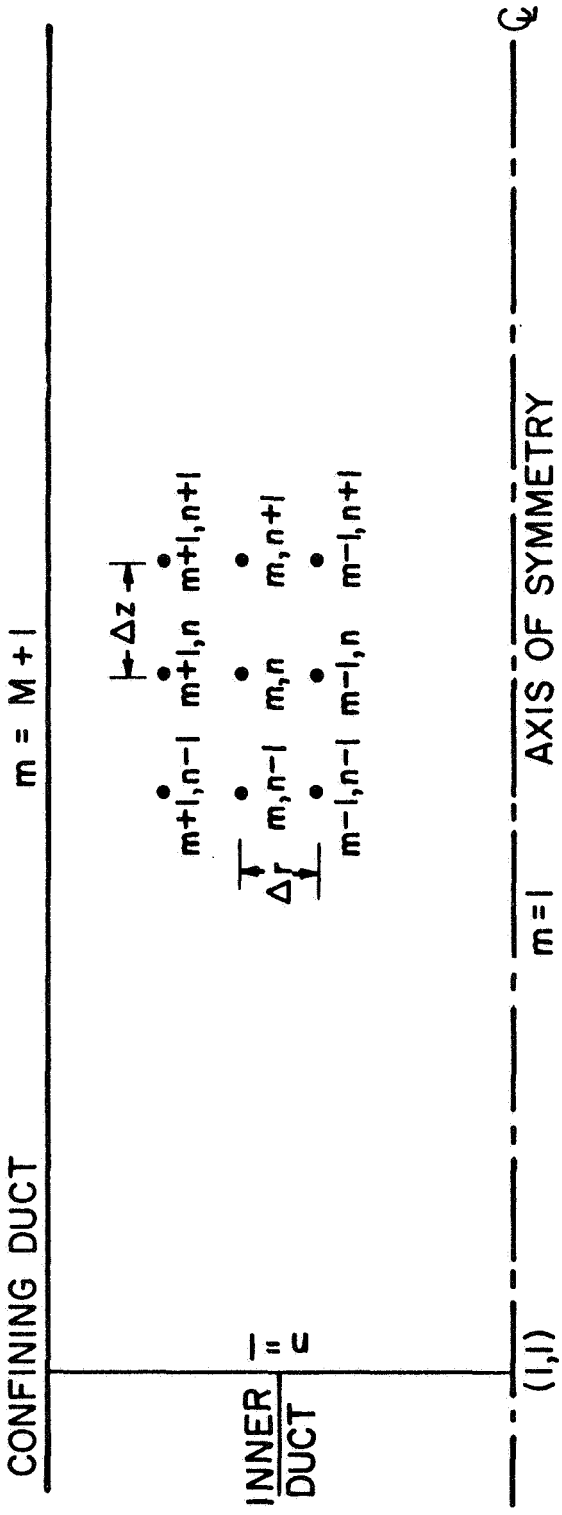

FIGURE 2. DISCRETIZED RECTANGULAR GRID SYSTEM IN JET ENTRANCE REGION

differences are used at the duct wall. Forward differences are used for the axial derivatives everywhere except in the continuity equation; the reason for this will be explained later.

The substitution of these finite difference approximations (FDAs) leads to linear explicit finite difference equations (FDEs) that are stable under certain conditions. These stability conditions are obtained by using the criterion which was developed by Karplus[22] based on an electric circuit theory. These conditions are realizable for non-negative axial velocities. Karplus' criterion has been successfully used by Wu[31] for a two-dimensional laminar incompressible flow problem, by Schuyler and Torda[32] for a two-dimensional laminar compressible flow problem, and by Fejer et al[17] and Agarwal and Torda[18] for confined coaxial axisymmetric laminar jet mixing. The numerical stability of the present problem is also studied by using von Neumann's method[23] and the corresponding stability conditions are compared with those obtained by Karplus' method. The von Neumann and the Karplus methods, and the derivation of the stability conditions for the flow problem using both these methods are presented in Appendix C. Besides stability, consistency and convergence must also be satisfied so that the numerical solution is meaningful. For the present problem, consistency and convergence are shown to be ensured in Appendix B.

The FDEs corresponding to the flow equations and the boundary conditions are now presented. The stability conditions for the basic equations are also given.

3.2 Finite Difference Equations and Stability Conditions

3.2.1 Governing Difference Equations

Momentum Equation

Using the above scheme, Equation (66) can be written at the general grid point (m,n) as

$$\frac{v_z(m,n+1) - v_z(m,n)}{\Delta z} = -\left[\frac{1}{\rho v_z}\frac{dp}{dz}\right]_{m,n}$$

$$+\left[\mu\rho v_z r^2\left[\frac{d\varphi}{d\psi}\right]^2\right]_{m,n}\left[\frac{v_z(m+1,n) - 2v_z(m,n) + v_z(m-1,n)}{\Delta\varphi^2}\right]$$

$$+\left[\mu\rho v_z r^2\frac{d^2\varphi}{d\psi^2} + 2\mu\frac{d\varphi}{d\psi}\right]_{m,n}\left[\frac{v_z(m+1,n) - v_z(m-1,n)}{2\Delta\varphi}\right]$$

$$+\left[r^2\left[\frac{d\varphi}{d\psi}\right]^2\right]_{m,n}\left[F_M\right]_{m,n}\left[\frac{v_z(m+1,n) - v_z(m-1,n)}{2\Delta\varphi}\right] \qquad (87a)$$

where

$$F_M = \mu\rho\frac{\partial v_z}{\partial\varphi} + \mu v_z\frac{\partial\rho}{\partial\varphi} + \rho v_z\frac{\partial\mu}{\partial\varphi} \qquad (87b)$$

Solving explicitly for $v_z(m,n+1)$, Equation (87a) yields

$$v_z(m,n+1) = v_z(m,n) +$$

$$\Delta z \left\{ \begin{array}{l} -\left[\frac{1}{\rho v_z}\frac{dp}{dz}\right]_{m,n} \\ \\ +\left[\mu\rho v_z r^2 \left[\frac{d\varphi}{d\psi}\right]^2\right]_{m,n}\left[\frac{v_z(m+1,n) - 2v_z(m,n) + v_z(m-1,n)}{\Delta\varphi^2}\right] \\ \\ +\left[\mu\rho v_z r^2 \frac{d^2\varphi}{d\psi^2} + 2\mu\frac{d\varphi}{d\psi}\right]_{m,n}\left[\frac{v_z(m+1,n) - v_z(m-1,n)}{2\Delta\varphi}\right] \\ \\ +\left[r^2\left[\frac{d\varphi}{d\psi}\right]^2\right]_{m,n}\left[F_M\right]_{m,n}\left[\frac{v_z(m+1,n) - v_z(m-1,n)}{2\Delta\varphi}\right] \end{array} \right\} \qquad (88)$$

The numerical stability conditions for Equation (88) are derived in Appendix B using Karplus' and von Neumann's methods. These conditions are

1. $\Delta\varphi$ is not limited from stability considerations and is thus selected from the required resolution and the accuracy of the flow problem.

2. $$\Delta z < \left[\frac{1}{2\nu}\frac{1}{r^2\rho^2 v_z}\frac{1}{\left[\frac{d\varphi}{d\psi}\right]^2}\right]_{m,n} \Delta\varphi^2 \tag{89}$$

Centerline Momentum Equation

Equation (85) is only valid at the centerline and can be written as

$$\frac{v_z(m,n+1) - v_z(m,n)}{\Delta z} = -\left[\frac{1}{\rho v_z}\frac{dp}{dz}\right]_{m,n} + \mu_{m,n}\left[\frac{v_z(m+1,n) - 2v_z(m,n) + v_z(m-1,n)}{\Delta\varphi^2}\right] \tag{90}$$

Here, $m = 1$, and from the assumption of axial symmetry, $v_z(m+1,n) = v_z(m-1,n)$. Substituting this value and solving explicitly for $v_z(m,n+1)$, Equation (90) gields

$$v_z(m,n+1) = v_z(m,n) + \Delta z\left[-\left[\frac{1}{\rho v_z}\frac{dp}{dz}\right]_{m,n} + 2\mu(m,n)\left[\frac{v_z(m+1,n) - v_z(m,n)}{\Delta\varphi^2}\right]\right] \tag{91}$$

The stability conditions for this equation are derived in Appendix B and are

1. no restriction on $\Delta\varphi$

2. $$\Delta z < \left[\frac{1}{2\mu}\right]_{m,n} \Delta\varphi^2 \qquad (92)$$

It may be shown that the centerline momentum equation is unconditionally stable if the exponent in the φ-transformation is unity.

For a given value of m, condition (89) is more restrictive than condition (92) and, hence, the step size computed from condition (89) was used throughout the flow field. Also, one may be concerned about the effect on the stability criterion of the pressure gradient term appearing in both Equations (88) and (91). Since the momentum equation is used to compute $v_z(m,n+1)$ by an explicit scheme, the values of all other quantities appearing in Equations (88) or (91) are either specified or computed prior to this stage. In particular, $\left.\frac{dp}{dz}\right|_{m,n}$ appearing in Equations (88) and (91) is a known quantity and, hence, cannot contribute to instability.

Diffusion Equation

Using the explicit scheme, Equation (67) can be written at the general grid point (m,n) as

$$\frac{\omega_1(m,n+1) - \omega_1(m,n)}{\Delta z} =$$

$$\left[r^2\rho^2 D_{12} v_z \left[\frac{d\varphi}{d\psi}\right]^2\right]_{m,n}\left[\frac{\omega_1(m+1,n) - 2\omega_1(m,n) - \omega_1(m-1,n)}{\Delta\varphi^2}\right]$$

$$+\left[r^2\rho^2 D_{12} v_z \frac{d^2\varphi}{d\psi^2} + 2\rho D_{12}\frac{d\varphi}{d\psi}\right]_{m,n}\left[\frac{\omega_1(m+1,n) - \omega_1(m-1,n)}{2\Delta\varphi}\right]$$

$$+\left[r^2\left[\frac{d\varphi}{d\psi}\right]^2\right]_{m,n}\left[F_D\right]_{m,n}\left[\frac{\omega_1(m+1,n) - \omega_1(m-1,n)}{2\Delta\varphi}\right] \qquad (93a)$$

where

$$F_D = \rho^2 D_{12}\frac{\partial v_z}{\partial\varphi} + 2\rho D_{12}\frac{\partial\rho}{\partial\varphi} + \rho^2 v_z\frac{\partial D_{12}}{\partial\varphi} \qquad (93b)$$

Solving explicitly for $\omega_1(m,n+1)$, Equation (93) yields

$$\omega_1(m,n+1) = \omega_1(m,n)$$

$$+\Delta z\left[\begin{array}{l}\left[r^2\rho^2 D_{12} v_z\left[\frac{d\varphi}{d\psi}\right]^2\right]_{m,n}\left[\frac{\omega_1(m+1,n) - 2\omega_1(m,n) + \omega_1(m-1,n)}{\Delta\varphi^2}\right] \\ +\left[r^2\rho^2 D_{12} v_z\frac{d^2\varphi}{d\psi^2} + 2\rho D_{12}\frac{d\varphi}{d\psi}\right]_{m,n}\left[\frac{\omega_1(m+1,n) - \omega_1(m-1,n)}{2\Delta\varphi}\right] \\ +\left[r^2\left[\frac{d\varphi}{d\psi}\right]^2\right]_{m,n}\left[F_D\right]_{m,n}\left[\frac{\omega_1(m+1,n) - \omega_1(m-1,n)}{2\Delta\varphi}\right]\end{array}\right] \qquad (94)$$

The numerical stability conditions, obtained in Appendix B for Equation (94) are

1. no restriction on $\Delta\varphi$

2. $$\Delta z < \left[\frac{N_{Sc}}{2\nu} \frac{1}{r^2 \rho^2 v_z} \frac{1}{\left[\frac{d\varphi}{d\psi}\right]^2} \right]_{m,n} \Delta\varphi^2 \qquad (95)$$

Centerline Diffusion Equation

Equation (86) is valid only at the centerline and can be written as

$$\frac{\omega_1(m,n+1) - \omega_1(m,n)}{\Delta z} = \left[\rho D_{12}\right]_{m,n} \left[\frac{\omega_1(m+1,n) - 2\omega_1(m,n) + \omega_1(m-1,n)}{\Delta\varphi^2} \right] \qquad (96)$$

Here, $m = 1$ and from the assumption of axial symmetry, $\omega_1(m+1,n) = \omega_1(m-1,n)$. Substituting this value and solving explicitly for $\omega_1(m,n+1)$, Equation (96) yields

$$\omega_1(m,n+1) = \omega_1(m,n) + 2\Delta z \left[\rho D_{12}\right]_{m,n} \left[\frac{\omega_1(m+1,n) - \omega_1(m,n)}{\Delta\varphi^2} \right] \qquad (97)$$

The stability conditions for this equation are derived in Appendix B. These conditions are

1. no restriction on $\Delta\varphi$

2. $$\Delta z < \left[\frac{1}{2\rho D_{12}}\right]_{m,n} \Delta\varphi^2 \tag{98}$$

If the exponent in the φ-transformation is unity, it can be shown that the centerline diffusion equation is unconditionally stable.

For a given value of m, condition (95) is more restrictive than condition (98) and, hence, the step size computed from condition (95) is used throughout the flow field.

Equation of Constraint

Using the explicit scheme, Equation (68) can be written as

$$\left.\frac{dp}{dz}\right|_{m,n} = \frac{1}{\sum_{m=1}^{M} \frac{\Delta\varphi}{\left[\rho v_z^2 \frac{d\varphi}{d\psi}\right]_{m,n}}} \left[\left[C_\rho v_z \rho D_{12} \frac{\partial^2 \omega_1}{\partial\varphi^2} + \rho\mu \frac{\partial^2 v_z}{\partial\varphi^2}\right]_{1,n} \frac{\Delta\varphi}{\left[\rho v_z \frac{d\varphi}{d\psi}\right]_{1,n}} + \sum_{m=2}^{M} \left[I_1 + I_2 + I_3\right]_{m,n} \frac{\Delta\varphi}{\left[\rho v_z \frac{d\varphi}{d\psi}\right]_{m,n}} \right] \tag{99}$$

where

$$C_\rho = \frac{\rho_{p,1} - \rho_{p,2}}{M_1 M_2 \left[\frac{\omega_1}{M_1} + \frac{\omega_2}{M_2}\right]^2} \tag{100}$$

$$I_1 = -\left[\rho v_r r \frac{d\varphi}{d\psi}\right]_{m,n} \left[\begin{array}{l} \rho(m,n)\left[\dfrac{v_z(m+1,n) - v_z(m-1,n)}{2\Delta\varphi}\right] \\ \\ + v_z(m,n)\left[\dfrac{\rho(m+1,n) - \rho(m-1,n)}{2\Delta\varphi}\right] \end{array}\right] \quad (101)$$

$$I_2 = C_\rho v_z(m,n)\left[\frac{\omega_1(m,n+1) - \omega_1(m,n)}{\Delta z}\right] \quad (102)$$

It should be noted here that $\omega_1(m,n+1)$ is known at this stage for all m.

$$I_3 = \rho(m,n)\left[\begin{array}{l} \left[\mu\rho v_z r^2\left[\dfrac{d\varphi}{d\psi}\right]^2\right]_{m,n}\left[\dfrac{v_z(m+1,n) - 2v_z(m,n) + v_z(m-1,n)}{\Delta\varphi^2}\right] \\ \\ +\left[\mu\rho^2 v_z r^2 \dfrac{d^2\varphi}{d\psi^2} + 2\mu\dfrac{d\varphi}{d\psi}\right]_{m,n}\left[\dfrac{v_z(m+1,n) - v_z(m-1,n)}{2\Delta\varphi}\right] \\ \\ +\left[r^2\left[\dfrac{d\varphi}{d\psi}\right]^2\right]_{m,n}\left[F_M\right]_{m,n}\left[\dfrac{v_z(m+1,n) - v_z(m-1,n)}{2\Delta\varphi}\right] \end{array}\right] \quad (103)$$

The right hand side of Equation (99) has no terms involving the pressure p. Therefore, Equation (99) is always stable.

Equation for Determining v_r

Equation (69) is not of the appropriate form for calculating the radial velocity v_r since no axial derivative of v_r appears in this equation. Hence, suitable finite difference forms of Equation (69) are necessary for the explicit scheme used. The form selected for use was based on an error analysis. The development of this form of the continuity equation is shown in Appendix A (Equation A-26).

Equation (A-26), used for determining v_r, is written at the fictitious points $(m + \frac{1}{2}, n + 1)$ instead of $(m, n + 1)$ in order to retain the use of central differences for the transverse derivatives and, thus, maintain the consistent accuracy of the finite difference scheme. This enables the determination of v_r for all values of m, which would not be possible if the transverse derivatives were written at the regular grid points $(m, n + 1)$. The axial derivatives in the continuity equation are evaluated by using backward differences, since forward differences would not yield an explicit representation at this stage. Thus

$$\left.\frac{\partial v_z}{\partial \varphi}\right|_{m+1/2,n+1} = \frac{v_z(m+1,n+1) - v_z(m,n+1)}{2\,\frac{\Delta\varphi}{2}} \tag{104}$$

that is,

$$\left.\frac{\partial v_z}{\partial \varphi}\right|_{m+1/2,n+1} = \frac{v_z(m+1,n+1) - v_z(m,n+1)}{\Delta\varphi} \tag{105}$$

Similarly

$$\left.\frac{\partial v_z}{\partial z}\right|_{m+1/2,n+1} = \frac{1}{2}\left[\left.\frac{\partial v_z}{\partial z}\right|_{m+1,n+1} + \left.\frac{\partial v_z}{\partial z}\right|_{m,n+1}\right] \tag{106}$$

that is,

$$\left.\frac{\partial v_z}{\partial z}\right|_{m+1/2,n+1} = \frac{1}{2}\left[\frac{v_z(m+1,n+1) - v_z(m+1,n)}{\Delta z} + \frac{v_z(m,n+1) - v_z(m,n)}{\Delta z}\right] \tag{107}$$

Forms similar to the above FDAs may be derived for $\frac{\partial \rho}{\partial \varphi}$ and $\frac{\partial \rho}{\partial z}$. Substituting these FDAs into Equation (A-26) yields

$$v_r(m+1,n+1) = \frac{1}{D(m,n+1)}\left[\begin{array}{l}\left[\rho v_r r\right]_{m,n+1} \\ \\ + \frac{1}{2}\left[\eta_1(m,n+1) + \eta_2(m,n+1) + \eta_2(m+1,n+1)\right]\Delta r_m^2\end{array}\right] \tag{108a}$$

where

$$\Delta r_m^2 = \frac{r^2(m+1,n+1) - r^2(m,n+1)}{2} \tag{108b}$$

$$D(m,n+1) = \left[\rho r\right]_{m+1,n+1} \left[1 - \left[\frac{1}{2}\rho \frac{d\varphi}{d\psi}\right]_{m+1,n+1} \left[\frac{v_z(m+1,n+1) - v_z(m,n+1)}{\Delta\varphi}\right] + \left[\frac{1}{2} v_z \frac{d\varphi}{d\psi}\right]_{m+1,n+1} \left[\frac{\rho(m+1,n+1) - \rho(m,n+1)}{\Delta\varphi}\right] \Delta r_m^2 \right] \tag{109}$$

$$\eta_1(m,n+1) = \left[\rho^2 v_r r \frac{d\varphi}{d\psi}\right]_{m,n+1} \left[\frac{v_z(m+1,n+1) - v_z(m,n+1)}{\Delta\varphi}\right] + \left[\rho v_r r v_z \frac{d\varphi}{d\psi}\right]_{m,n+1} \left[\frac{\rho(m+1,n+1) - \rho(m,n+1)}{\Delta\varphi}\right] \tag{110}$$

$$\eta_2(m,n+1) = -\rho(m,n+1) \left[\frac{v_z(m,n+1) - v_z(m,n)}{\Delta z}\right] - v_z(m,n+1) \left[\frac{\rho(m,n+1) - \rho(m,n)}{\Delta z}\right] \tag{111}$$

It can easily be shown that Equation (108) is unconditionally stable.

3.2.2 Inverse Transformation

Using the explicit scheme, Equation (64) for $m = 2,3,..,M$ can be written as

$$r^2(m,n) = r^2(m-1,n) + 4\sum_{m=2}^{M}\left[\frac{\varphi}{\rho v_z}\right]_{m,n}\Delta\varphi \tag{112}$$

For $m = 1$,

$$r(1,n) = 0 \tag{113a}$$

and for $m = M + 1$

$$r(M + 1,n) = R \tag{113b}$$

3.2.3 Auxiliary Expressions

The auxiliary expressions (70), (71) and (72), when transformed into FDEs, have the following form.

Expression for Density

$$\rho(m,n) = \frac{\dfrac{\omega_1(m,n)}{M_1}}{\dfrac{\omega_1(m,n)}{M_1} + \dfrac{\omega_2(m,n)}{M_2}}\left[\rho_{p,1} - \rho_{p,2}\right] + \rho_{p,2} \tag{114}$$

Expression for Viscosity

$$\mu(m,n) = \sum_{i=1}^{2} \frac{x_i(m,n)\mu_{p,i}}{\sum_{j=1}^{2} x_j(m,n)\,\Phi_{i,j}} \tag{115}$$

Expression for Binary Diffusivity

$$D_{12} = \frac{BT^{3/2}\left[\frac{M_1 + M_2}{M_1 M_2}\right]^{1/2}}{P\sigma_{12}^2\, W_{(1)}^{(1)}\,(1 - \Delta)} \tag{116}$$

It may be recalled that in this particular problem, D_{12} is assumed to be constant.

It may be shown that Equations (114), (115) and (116) are unconditionally stable.

3.2.4 Boundary Conditions

The boundary conditions, given by Equations (78) through (80), have the following finite difference representations.

1. At $n = 1$

It was mentioned in Chapter 2 that the boundary conditions of the φ-z plane, $\lambda_1(\varphi)$, $\lambda_2(\varphi)$, $\lambda_3(\varphi)$ and $\lambda_4(\varphi)$, are chosen to be

constants for this particular problem. These constants are U_1, U_2, unity and zero respectively.

$$v_z(m,1) = \begin{cases} U_1 & 1 \leq m \leq \frac{\Phi_1}{\Delta\varphi} \\ U_2 & \frac{\Phi_1}{\Delta\varphi} < m \leq M+1 \end{cases} \tag{117a}$$

$$v_r(m,1) = 0 \qquad 1 \leq m \leq M+1 \tag{117b}$$

$$\omega_1(m,1) = \begin{cases} 1 & 1 \leq m \leq \frac{\Phi_1}{\Delta\varphi} \\ 0 & \frac{\Phi_1}{\Delta\varphi} < m \leq M+1 \end{cases} \tag{117c}$$

2. <u>At m = 1 for all n > 0</u>

$$v_r(m,1) = 0 \tag{118a}$$

$$\frac{v_z(m+1,n) - v_z(m-1,n)}{2\Delta\varphi} = 0 \qquad \text{where} \quad m = 1 \tag{118b}$$

$$\frac{\omega_1(m+1,n) - \omega_1(m-1,n)}{2\Delta\varphi} = 0 \qquad \text{where} \quad m = 1 \tag{118c}$$

3. At $m = M+1$ for all $n > 0$

$$v_r(M+1,n) = 0 \tag{119a}$$

$$v_z(M+1,n) = 0 \tag{119b}$$

$$\frac{\omega_1(M+1,n) - \omega_1(M,n)}{\Delta\varphi} = 0 \tag{119c}$$

Thus, the governing equations and boundary conditions of the flow problem have been transformed to finite difference equations using the explicit scheme. In order to solve the problem, Equations (88), (91), (94), (97), (99), (108) and (112) through (119) were programmed for the IBM 360/40 computer. The numerical stability of these finite difference equations was ensured by satisfying conditions (89) and (95).

3.3 Sequence of Operations for Solution of FDEs

1. The set of flow parameters U_1, U_2, $\rho_{p,1}$, $\rho_{p,2}$, R_1, R are specified and are assigned for the initial section of a grid system in the r-z plane.

2. At this initial section, the values of μ_1, μ_2, D_{12} are either specified, or are computed from Equations (114), (115) and (116)

using prescribed values of M_1, M_2, $\rho_{p,1}$, $\rho_{p,2}$, T, etc.

3. Ψ is evaluated using Equation (21) with r = R. Φ is then determined from Equation (59). Subsequently, $\Delta\varphi$ is obtained as $\frac{\Phi}{M}$.

4. Δz is computed at n = 1 for all m from the stability conditions (89) and (95). The most restrictive of all these values is used in further computations.

5. $\omega_1(m,n+1)$ is evaluated using Equation (97) for m = 1, Equation (94) for m = 2,3,..,M and the boundary condition (118c) for m = M + 1.

6. $\left.\frac{dp}{dz}\right|_{m,n}$ is computed using Equation (99).

7. $v_z(m,n+1)$ is determined using Equation (91) for m = 1, Equation (88) for m = 2,3..,M and the boundary condition (118b) for m = M + 1.

8. r(m,n+1) is determined using Equation (112) for m = 2,3, ..,M and the boundary conditions (113a) and (113b) for m = 1 and m = M + 1 respectively.

9. $v_r(m,n+1)$ is computed using the boundary condition (118a) for m = 1, Equation (108) for m = 2,3,..,M, and the boundary condition (119a) for m = M + 1.

10. The value of n is incremented by unity and steps 5 through 9 are repeated until a fixed distance z is reached where the stability conditions (89) and (95) are checked.

11. Steps 5 through 10 are repeated until the flow is fully developed.

12. The values of the fully developed flow parameters as obtained from the above numerical procedure are compared with their values computed theoretically.

This sequence of operations is summarized in the flow diagram presented in Figure 3.

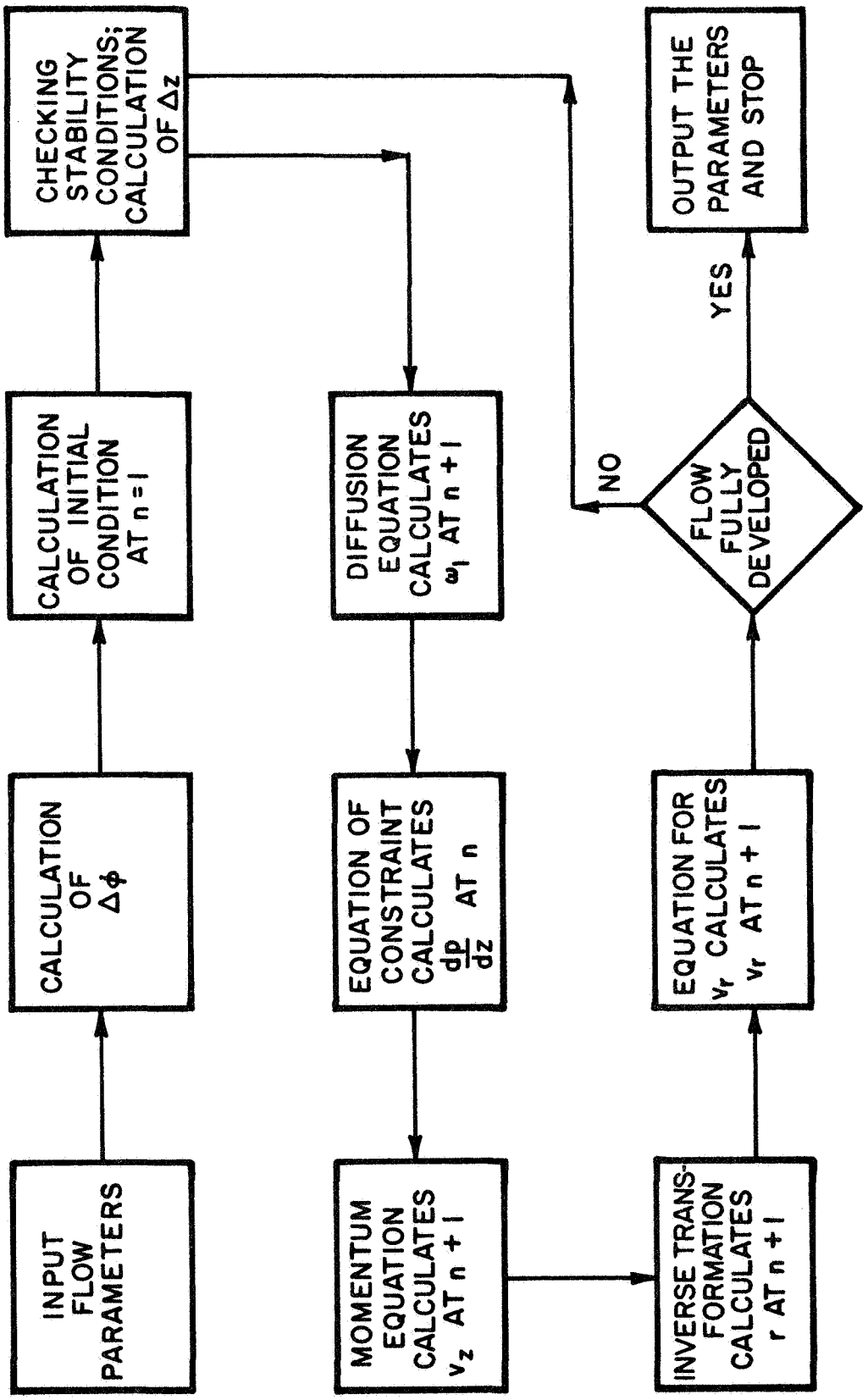

FIGURE 3. FLOW DIAGRAM FOR NUMERICAL SOLUTION.

CHAPTER 4

RESULTS AND DISCUSSION

4.1 Introduction

A detailed parametric study of confined jet mixing was carried out using the finite difference method developed in the last chapter. The significance of the results of this study depends, of course, on the validity of the mathematical model used to formulate the physical flow problem. Before presenting the results obtained, it is necessary to give some explanation on the use of boundary layer equations describing the flow system considered. A brief discussion is also presented for some points of special interest in the von Mises transformation as well as the φ-transformation. Finally, it is important to mention the possible checks used to validate the present results which are next discussed.

4.2 On the Use of Boundary Layer Equations

Boundary layer equations are known to be valid for high Reynolds numbers in the region adjoining the wall. These equations have been used for the entire flow region of the confining pipe and justification

of their use is discussed here. The main assumptions in obtaining these equations are

1. $v_r \ll v_z$

2. $\frac{\partial^2 v_z}{\partial z^2} \ll \frac{\partial^2 v_z}{\partial r^2}$

3. $\frac{\partial^2 \omega_1}{\partial z^2} \ll \frac{\partial^2 \omega_1}{\partial r^2}$

As far as the axial momentum equation is concerned, only the term $\frac{\partial^2 v_z}{\partial z^2}$ has been neglected under these assumptions. In the confined jet mixing, sufficiently downstream from the jet exit section, the boundary layer assumptions hold good since the flow characteristics there are similar to those of the developing flow in the entrance region of a pipe. In this region, the axial velocity $v_z(r,z)$ is a smooth function and satisfies $\frac{\partial^2 v_z}{\partial z^2} \ll \frac{\partial^2 v_z}{\partial r^2}$; also $v_r \ll v_z$. However, in the region close to the jet exit section, the assumption $v_r \ll v_z$ may not be satisfactorily justified, but the nature of $v_z(r,z)$ in this region is such that $\frac{\partial^2 v_z}{\partial z^2} \ll \frac{\partial^2 v_z}{\partial r^2}$. This can be seen from the fact that a considerable transverse gradient of v_z exists near the jet exit. Therefore, the momentum exchange between the two streams is large in this region. Further, for the present

problem, the flow outside the boundary layer is viscous also and hence the boundary layer equations may still be used for sufficiently large Reynolds numbers. A similar argument holds good for neglecting the term $\frac{\partial^2 \omega_1}{\partial z^2}$ in the diffusion equation. The use of the boundary layer equations was also supported by the success with which several investigators (References 8, 12, 13 and 14) applied them to the study of unconfined mixing. In particular, Weinstein and Todd[13] computed the radial and axial derivatives of v_z and ω_1 and showed that the boundary layer assumptions are valid for the unconfined jet mixing system.

4.3 On the Use of von Mises and the φ Transformations

Several researchers have analyzed unconfined jet mixing problems using the von Mises transformation in order to avoid the severe numerical instabilities encountered in the physical plane. These instabilities become further enhanced in the case of confined jet mixing because of the boundary conditions at the confining wall. The numerical stability analysis of the present flow problem in the physical plane imposes an upper limit on the step size Δr, in the r direction; further, the maximum step size Δz, in the z direction, is limited by a function of Δr^2. These stability conditions are very stringent. On the other hand, in the von Mises plane, the step size $\Delta\psi$ in the transverse

direction has no stability restriction, although Δz is still restricted by a function of $\Delta\psi^2$. The von Mises transformation has been used in the present analysis also, and certain difficulties which are associated with this transformation are mentioned here.

The order of accuracy of the finite difference method is no longer maintained uniform throughout the flow field since in the interior of the flow field, central differences are used for the transverse derivatives, but either forward or backward differences are used at the boundaries. The limiting differential equations at the centerline contain first order transverse derivatives which have to be represented by forward differences. Since the transverse derivative of ω_1 is prescribed at the wall, backward differences have to be used to evaluate ω_1 at this boundary.

The results are desired in the physical plane, therefore, additional calculations are necessary to transform the obtained values of the flow parameters back to the physical plane. This requires additional computer time. Also, use of the von Mises transformation becomes impractical as the ratio of mass flux of outer to inner streams increases, resulting in a decrease in the number of grid points representing the inner stream. The latter number becomes undesirably small

for certain cases, with large mass flux ratios, investigated in the present work. Hence, to obtain a proper finite difference representation of the inner stream for these large mass flux ratios without unreasonably increasing the number of steps in the ψ direction, the φ-transformation was used to stretch the ψ coordinate in the region of the inner stream.

In addition to representing the inner stream suitably the φ-transformation simultaneously removes the inconsistency in the order of accuracy of the finite difference method at the centerline of the von Mises plane since the flow problem in the φ-z plane is axisymmetric. The stability conditions are comparable to those in the von Mises plane. It is noted here that the mathematical model of the flow problem in the von Mises plane may be considered as a special case of the model in the φ-z plane. Hence, the complete finite difference formulation of the problem was presented only in the φ-z plane.

4.4 Validation of the Results

The analysis developed is used to investigate coaxial confined laminar mixing of jets with greatly different densities and variable physical and transport properties. To the best knowledge of the authors, this specific problem has not been treated by others, either

experimentally or analytically. Therefore, evaluation of the results by direct comparison is not possible and an indirect method is used to assess reliance on the results.

Extensive analytical and experimental results are available for the entrance flow in a pipe. A computer program was written to solve the classical entrance flow problem using the boundary layer equations in the physical plane. Comparing the results with those obtained by Lavan and Fejer[33] using the Navier Stokes equations, the maximum deviation observed is 3.5 percent in the region close to the jet exit section and the deviation decreases with distance downstream. The classical entrance flow problem was solved also in the von Mises plane using the present program. Comparison of these results with the solution of the Navier Stokes equations[33] shows a maximum deviation of almost 8 percent for the fully developed flow. This comparison gives an estimate of the expected accuracy of the results obtained by solving the problem in the von Mises plane. Further, only a small deviation was observed between the solutions for the confined jet mixing problem in the φ-z plane and those in the von Mises plane.

As a partial check on the results obtained by the present method, the fully developed values of the flow parameters, namely, $v_z(r,z)$,

$\omega_1(r,z)$ and $\frac{dp}{dz}$, are compared with the corresponding asymptotic values that were obtained independently from simple theoretical considerations. From the invariance of mass and volume flow rates at any section and the parabolic velocity profiles in the fully developed flow, $v_z(r,z)$ and $\omega_1(r,z)$ at the end section are expressed in terms of the inlet parameters, namely, velocities, densities and cross-sectional areas. The axial pressure gradient $\frac{dp}{dz}$ is evaluated also from the momentum equation after substituting appropriate values for the fully developed flow. The agreement with these asymptotic values gives further reliance on the numerical results.

4.5 Discussion of Results

The present method is used to study the mixing and developing phenomena of a laminar circular jet in a confined coaxial flow. Results are obtained in the form of velocity and mass fraction fields and the effects of the following parameters on the mixing are studied.

1. Velocity Ratio $\frac{U_2}{U_1}$
2. Density Ratio $\frac{\rho_1}{\rho_2}$
3. Radius Ratio $\frac{R_1}{R}$

4. Reynolds Number $N_{Re,2}$

5. Schmidt Number $N_{Sc,2}$

6. Viscosity Ratio $\frac{\mu_2}{\mu_1}$

(Subscripts 1 and 2 refer to the inner and the outer jets, respectively.) The Reynolds number used for the parametric study is that of the outer stream and the Schmidt number is based on the viscosity of the outer stream. In order to vary density ratio, Schmidt number and viscosity ratio independently of one another, the numerical values of densities, diffusivity and viscosities are assumed instead of being calculated from the auxiliary expressions.

A total of 57 cases is investigated for the steady confined coaxial circular jet mixing problem and the effects of the variation of the above mentioned parameters are studied. For the cases in vestigated, the values of these parameters are presented in tabular form in Appendix D. The basis of these runs is an air-freon system; a similar system is also being experimentally investigated by Weinstein and his associates at the Illinois Institute of Technology. The range of values of the parameters studied includes many physical systems of practical interest. Some combinations of these parameters lead to an

adverse pressure gradient in the initial region of the flow field and this behavior of the flow may be attributed to the discontinuities in the initial profiles. If this region is very short, the computed fully developed flow parameters still compare well with the corresponding asymptotic values calculated independently from simple theoretical considerations. However, if the adverse pressure gradient persists up to a sufficient length of the initial region, the agreement between the asymptotic flow parameters is only fair. In some other cases, the pressure gradient is favorable but oscillatory; satisfactory agreement is still obtained between the fully developed values of the flow parameters. In all such cases, the initial mixing region is most affected.

Some of the parameters to be investigated in this study demand an unreasonably small step size Δz in order to obtain a stable solution. The increased number of computations leads to inaccuracies, the effect of which is manifested in the fully developed centerline velocity. In such a case, the centerline velocity exceeds the corresponding asymptotic value computed independently from simple theoretical considerations.

It may be recalled here that the transformation of the problem from the physical plane to the von Mises plane, or further to the φ-z

plane, was performed mainly to avoid numerical instabilities at high velocity ratios. However, it was found later that when the velocity ratio $\frac{U_2}{U_1}$ reached a value where a stable solution was not obtainable, increase of the density ratio $\frac{\rho_1}{\rho_2}$ stabilized the solution. Hence, the mass flux ratio $\frac{U_2\rho_2}{U_1\rho_1}$, and not the velocity ratio $\frac{U_2}{U_1}$ alone, is the deciding parameter for a stable convergent numerical solution. Similarly, decrease of the radius ratio $\frac{R_1}{R}$ further increases the range of mass flux ratios for which a stable solution is obtainable. Thus, some combination of $\frac{U_2}{U_1}$, $\frac{\rho_1}{\rho_2}$ and $\frac{R_1}{R}$ must be the parameter governing the stability of the solution. This suggests that some grouping of all the parameters of the problem should be the deciding criterion for the existence of a stable numerical solution. Although this idea was explored to some extent, no suitable group could be formed which would ensure a stable solution.

Some of the investigated cases demanded a step size considerably smaller than those predicted by stability analysis; these cases have been studied only for small distances downstream due to the increased computer time requirements.

The results of the 57 cases investigated for the parametric study present the effects of the six parameters - $\frac{U_2}{U_1}$, $\frac{\rho_1}{\rho_2}$, $\frac{R_1}{R}$, $N_{Re,2}$, $N_{Sc,2}$, and $\frac{\mu_2}{\mu_1}$ - on

1. the mass fraction potential core L_{ω_1}

2. the velocity potential core L_v

3. the centerline velocity $v_{z,1}$

4. the wall mass fraction $\omega_{1,w}$

and 5. the index of the effect of mixing η

The results of some selected runs are presented in order to show typical effects of the parameters of the problem. The developing profiles of axial velocity v_z and mass fraction ω_1 are also presented for some typical runs.

4.5.1 Effects of Flow Parameters on L_{ω_1}*

Figures 4 through 8 present the effects of the various parameters on L_{ω_1}. Figure 4 shows that L_{ω_1} decreases as $\frac{U_2}{U_1}$ increases, but L_{ω_1} increases as $\frac{\rho_1}{\rho_2}$ increases. The fractional increase of L_{ω_1} due to an increase in $\frac{\rho_1}{\rho_2}$ is larger for higher $\frac{U_2}{U_1}$. Also, L_{ω_1} decreases very rapidly for $\frac{U_2}{U_1}$ between 1 and 5. It must be mentioned here that the case with $\frac{\rho_1}{\rho_2} = 8.3$ could not be investigated for $\frac{U_2}{U_1}$ less than 5 for reasons of numerical instability.

---

* L_{ω_1} is the value of z where the mass fraction ω_1 at the centerline has changed by less than five percent of its original centerline value.

The effect of change in $N_{Re,2}$ at two different density ratios is presented in Figure 5. These results are for the case of $\frac{U_2}{U_1} = 5$ and $\frac{R_1}{R} = 0.563$. It is seen that L_{ω_1} increases with increase in $N_{Re,2}$ as well as with increase in $\frac{\rho_1}{\rho_2}$. The increase of L_{ω_1} with $N_{Re,2}$ is almost linear. Comparison of Figure 5 with Figure 6 shows that when $\frac{R_1}{R}$ is decreased from 0.563 to 0.28 and $\frac{U_2}{U_1}$ is increased from 5 to 30, the nature of variation of L_{ω_1} with respect to both $N_{Re,2}$ and $\frac{\rho_1}{\rho_2}$ remains unchanged. However, the value of L_{ω_1} is reduced approximately 80-fold in the latter case. Figure 7 shows that L_{ω_1} increases almost linearly with $N_{Sc,2}$. From Figures 5, 6, and 7, it is seen that the effect of increase in $\frac{\rho_1}{\rho_2}$ is larger at higher values of $N_{Re,2}$ and $N_{Sc,2}$. Figure 8 shows that the effect of change in $\frac{\mu_2}{\mu_1}$ on L_{ω_1} is rather small. At $\frac{\rho_1}{\rho_2} = 4.2$, the changes in L_{ω_1} are almost linear, but this is not true for $\frac{\rho_1}{\rho_2} = 8.3$, since a maximum is observed in the vicinity of $\frac{\mu_2}{\mu_1} = 1.75$. Also, L_{ω_1} increases in the same proportion as $\frac{\rho_1}{\rho_2}$.

4.5.2 Effects of Flow Parameters on L_v*

The effects of the various parameters on L_v are presented in Figures 9 through 12. Figure 9 shows that L_v increases with increase in $\frac{U_2}{U_1}$, the increase in L_v being larger at higher values of $\frac{U_2}{U_1}$. For $\frac{U_2}{U_1}$ less than 6, an increase in $\frac{\rho_1}{\rho_2}$ increases L_v, but for $\frac{U_2}{U_1}$ greater than 6, higher $\frac{\rho_1}{\rho_2}$ causes a reduction in L_v. Thus, in the vicinity of $\frac{U_2}{U_1} = 6$, L_v may be insensitive to change in $\frac{\rho_1}{\rho_2}$.

Figure 10 shows that L_v increases with increase in $N_{Re,2}$. For $\frac{U_2}{U_1} = 5$ and $\frac{R_1}{R} = 0.563$, L_v decreases with reduction in $\frac{\rho_1}{\rho_2}$, the effect being smaller at lower values of $N_{Re,2}$. Similar behavior is also observed for $\frac{U_2}{U_1} = 30$ and $\frac{R_1}{R} = 0.28$, however, the reduction in L_v is comparatively smaller. It is seen from Figure 11 that L_v increases with increase in $N_{Sc,2}$, the increase being larger at higher $N_{Sc,2}$. An increase in $\frac{\rho_1}{\rho_2}$ decreases L_v and this decrease in L_v

---

* For unconfined mixing, L_v is usually defined as that value of z where the centerline axial velocity $v_{z,1}$ has changed by less than 5 percent of its original centerline value. According to this definition, there exists no potential core for the case of confined mixing of jets with large velocity ratio $\frac{U_2}{U_1}$. Hence, for confined mixing, L_v is defined as that value of z where the centerline axial velocity has the value $U_1 + 0.05\ (U_2 - U_1)$. The concept of a velocity potential core is thus retained by this definition.

increases with increase in $N_{Sc,2}$. Figure 12 shows that the variation of L_v with $\frac{\mu_2}{\mu_1}$ is entirely different from that with the other parameters discussed so far. A distinct maximum exists in the vicinity of $\frac{\mu_2}{\mu_1} \approx 1.4$. Also, an increase in $\frac{\rho_1}{\rho_2}$ shows a marked decrease in L_v .

4.5.3 Effects of Flow Parameters on $v_{z,1}$

Figures 13 through 18 present the effects of the parameters on the centerline axial velocity, $v_{z,1}$*. The effects of velocity ratio for two density ratios are shown in Figure 13. It is seen that for equal densities of the inner and outer streams, an increase in $\frac{U_2}{U_1}$ from 1.1 to 4 causes an increase in $v_{z,1}$ as may be expected; but for almost equal velocities of the inner and outer streams, an increase in $\frac{\rho_1}{\rho_2}$ from 1 to 4.2 causes a small decrease in $v_{z,1}$. An inflection is noticed in the curve for $\frac{U_2}{U_1} = 4$ indicating rapid changes in the rate of flow development in the initial region. The effect of an increase in $\frac{\rho_1}{\rho_2}$ is to reduce the centerline velocity in the mixing and the initial developing regions. This effect decreases with distance downstream so that beyond a certain value of z, the curves for different $\frac{\rho_1}{\rho_2}$ but same $\frac{U_2}{U_1}$ will merge together. This is in accordance with the known fact that, for a fixed velocity ratio, the asymptotic value of the centerline velocity is independent of the density ratio. The effect

* The centerline axial velocity $v_{z,1}$ is made non-dimensional with respect to U_1 .

of change in $\frac{\rho_1}{\rho_2}$ on $v_{z,1}$ is less pronounced at low velocity ratios. Figure 13 also shows that, for $\frac{U_2}{U_1} = 15$ and $\frac{\rho_1}{\rho_2} = 8.3$, inflection points occur in the initial region again indicating rapid changes in the rate of flow development. For $\frac{U_2}{U_1} = 5$ and both density ratios, the details of the initial portion of the $v_{z,1}$ curves are not clearly visible because of the scale used.

The effects of change in $\frac{R_1}{R}$ on the centerline velocity are presented in Figure 14. For a fixed velocity ratio, a decrease in $\frac{R_1}{R}$ from 0.563 to 0.28 causes an increase in $v_{z,1}$ in the entire flow field, as may be expected. In the initial region, the curve for $\frac{R_1}{R} = 0.28$ is considerably steeper than that for $\frac{R_1}{R} = 0.563$, thus indicating the rapidity with which the momentum deficiency is overcome in the former case.

Figure 15 shows that as $N_{Re,2}$ increases, $v_{z,1}$ decreases. However, for a fixed velocity ratio, the asymptotic values of the centerline velocities are the same for all the cases shown in Figure 15. Also, the nature of the curves is independent of $N_{Re,2}$. Comparison of Figures 15 and 16 shows that, as $\frac{U_2}{U_1}$ is increased from 5 to 30 and $\frac{R_1}{R}$ is decreased from 0.563 to 0.28, the effect of $N_{Re,2}$ remains almost unaltered. However, the inflection points observed in the initial region of Figure 15 are not seen in the cases of Figure 16

and steeper slopes of the $v_{z,1}$ curves are observed in the initial region indicating rapid mixing in this region.

The effects of change in $N_{Sc,2}$ on the centerline velocity are presented in Figure 17. The centerline velocity $v_{z,1}$ decreases in the entire flow field as $N_{Sc,2}$ increases from 0.75 to 2.0. The asymptotic values of $v_{z,1}$ should be the same for the three cases shown in this figure. The case for $N_{Sc,2} = 0.75$ was not investigated beyond $z = 65R$, since numerical stability demanded a very small Δz and, consequently, large computer time. For the case of $N_{Sc,2} = 2.0$, adverse pressure gradient was observed from $z = 0.16R$ to $z = 3.12R$, resulting in a trough in the $v_{z,1}$ curve in the initial region.

4.5.4 Effects of Flow Parameters on $\omega_{1,w}$

The influence of the parameters on the wall mass fraction $\omega_{1,w}$ are presented in Figures 19 through 24. Figure 19 shows that increase in $\frac{U_2}{U_1}$ decreases $\omega_{1,w}$, the decrease being smaller at higher $\frac{U_2}{U_1}$. Also, an increase in $\frac{\rho_1}{\rho_2}$ increases $\omega_{1,w}$ as may be expected. An increase in $\frac{U_2}{U_1}$ or a decrease in $\frac{\rho_1}{\rho_2}$ tends to reduce the spreading of the jets. As seen from Figure 20, reduction of $\frac{R_1}{R}$ from 0.563 to 0.28 causes a reduction of inner stream mass flow rate resulting in decrease of $\omega_{1,w}$. For the case with $\frac{R_1}{R} = 0.563$, the asymptotic

value of $\omega_{1,w}$ is attained at $z \approx 400R$, hence, a steep slope is still present at $z = 250R$ for this case.

Figure 21 shows that the effect of increasing $N_{Re,2}$ is to decrease the value of $\omega_{1,w}$ in the entire field. The three curves presented here are for the case of $\frac{U_2}{U_1} = 5$ and $\frac{R_1}{R} = 0.563$. These curves are similar and show that an increase of $N_{Re,2}$ delays the mixing to some extent. Also, all these curves should merge together beyond some value of z since the asymptotic value of ω_1 depends only on the density ratio, velocity ratio and area ratio which were maintained constant when $N_{Re,2}$ was varied. Comparison of Figures 21 and 22 shows that, as $\frac{U_2}{U_1}$ is increased from 5 to 30 and $\frac{R_1}{R}$ is decreased from 0.563 to 0.28, the effect of $N_{Re,2}$ remains almost unchanged. The flow is far from being fully mixed within the axial distance investigated and, hence, the curves in Figure 22 are diverging with steep slopes. The curves presented in Figure 22 show a similar behavior, but mixing is relatively faster in the initial region. Also, the asymptotic value of $\omega_{1,w}$ will be the same for all three curves of this figure.

The effects of variation of $N_{Sc,2}$ on $\omega_{1,w}$ are presented in Figure 23. An increase in $N_{Sc,2}$ shows a marked decrease in $\omega_{1,w}$

and in the rate of mixing. Mixing is exceptionally fast for the case of $N_{Sc,2} = 0.75$. This case was investigated only up to $z = 60R$ because the requirement of small Δz resulted in large computer time. The asymptotic value of $\omega_{1,w}$ will be the same for the three curves of Figure 23, since $\frac{U_2}{U_1}$, $\frac{\rho_1}{\rho_2}$ and $\frac{R_1}{R}$ are constant for these cases.

4.5.5 Effects of Flow Parameters on η

Figures 25 through 30 present the effects of the parameters on η where

$$\eta = \frac{\left[\begin{array}{l}\text{mass of species 1 in a given volume (between the entrance} \\ \text{section and a section downstream) of the confining duct}\end{array}\right]}{\left[\begin{array}{l}\text{mass of species 1 in the same volume had there been no} \\ \text{mixing}\end{array}\right]}$$

Expressed mathematically

$$\eta = \frac{2\pi \int_0^L \int_0^R \rho \omega_1 r \, dr \, dz}{\rho_{p,1} \, \pi R_1^2 L} \tag{120}$$

Thus, η may be considered as some index of the effect of mixing of the two streams. At $z = 0$, η is indeterminate, hence, the first point for the plotted curve is taken at a suitable small downstream distance. Also, since the results are obtained at values of z

which are some integral multiples of Δz and not of the confining duct radius R, the last points plotted are not the same for all the curves. Figure 25 shows that η decreases with increasing distance downstream. η also decreases as $\frac{U_2}{U_1}$ increases and η increases as $\frac{\rho_1}{\rho_2}$ increases. The effect of variation in $\frac{\rho_1}{\rho_2}$ is larger at higher values of $\frac{U_2}{U_1}$. As seen from Figure 26, η increases as $\frac{R_1}{R}$ increases. For the case of $\frac{R_1}{R} = 0.28$, η decreases very rapidly up to $z = 1R$ beyond which point the rate of decrease is gradual.

The effects of $N_{Re,2}$ on η are presented in Figure 27. For all three curves shown in this figure, $\frac{U_2}{U_1} = 5$ and $\frac{R_1}{R} = 0.563$. It is seen that η decreases gradually with downstream distance and η increases with increase in $N_{Re,2}$ and the curves exhibit a similar behavior. Comparison of Figures 27 and 28 shows that as $\frac{U_2}{U_1}$ is increased from 5 to 30 and $\frac{R_1}{R}$ is decreased from 0.563 to 0.28, the effect of $N_{Re,2}$ on η remains similar but it becomes less pronounced. However, the curves of Figure 28 show that the decrease of η is extremely rapid up to $z = 1R$.

Figure 29 shows the effect of $N_{Sc,2}$ on η. $N_{Sc,2}$ was varied by changing D_{12} only. Hence, as $N_{Sc,2}$ is increased, D_{12} is reduced, i.e., the diffusion process is slowed down. Since the velocity in the

outer stream is higher than in the inner stream, slower diffusion results in an increase of η, which is clearly seen from Figure 29.

It is noted here that the effect of change in $\frac{\mu_2}{\mu_1}$ on the centerline velocity $v_{z,1}$, the wall mass fraction $\omega_{1,w}$ and the mixing index η are presented in Figures 18, 24, and 30 respectively. The effect of change in $\frac{\mu_2}{\mu_1}$ is rather small and, hence, no definite trend of the results can be established from the above figures. For some of these cases, a positive pressure gradient or a negative oscillatory pressure gradient was also observed. Further investigation is necessary in order to determine the definite effects of $\frac{\mu_2}{\mu_1}$ variation on the jet mixing.

4.5.6 Velocity and Mass Fraction Fields for Typical Runs

Figures 31 through 34 show the development of the axial velocity profiles for Run Nos. 55, 43, 6, and 49, respectively*. At the entrance, i.e., $z = 0$, a discontinuity exists at $r = R_1$ due to the nature of the inlet velocity profile. A discontinuity exists also at $r = R$ because of the no-slip condition at the wall. These discontinuities are indicated by broken lines in the figures. Since the initial region is of particular interest, the velocity profiles are presented only up to $z = 10R$. The fully developed velocity profiles have also been presented

---

* The axial velocity is made non-dimensional with respect to U_1.

since they were used for partial verification of the results by comparing them with the asymptotic velocity profiles obtained independently from simple theoretical considerations. Figure 31 shows the results for the homogeneous case, i.e., $\frac{\rho_1}{\rho_2} = 1$, with $\frac{U_2}{U_1} = 1.1$, while Figures 32, 33, and 34 show the results for the heterogeneous cases with $\frac{\rho_1}{\rho_2} = 4.2$. The axial velocity profiles develop similarly for all the cases. For the heterogeneous cases, an increase in $\frac{U_2}{U_1}$ from 5 to 15 causes a reduction in the developing length. A further increase of $\frac{U_2}{U_1}$ to 30 with a simultaneous reduction of $\frac{R_1}{R}$ to 0.28 results in a considerable reduction of the developing length. Extrapolation of these results on this basis suggests that the developing length for the case with $\frac{U_2}{U_1} = 1.1$ should be greater than that for the case with $\frac{U_2}{U_1} = 5$. However, a simultaneous reduction in $\frac{\rho_1}{\rho_2}$ from 4.2 to 1 reduces the developing length sharply.

The developing profiles of mass fraction ω_1 are presented in Figures 35 through 37 for the heterogeneous cases with $\frac{\rho_1}{\rho_2} = 4.2$. At the entrance section, i.e., $z = 0$, a sharp discontinuity exists at $r = R_1$ on account of the nature of the inlet mass fraction profile and has been shown by broken lines in the figures. The mass fraction profiles are shown only for the near jet region which is of particular interest, and are presented for the same values of z for

which the axial velocity profiles have been discussed already. As $\frac{U_2}{U_1}$ increases from 5 to 15, comparison of Figures 35 and 36 shows an increase in the rate of mixing. Mixing is sharply enhanced for the case of $\frac{U_2}{U_1} = 30$ and $\frac{R_1}{R} = 0.28$. From the curves for the largest value of z presented it is seen that the flow in all three cases has not yet mixed fully since the mass fraction profile in the fully mixed state should be uniform. This may be verified from the fact that the Schmidt number N_{Sc} for the overall flow is slightly greater than unity.

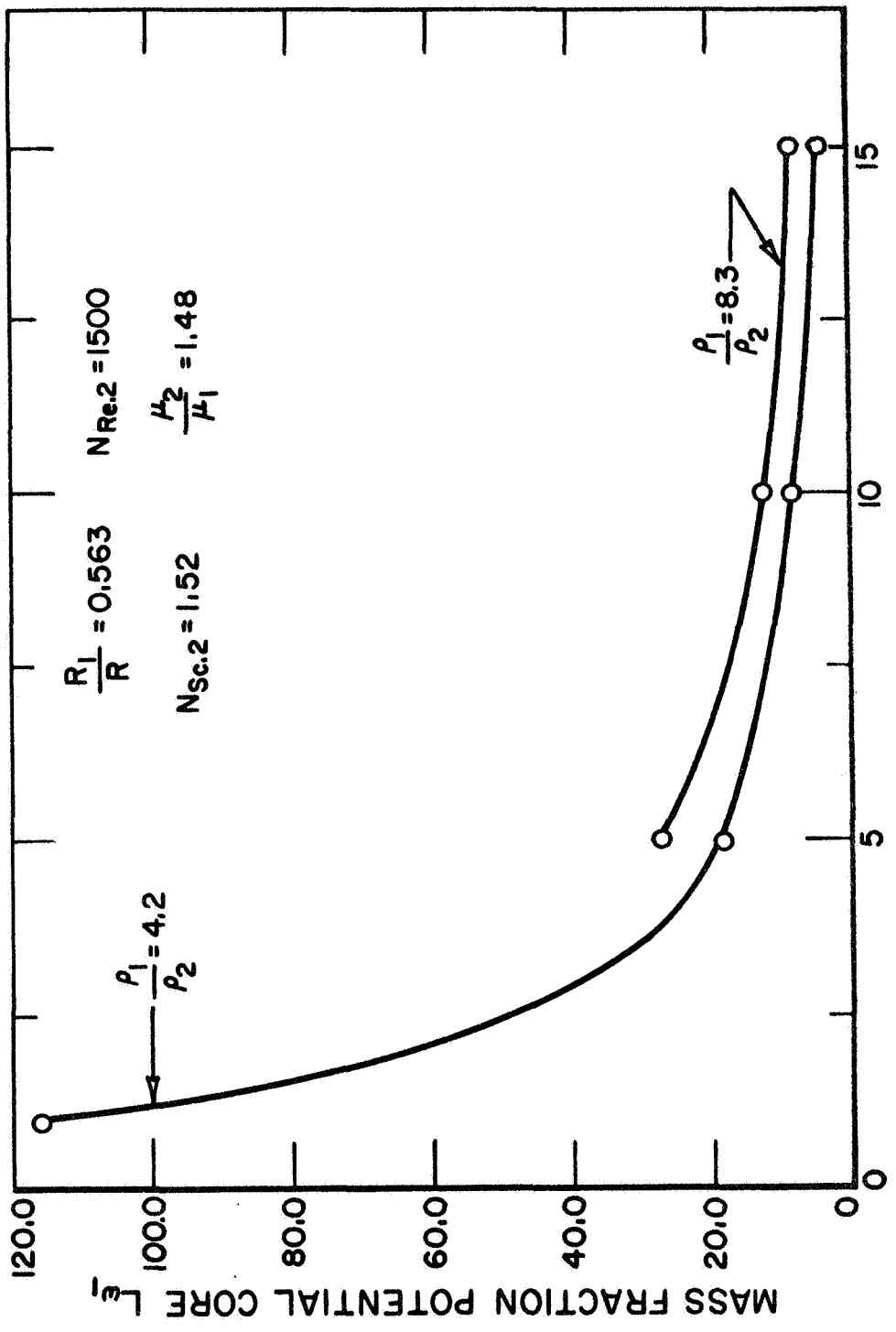

FIGURE 4. MASS FRACTION POTENTIAL CORE VS VELOCITY RATIO.

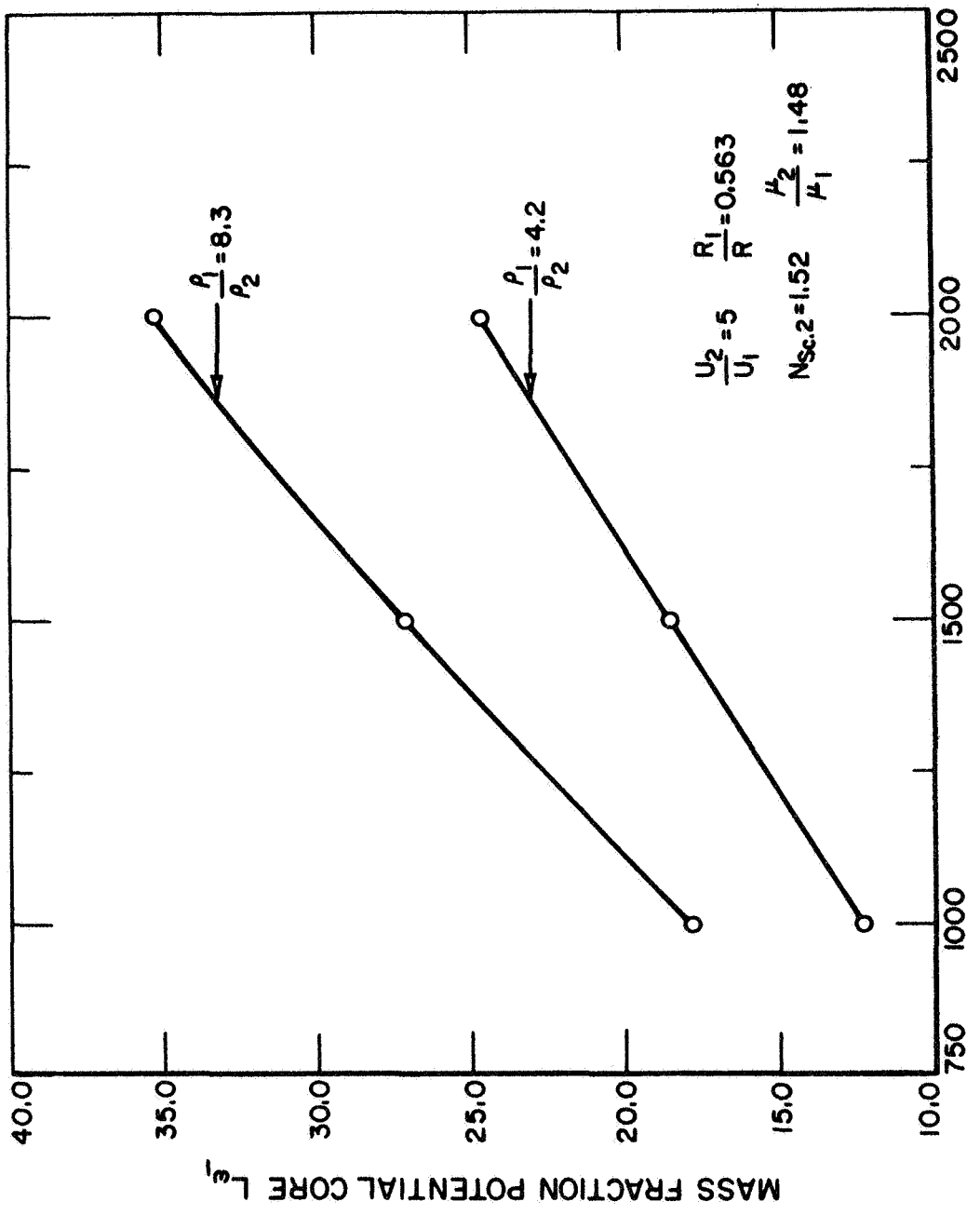

FIGURE 5. MASS FRACTION POTENTIAL CORE VS REYNOLDS NUMBER $N_{Re,2}$.

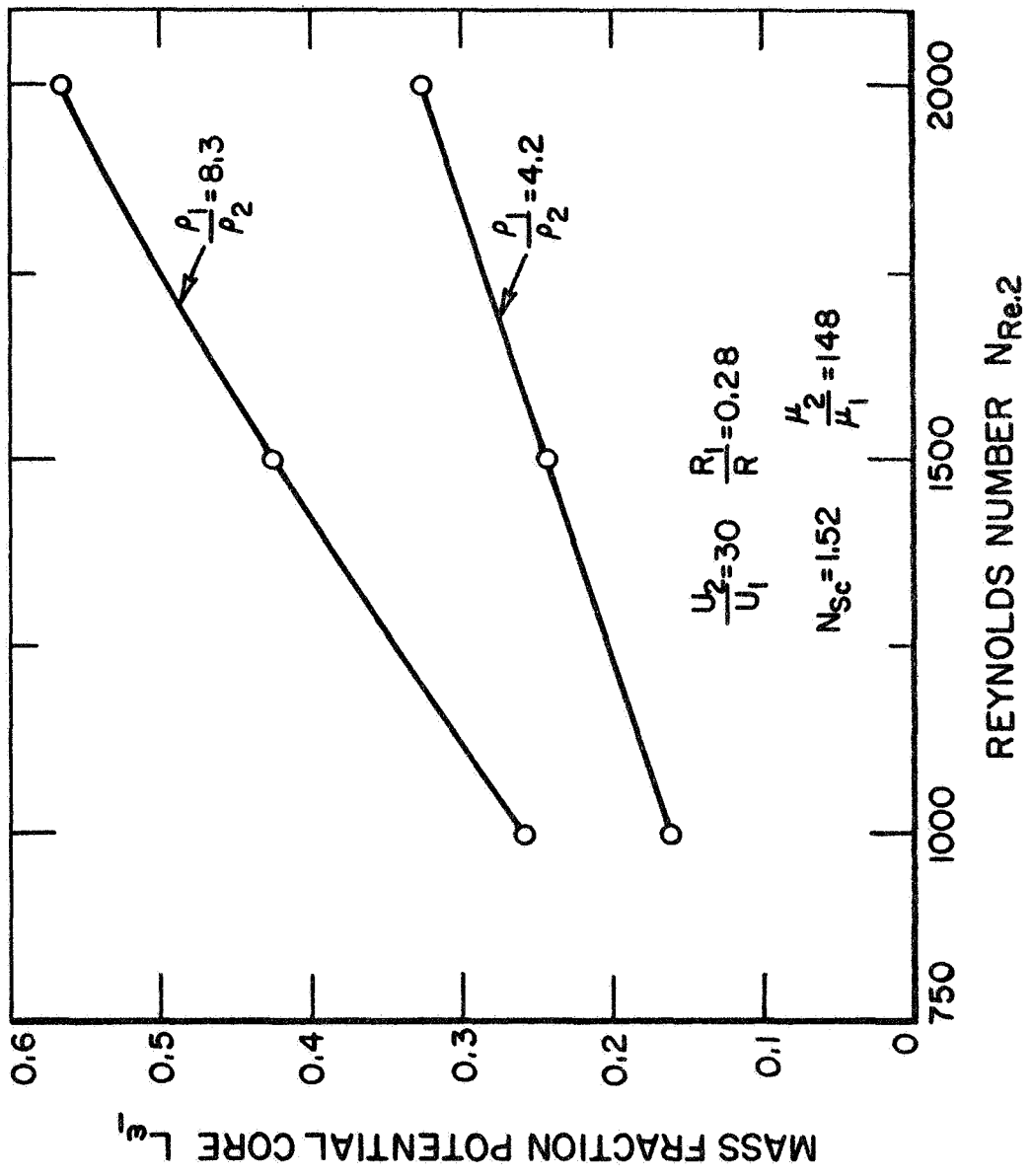

FIGURE 6. MASS FRACTION POTENTIAL CORE VS REYNOLDS NUMBER $N_{Re,2}$.

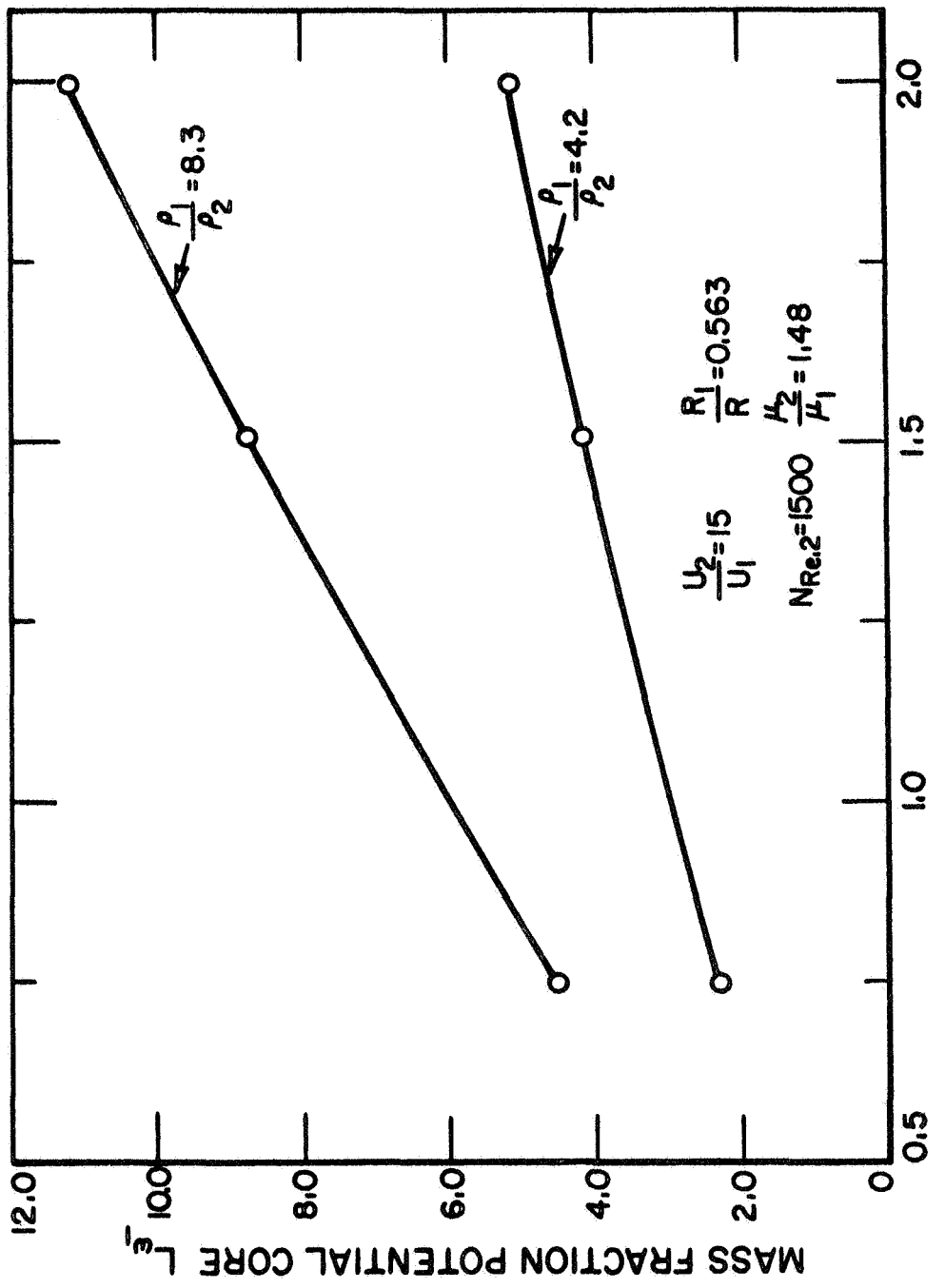

FIGURE 7. MASS FRACTION POTENTIAL CORE VS SCHMIDT NUMBER $N_{Sc,2}$.

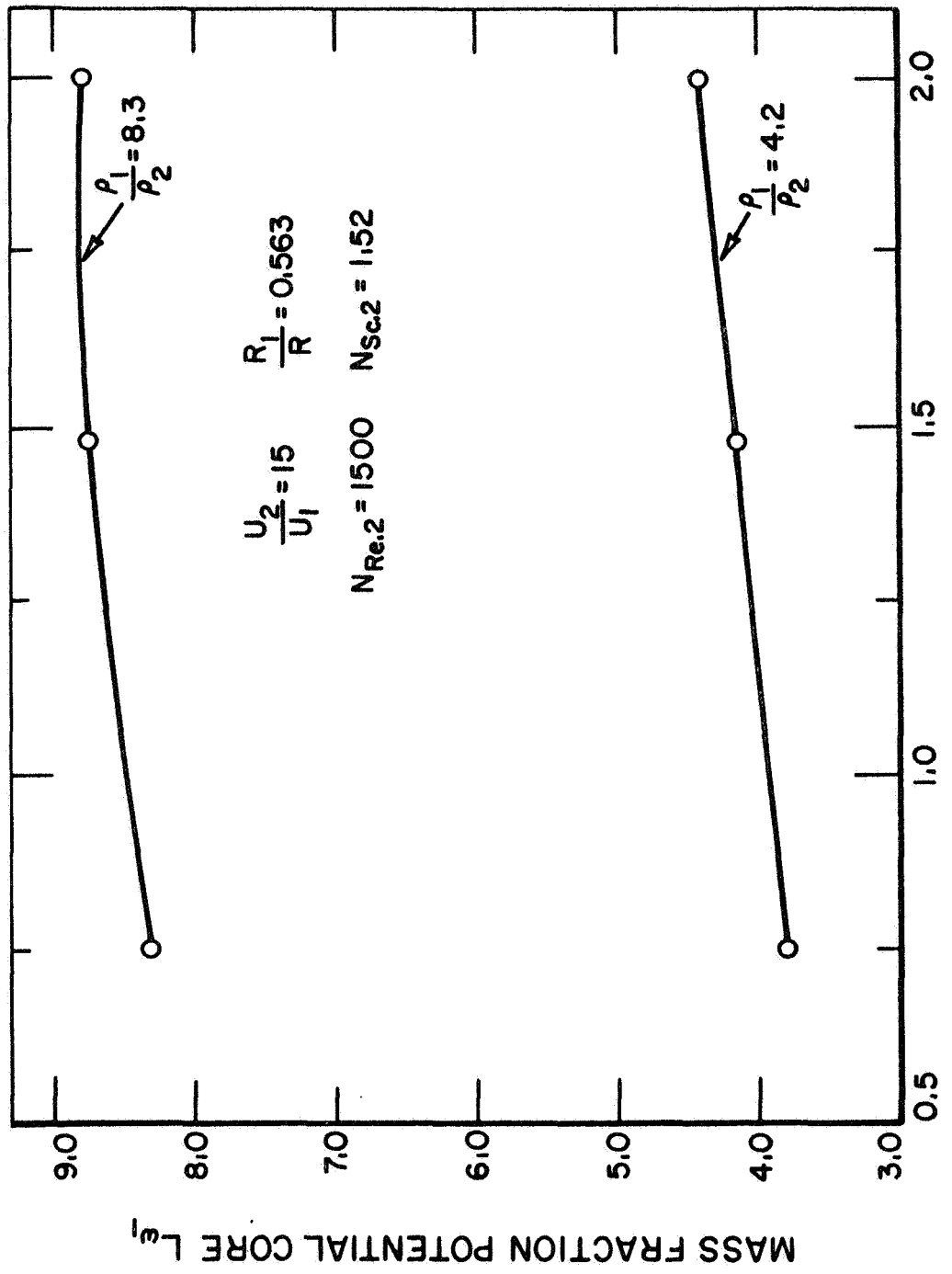

FIGURE 8. MASS FRACTION POTENTIAL CORE VS VISCOSITY RATIO.

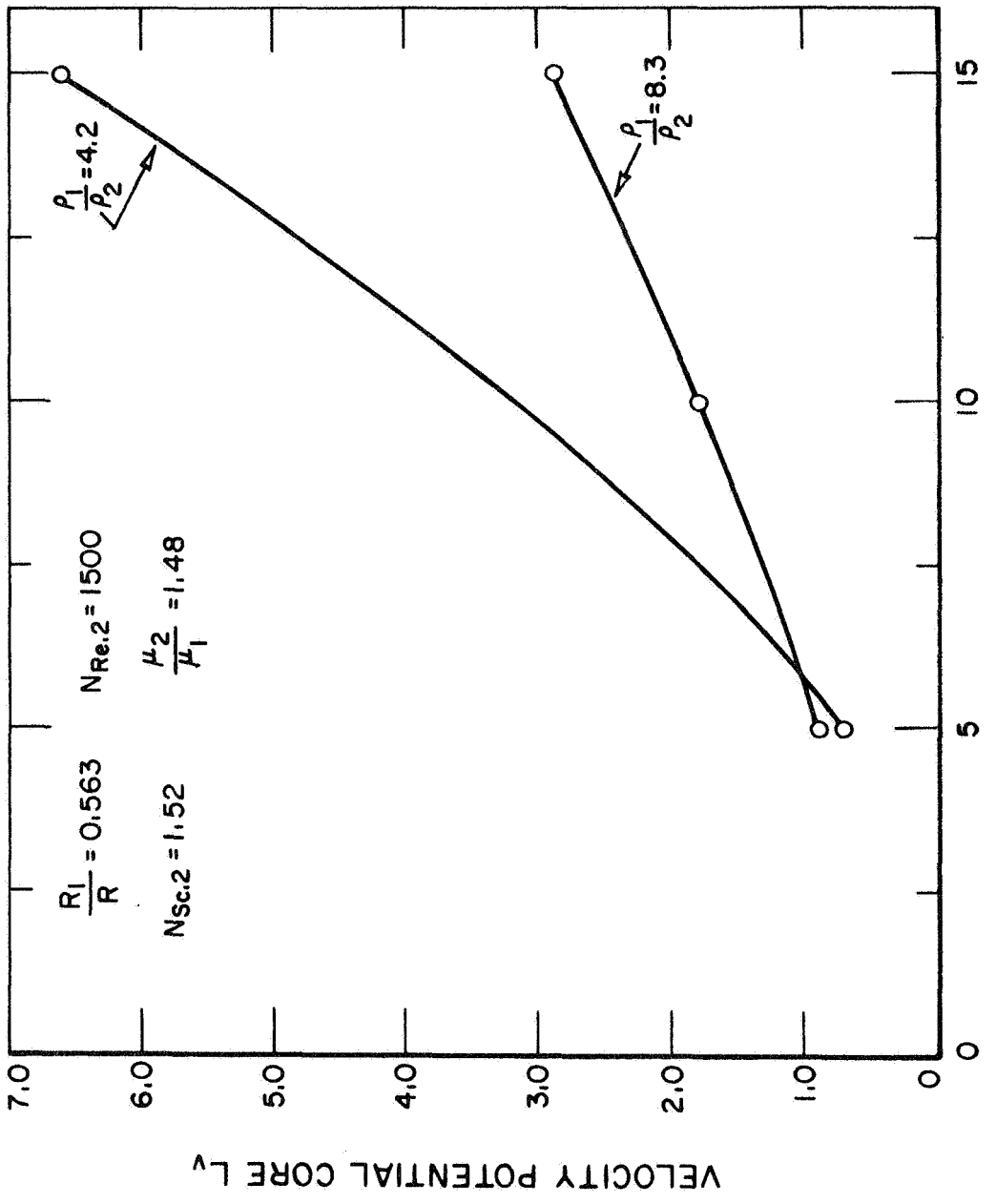

FIGURE 9. VELOCITY POTENTIAL CORE VS VELOCITY RATIO.

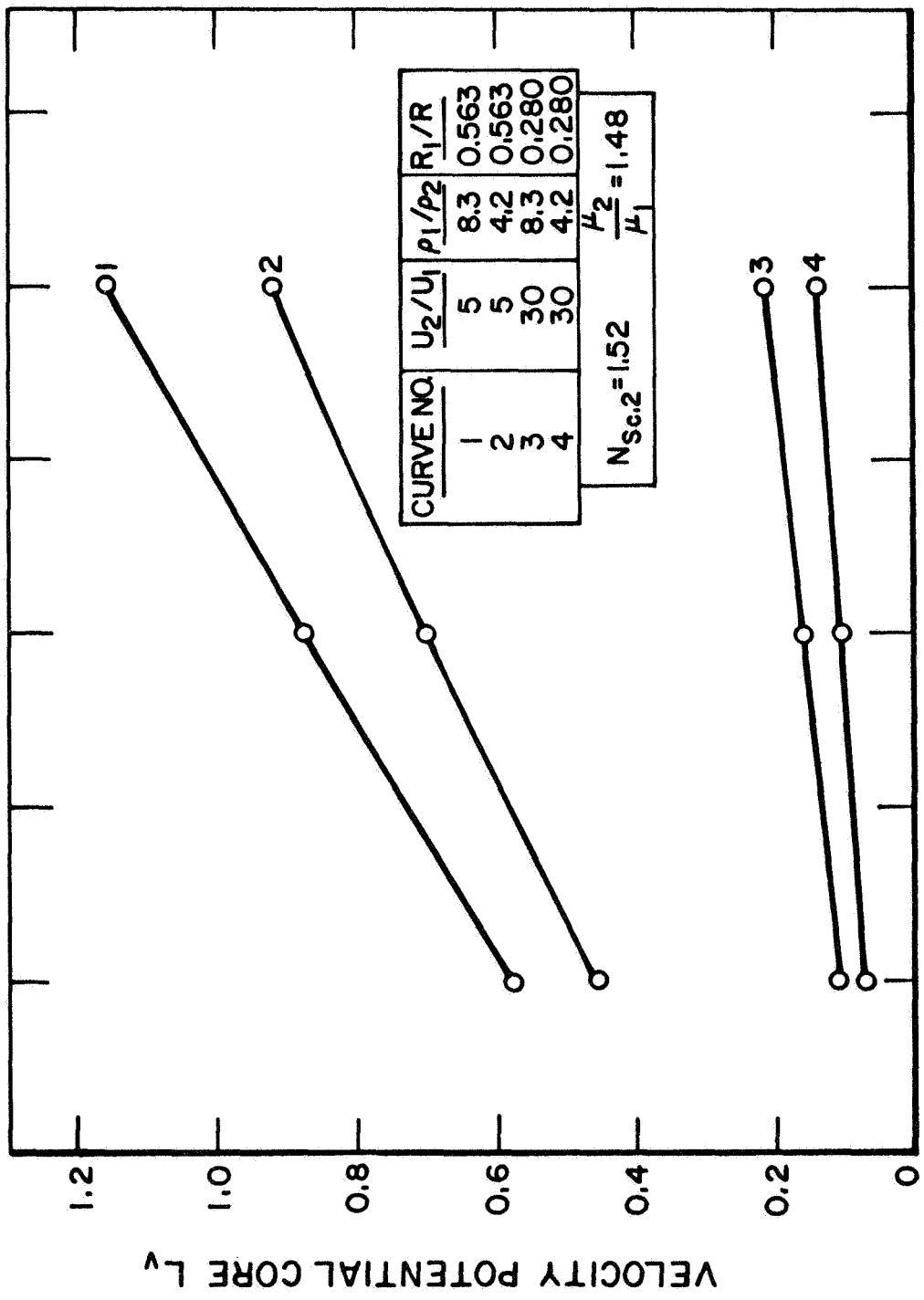

FIGURE 10. VELOCITY POTENTIAL CORE VS REYNOLDS NUMBER $N_{Re,2}$.

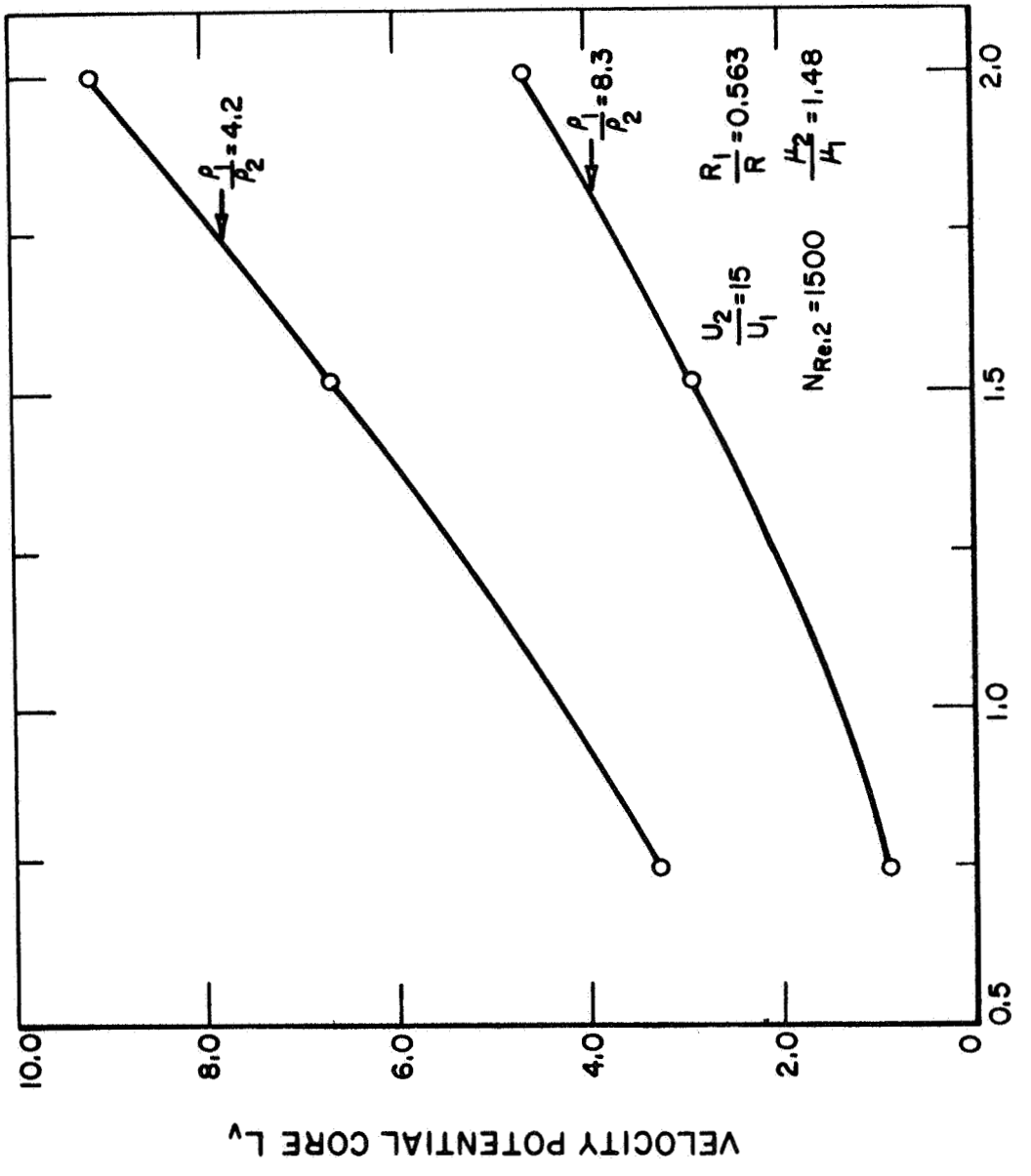

FIGURE 11. VELOCITY POTENTIAL CORE VS SCHMIDT NUMBER $N_{Sc,2}$.

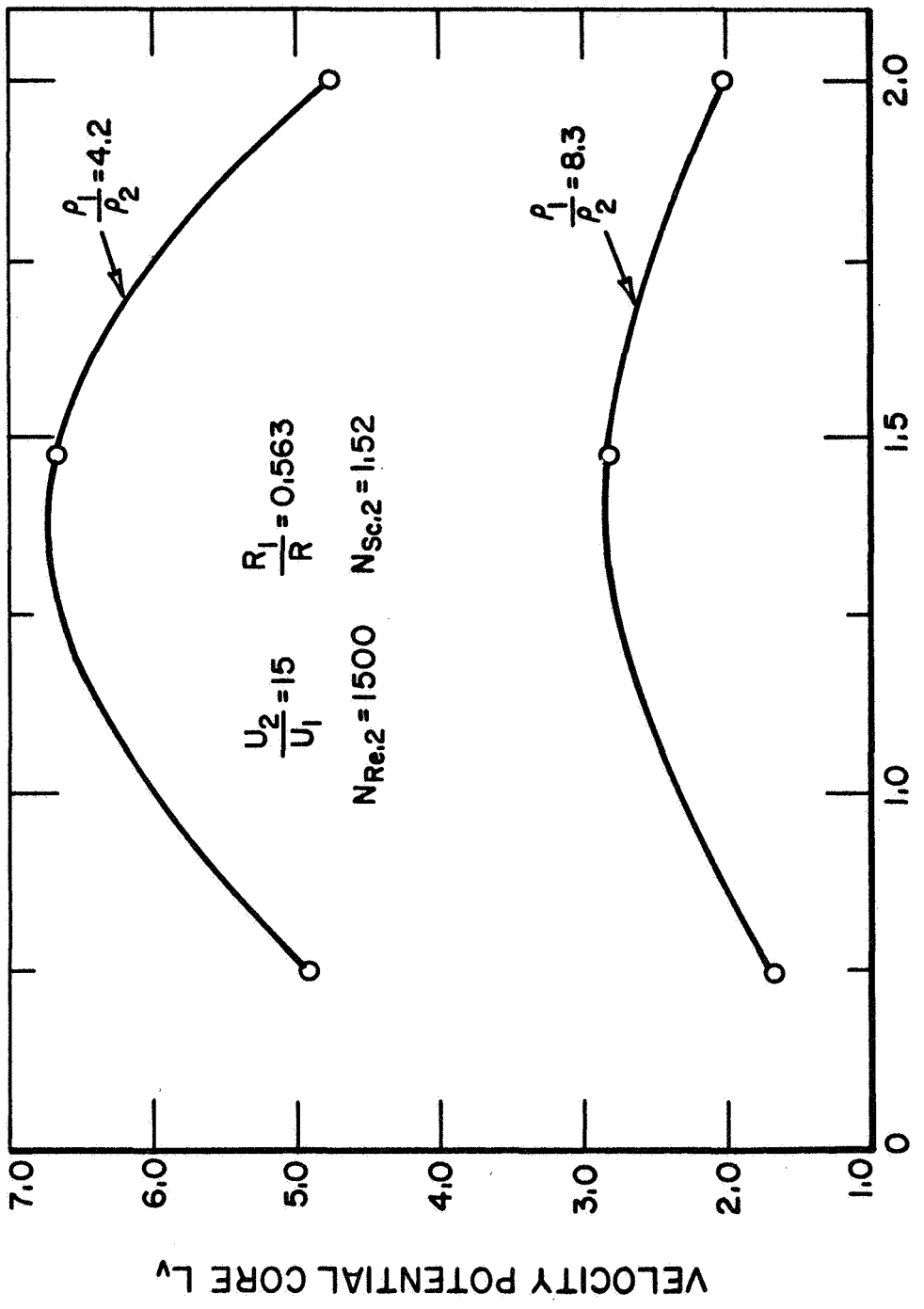

FIGURE 12. VELOCITY POTENTIAL CORE VS VISCOSITY RATIO.

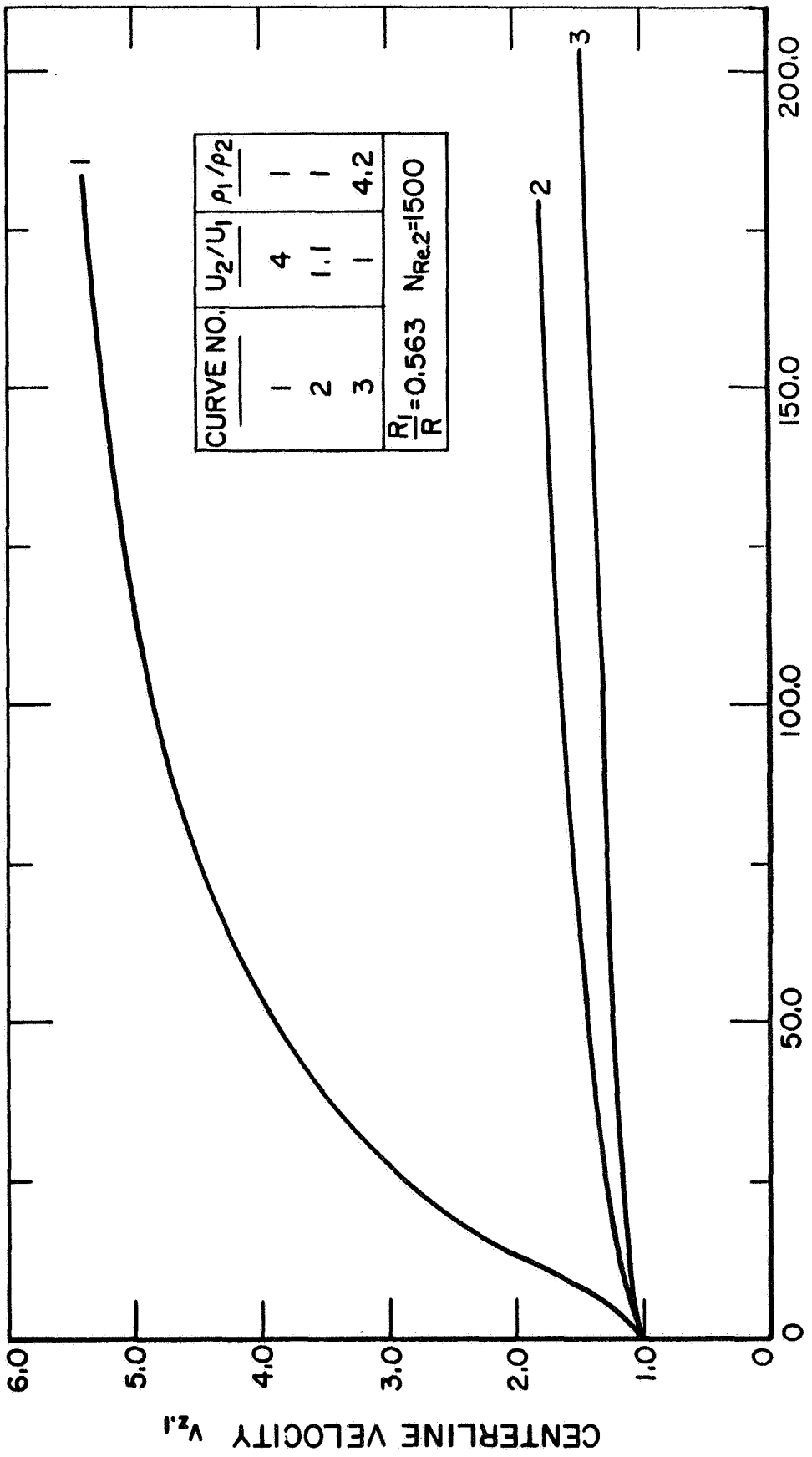

FIGURE 13. CENTERLINE VELOCITY VS DOWNSTREAM DISTANCE.

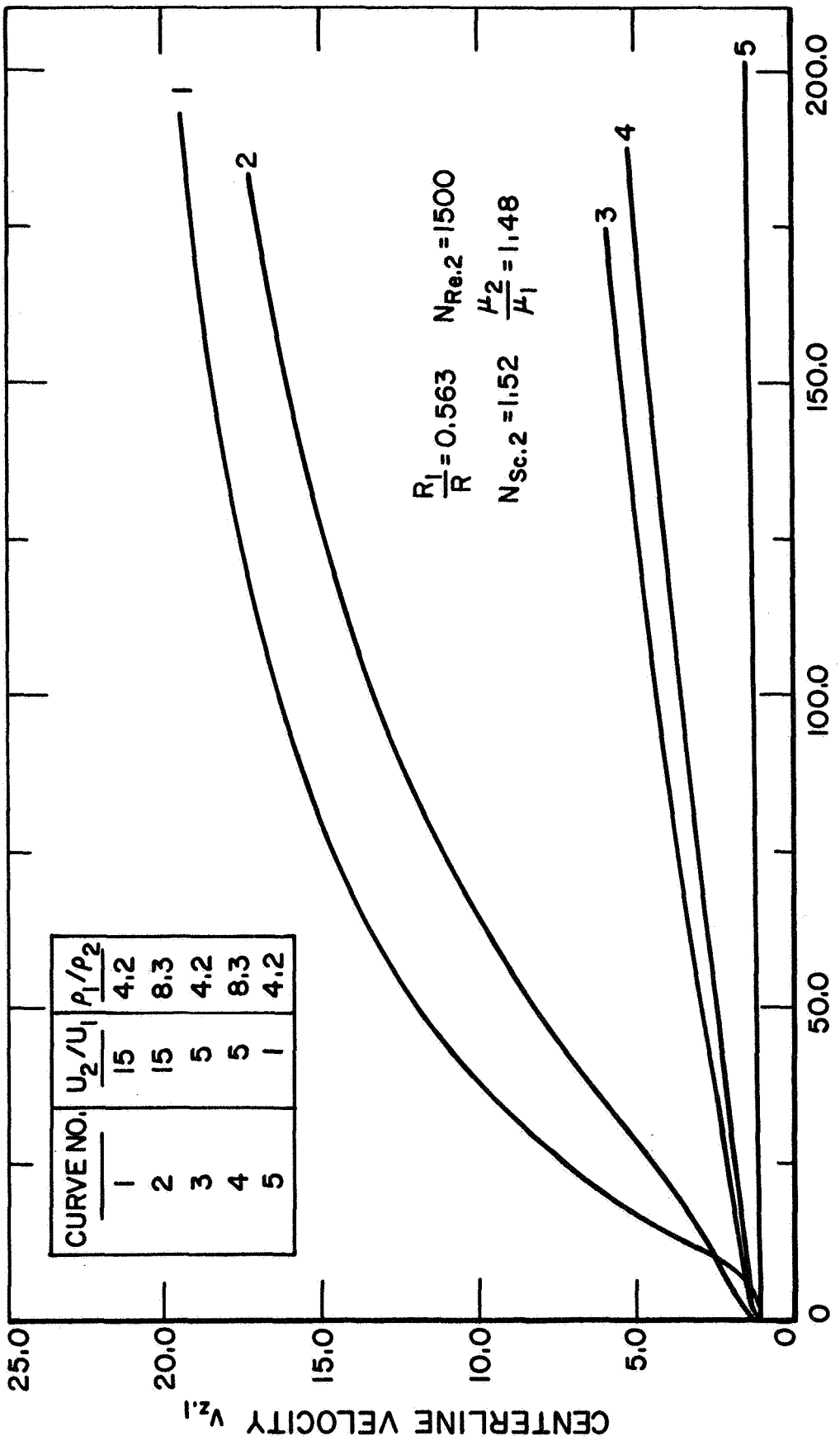

FIGURE 13. concluded. CENTERLINE VELOCITY VS DOWNSTREAM DISTANCE.

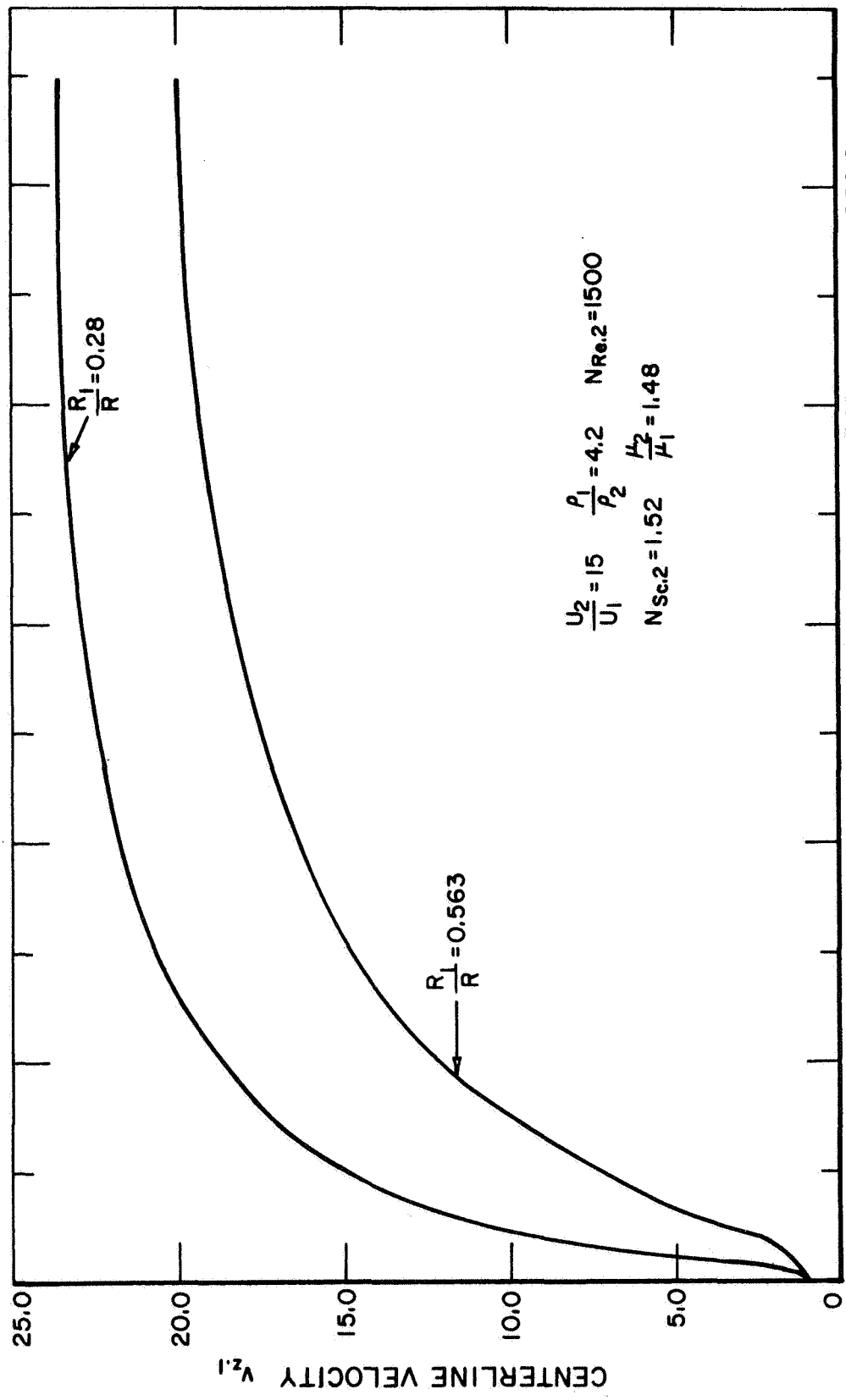

FIGURE 14. CENTERLINE VELOCITY VS DOWNSTREAM DISTANCE.

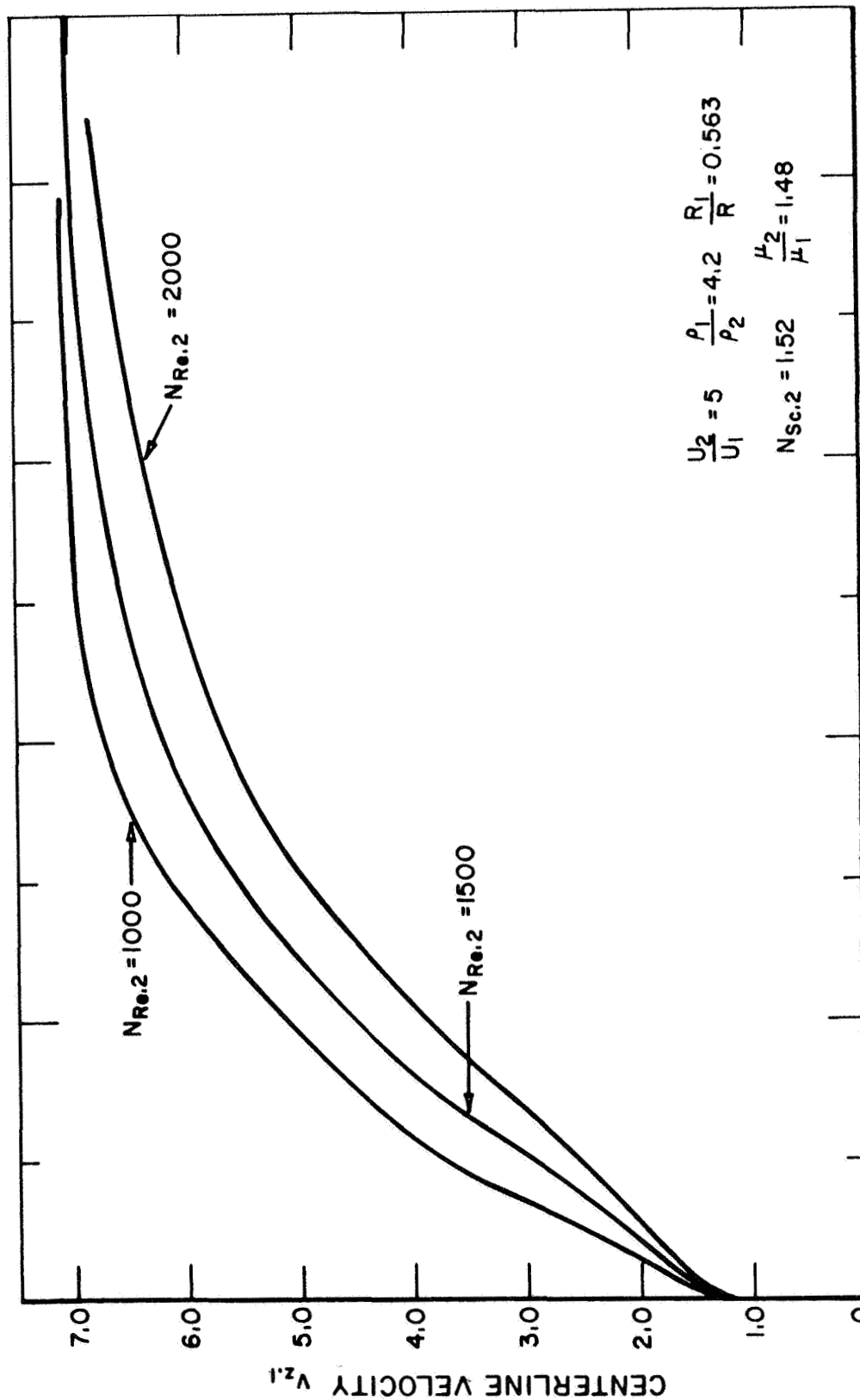

FIGURE 15. CENTERLINE VELOCITY VS DOWNSTREAM DISTANCE.

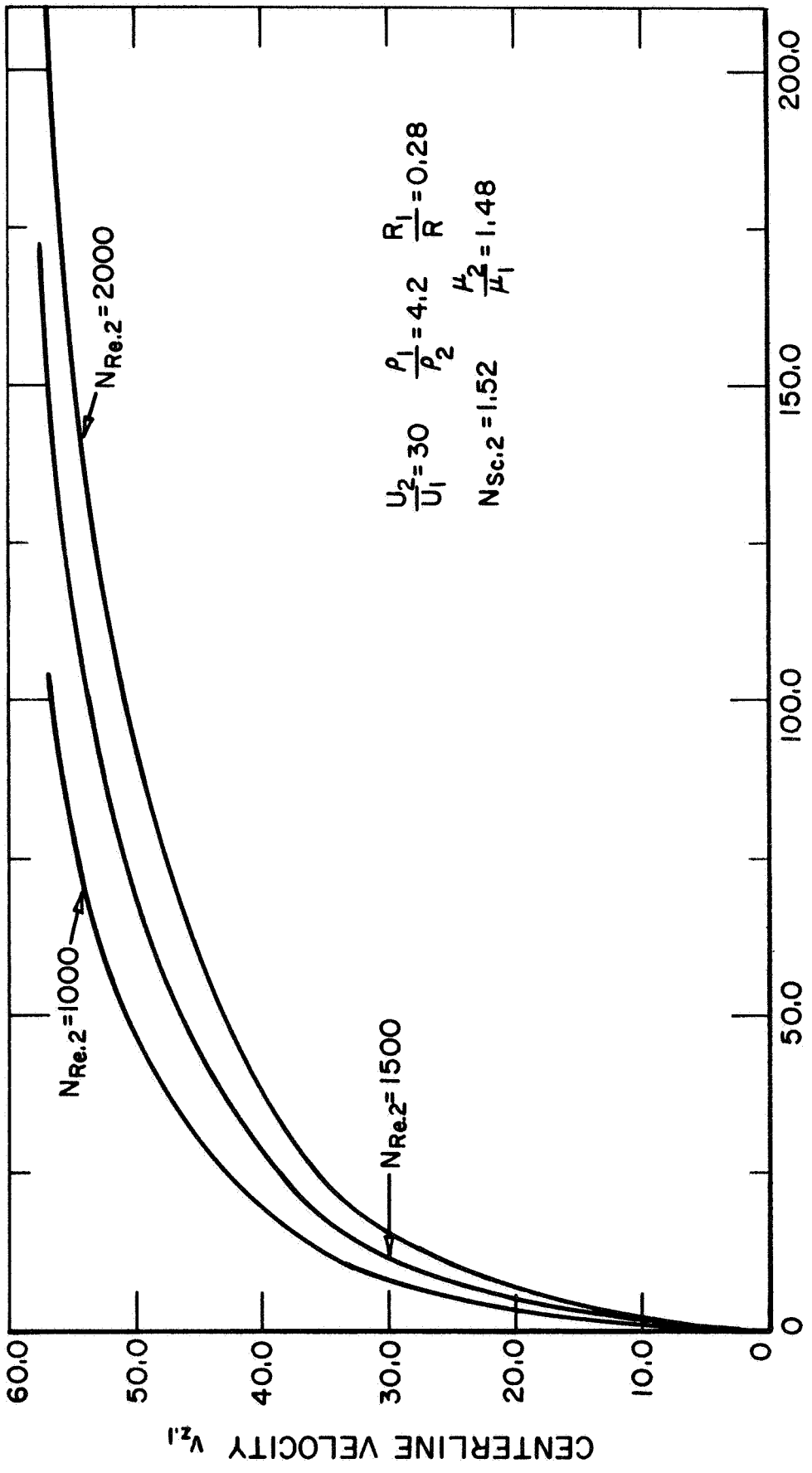

FIGURE 16. CENTERLINE VELOCITY VS DOWNSTREAM DISTANCE.

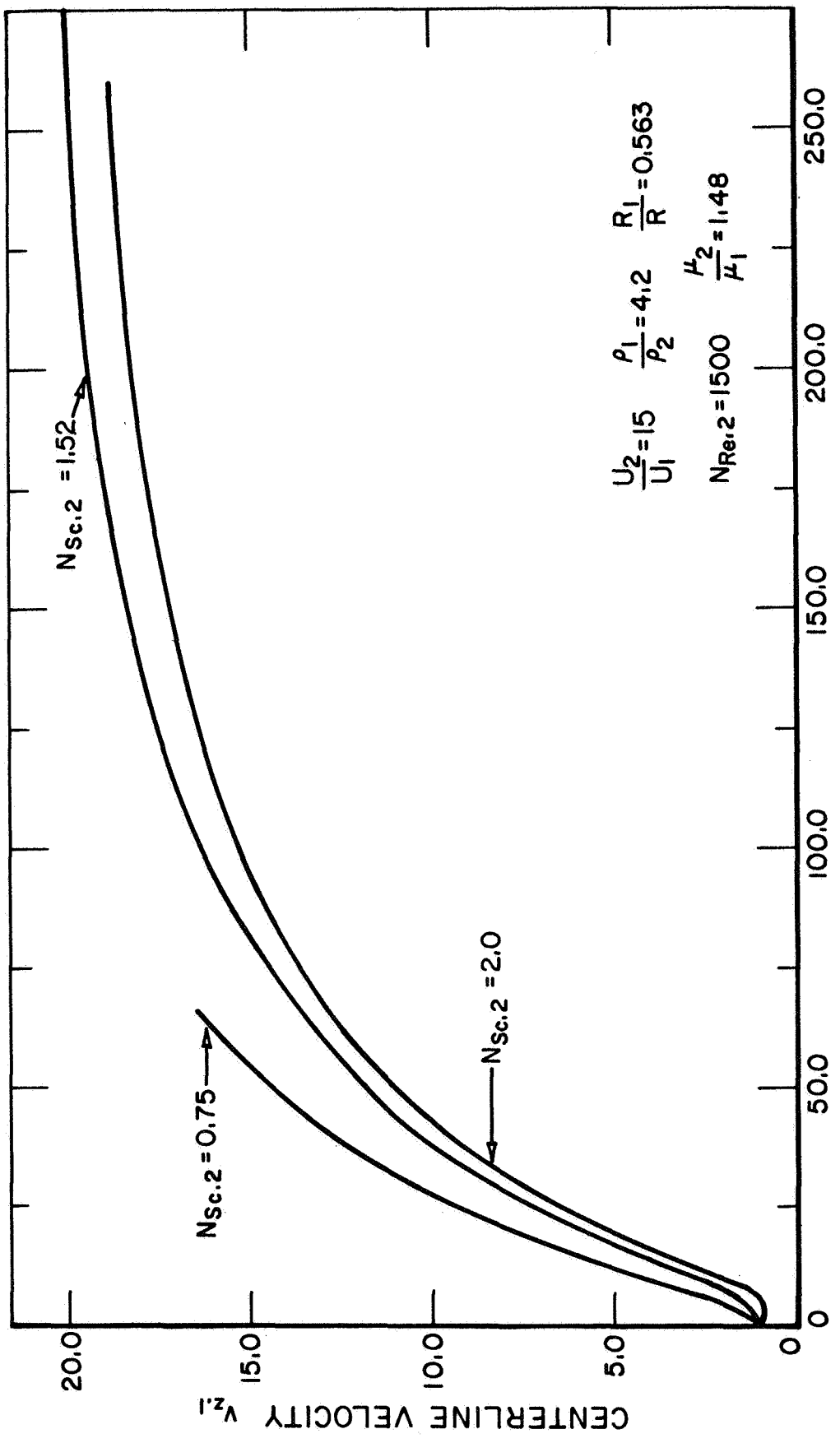

FIGURE 17. CENTERLINE VELOCITY VS DOWNSTREAM DISTANCE.

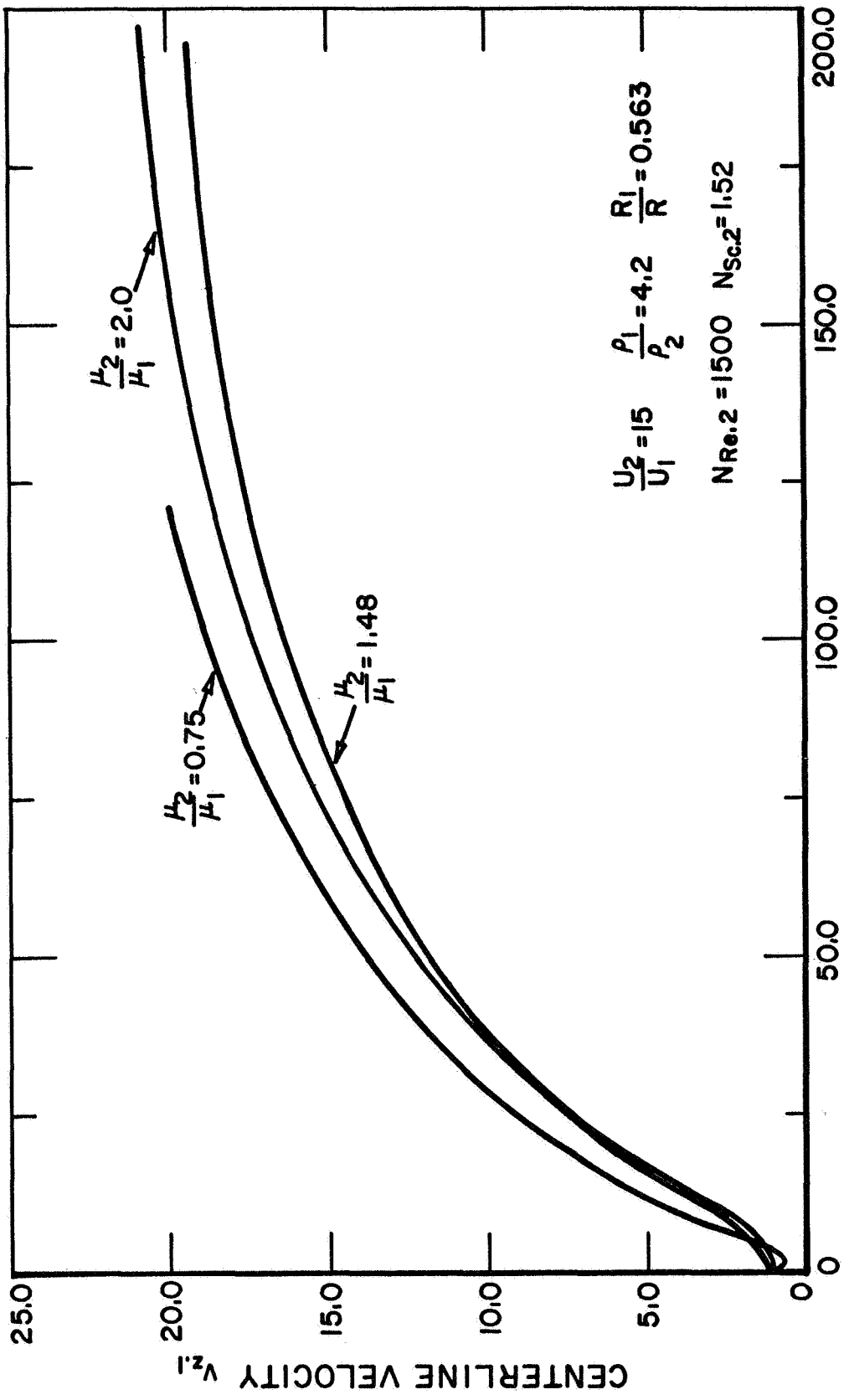

FIGURE 18. CENTERLINE VELOCITY VS DOWNSTREAM DISTANCE.

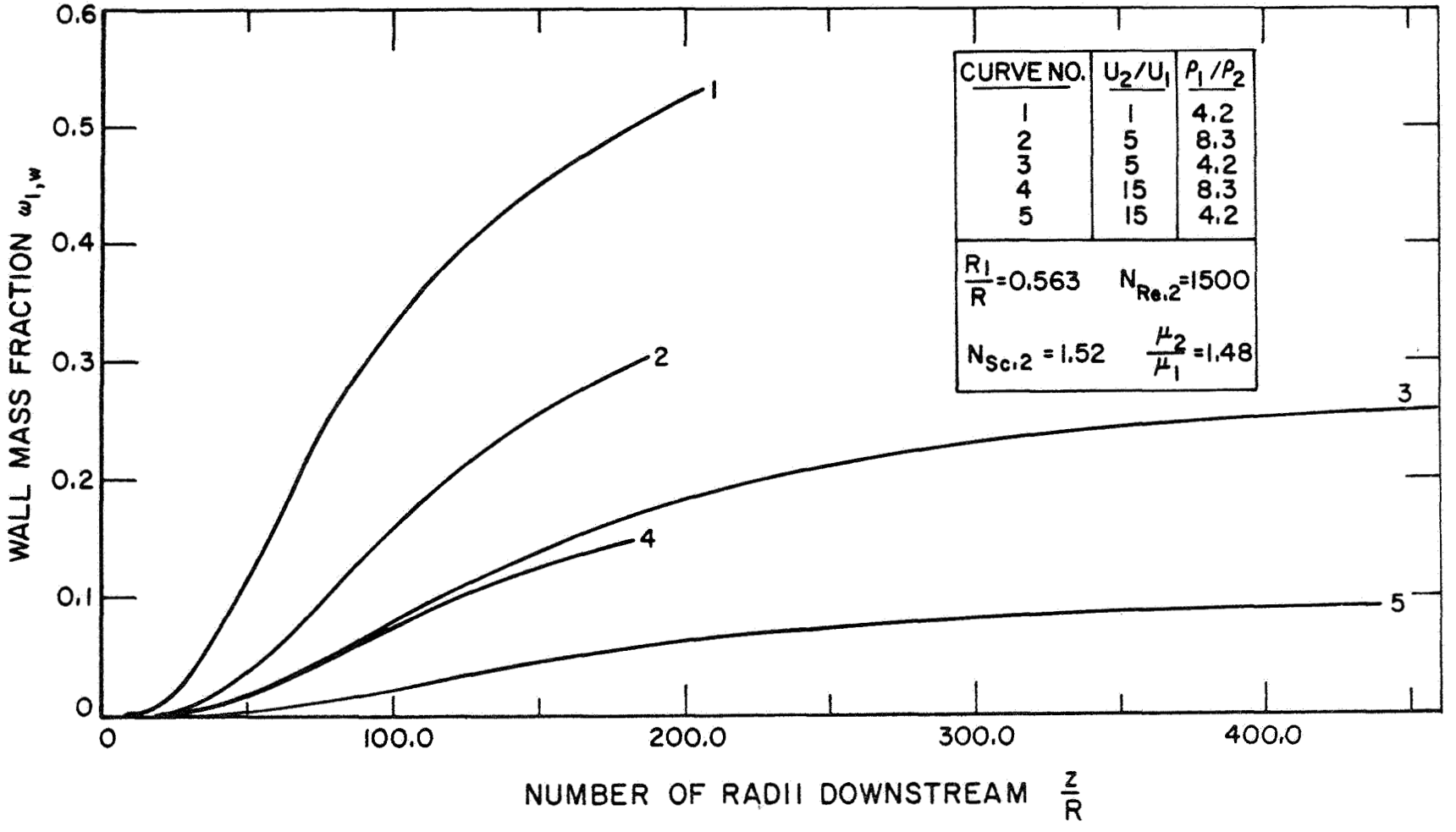

FIGURE 19. WALL MASS FRACTION VS DOWNSTREAM DISTANCE.

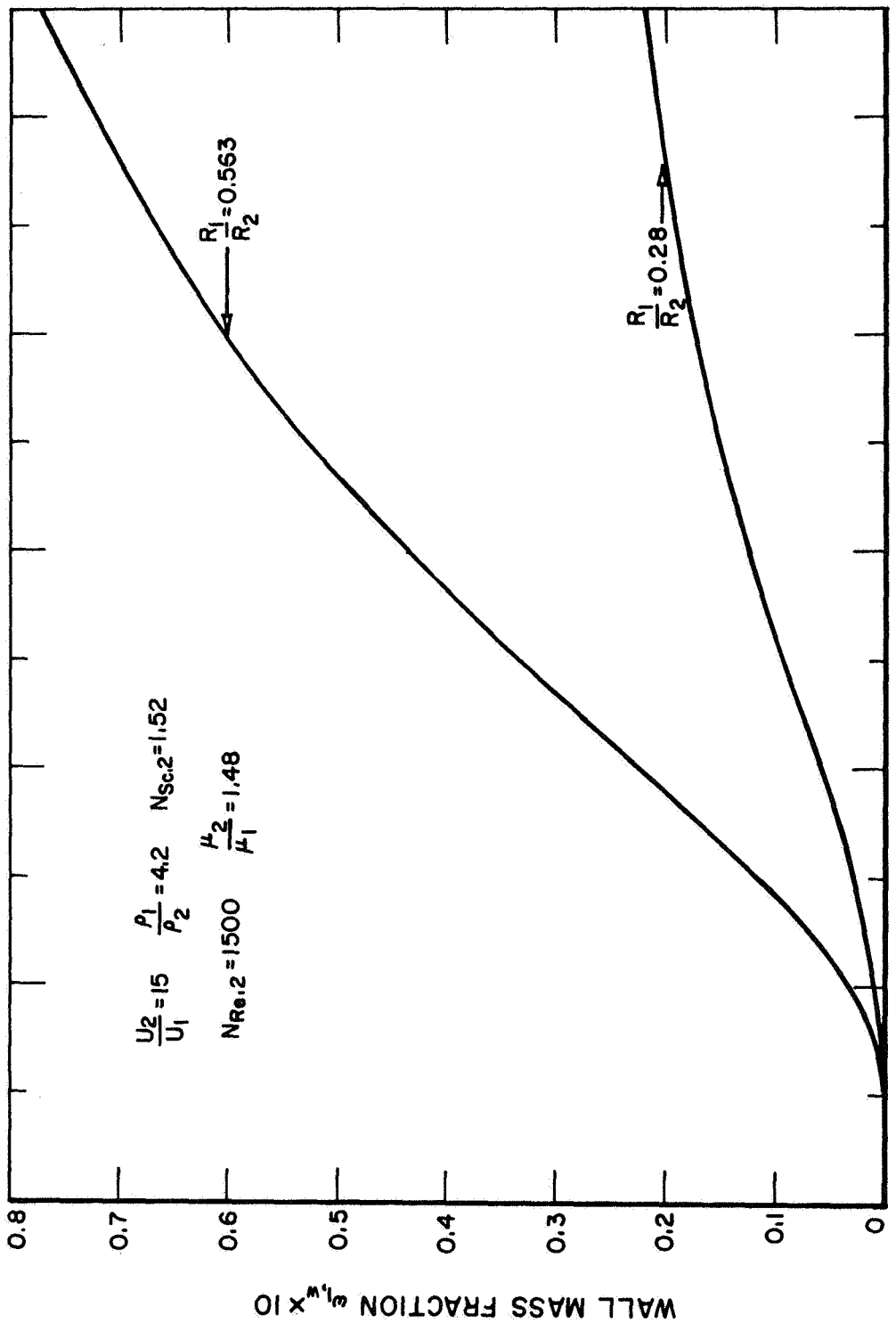

FIGURE 20. WALL MASS FRACTION VS DOWNSTREAM DISTANCE.

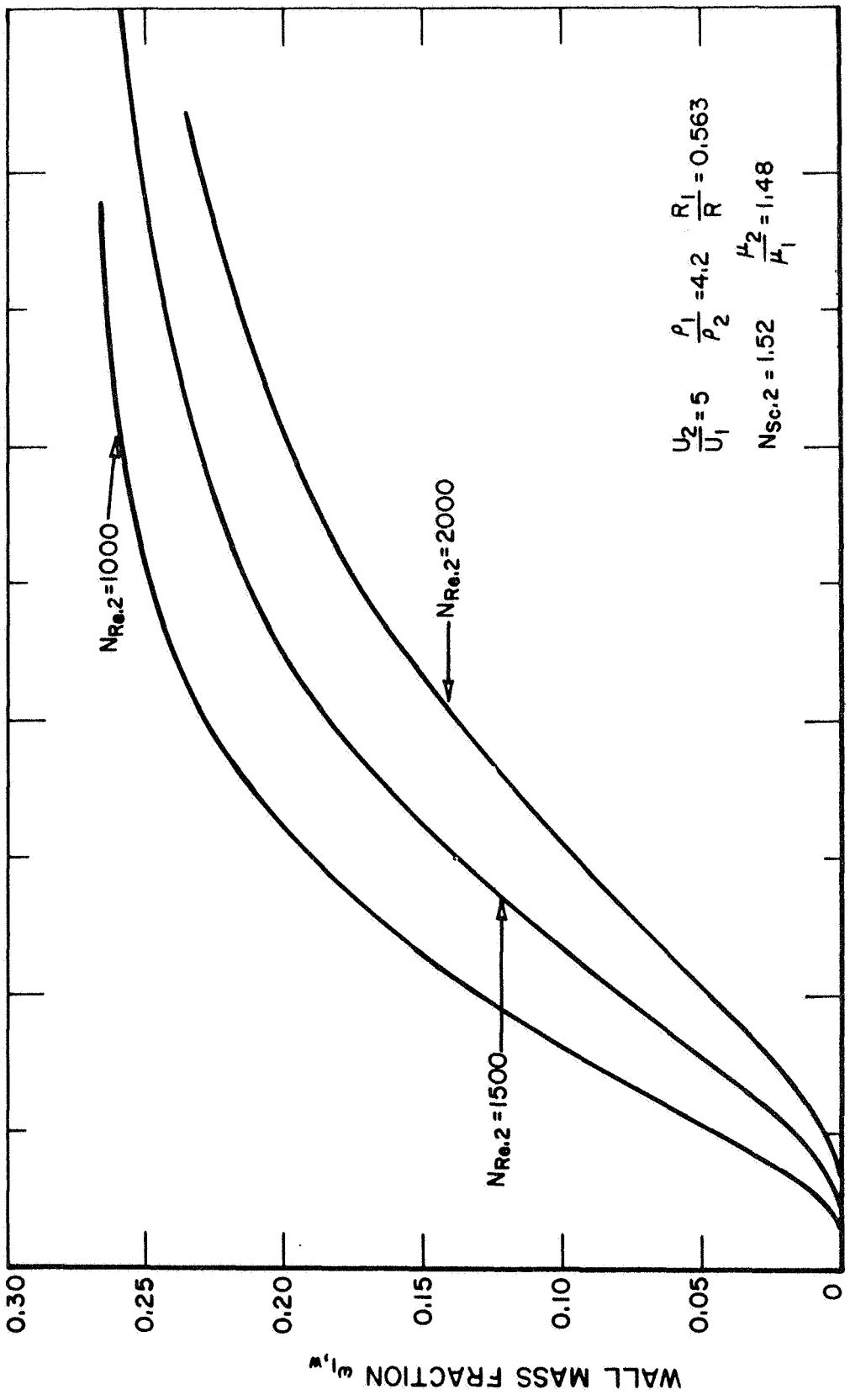

FIGURE 21. WALL MASS FRACTION VS DOWNSTREAM DISTANCE.

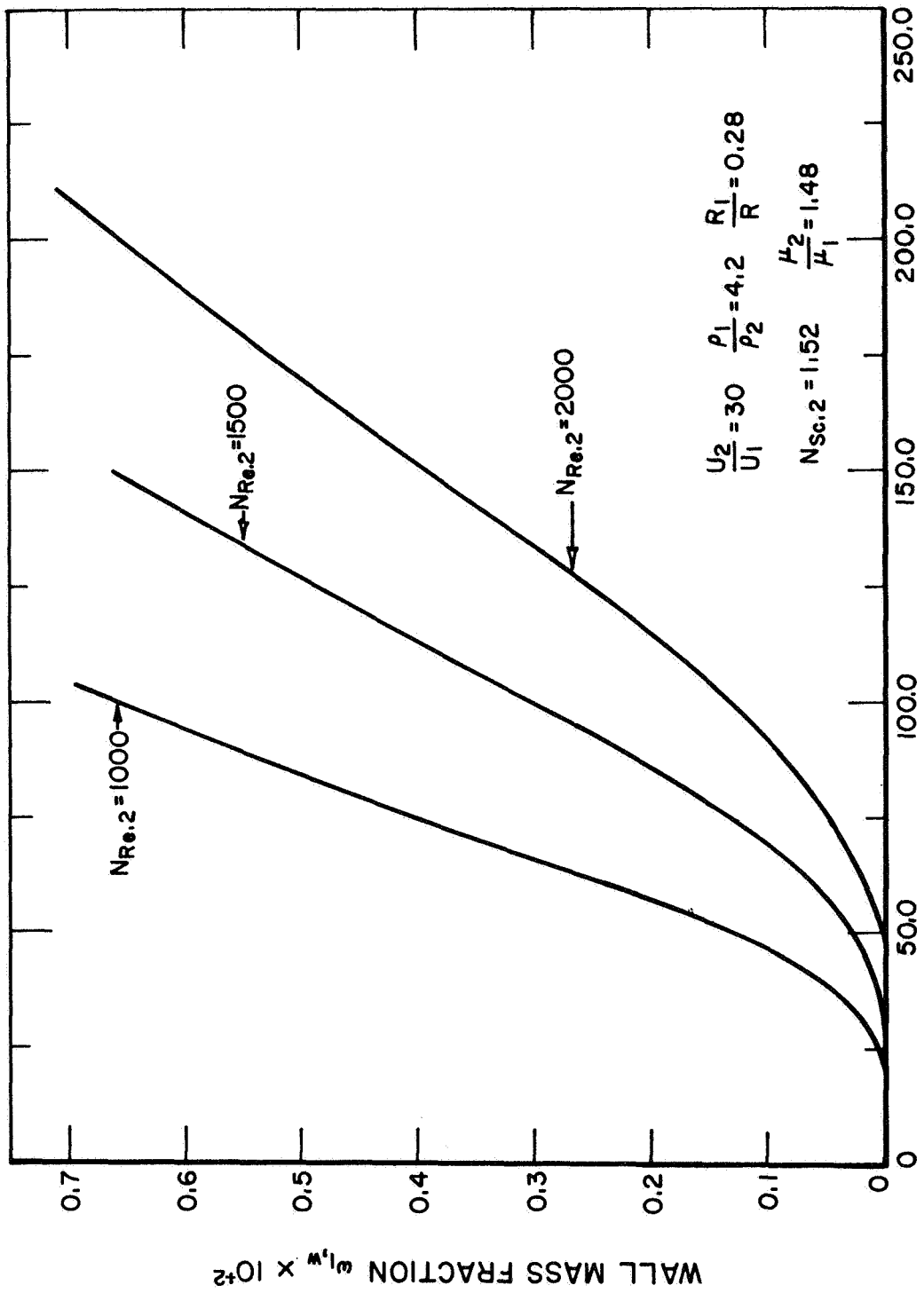

FIGURE 22. WALL MASS FRACTION VS DOWNSTREAM DISTANCE.

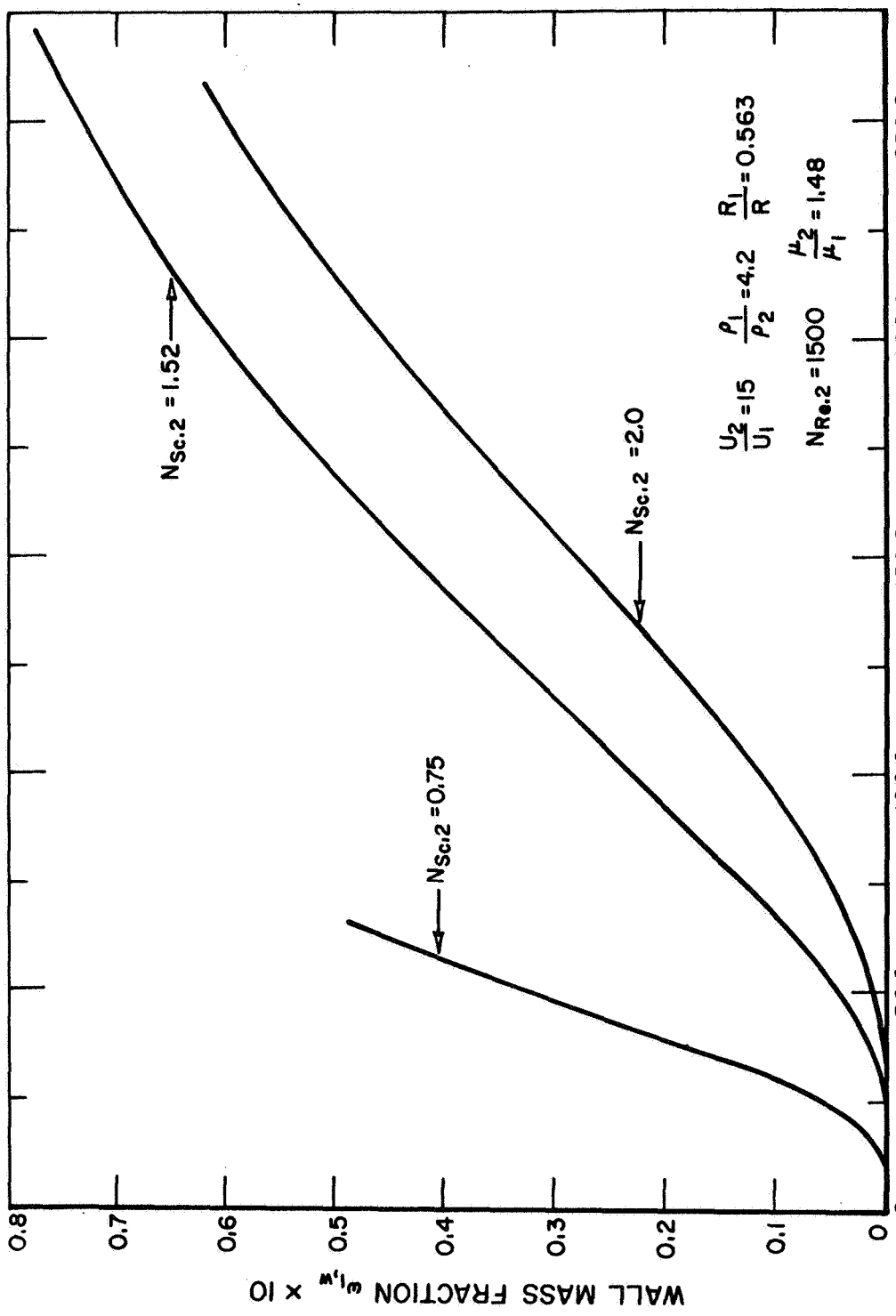

FIGURE 23. WALL MASS FRACTION VS DOWNSTREAM DISTANCE.

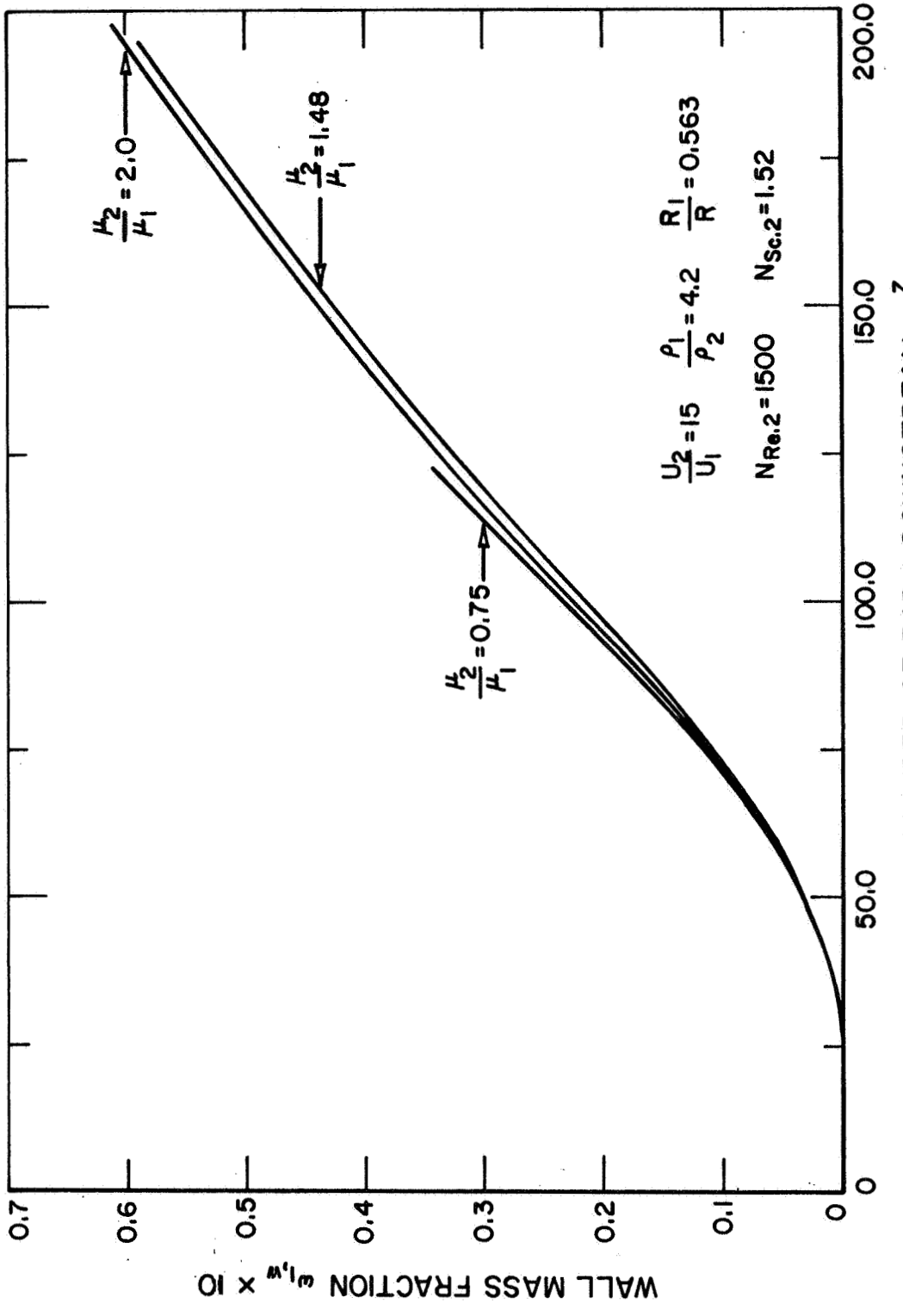

FIGURE 24. WALL MASS FRACTION VS DOWNSTREAM DISTANCE.

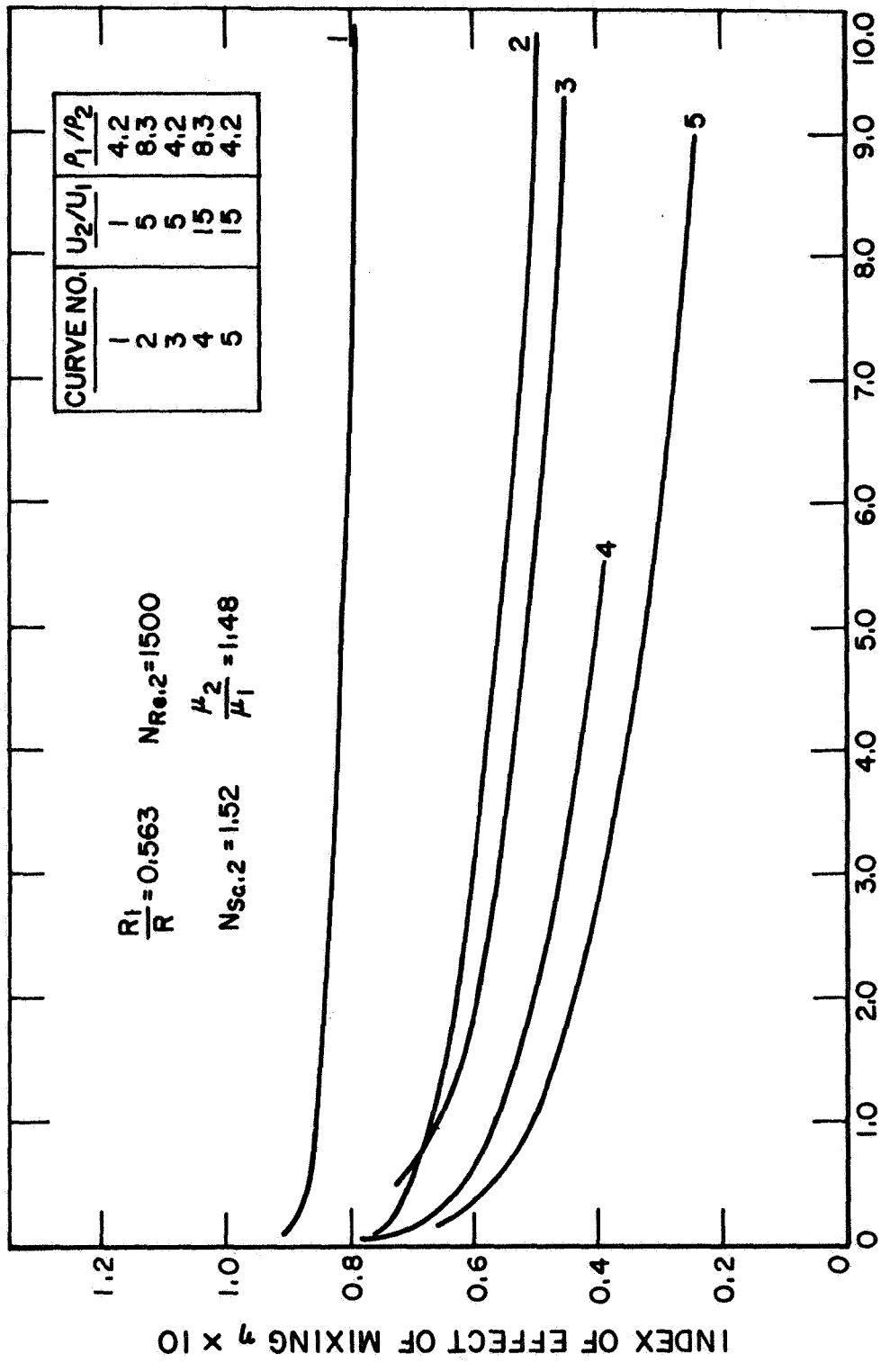

FIGURE 25. INDEX OF EFFECT OF MIXING VS. DOWNSTREAM DISTANCE

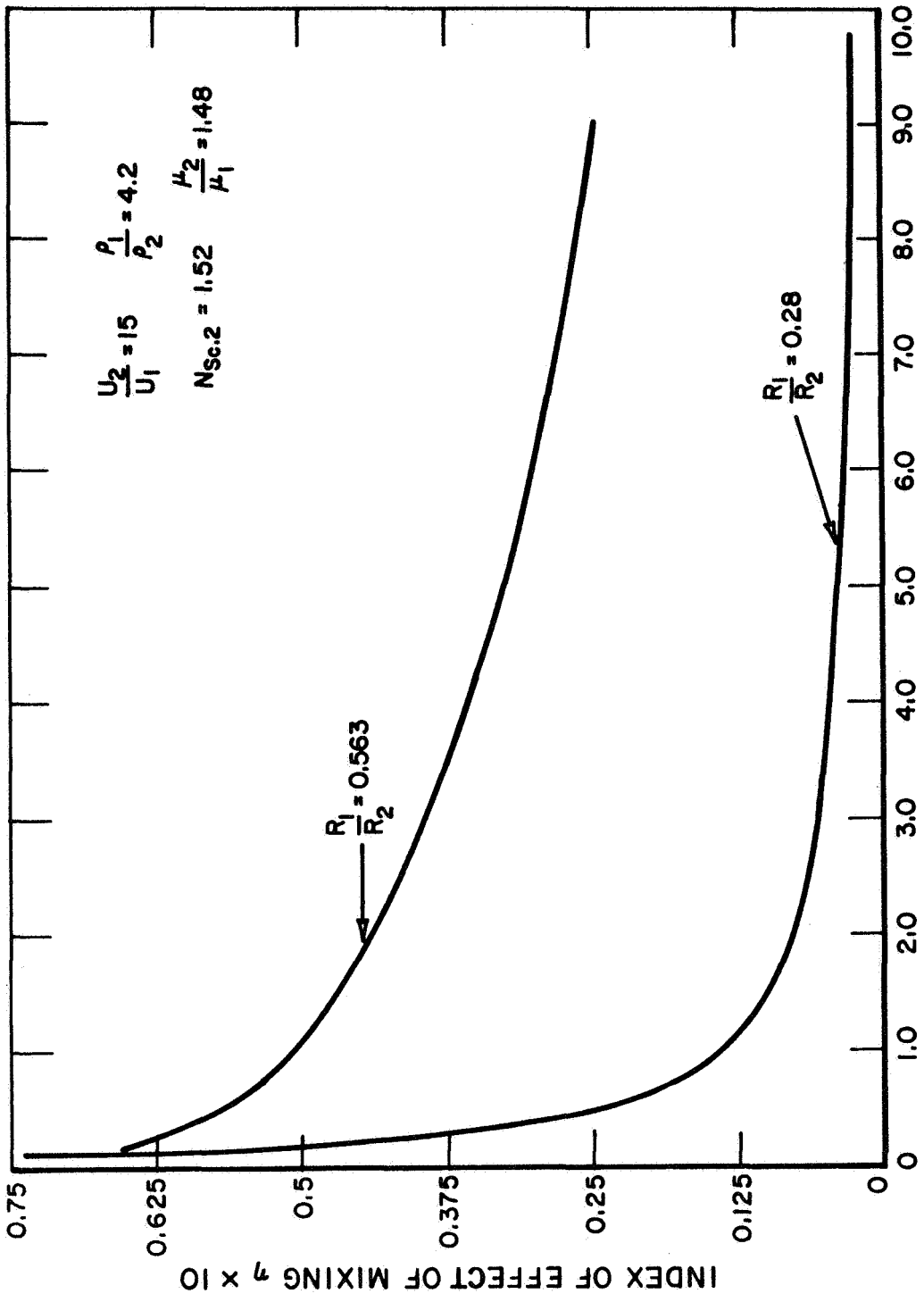

FIGURE 26. INDEX OF EFFECT OF MIXING VS. DOWNSTREAM DISTANCE

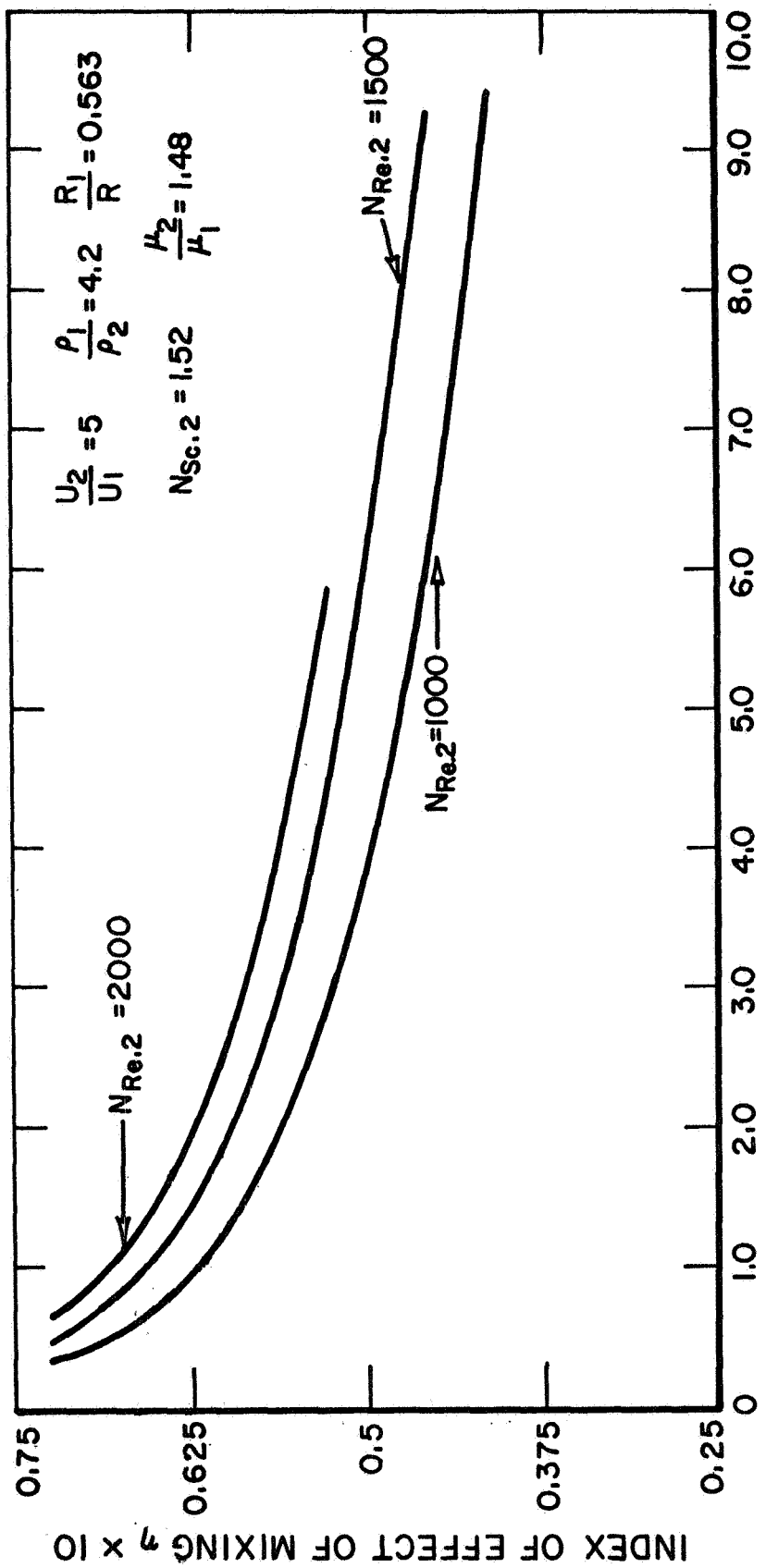

FIGURE 27. INDEX OF EFFECT OF MIXING VS. DOWNSTREAM DISTANCE

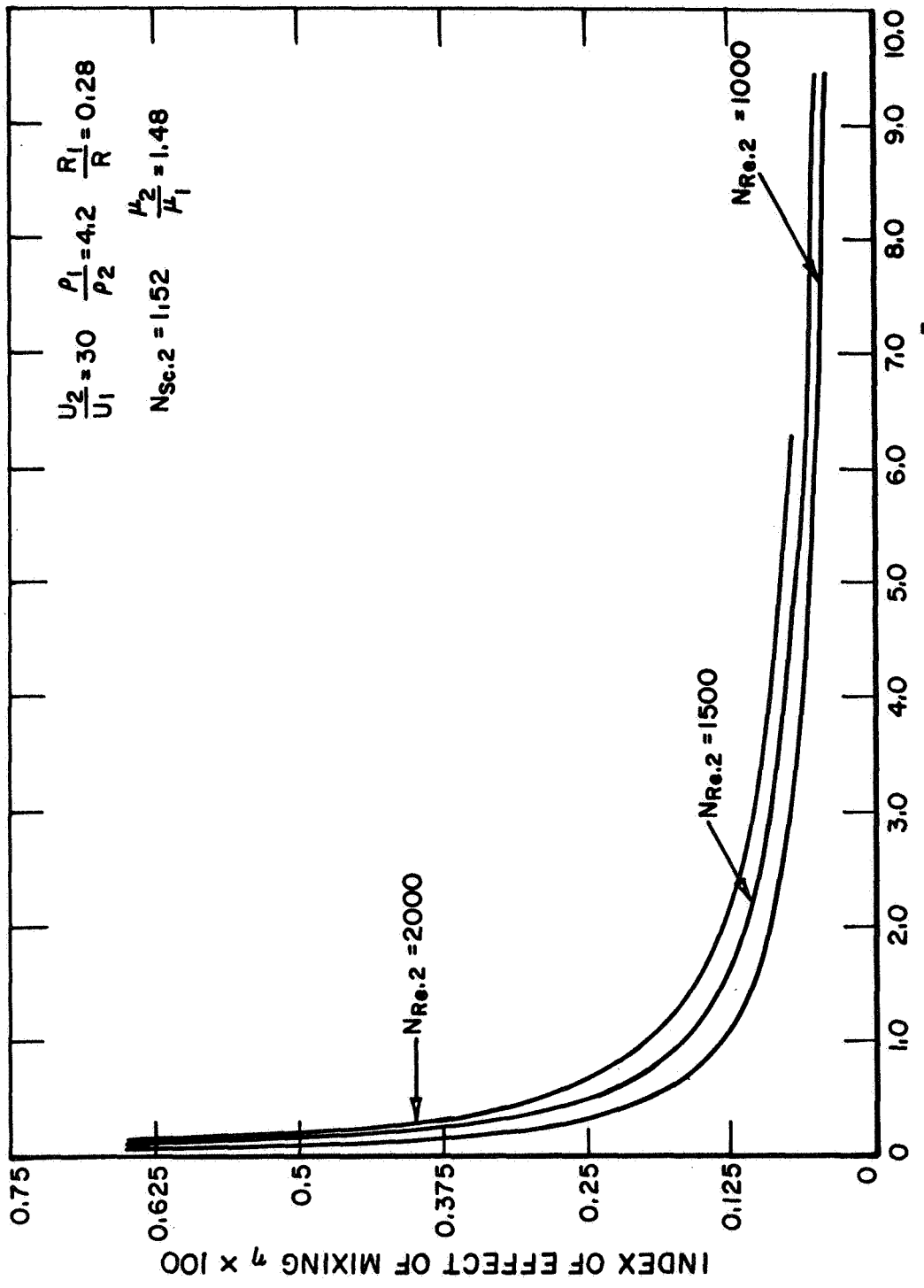

FIGURE 28. INDEX OF EFFECT OF MIXING VS. DOWNSTREAM DISTANCE

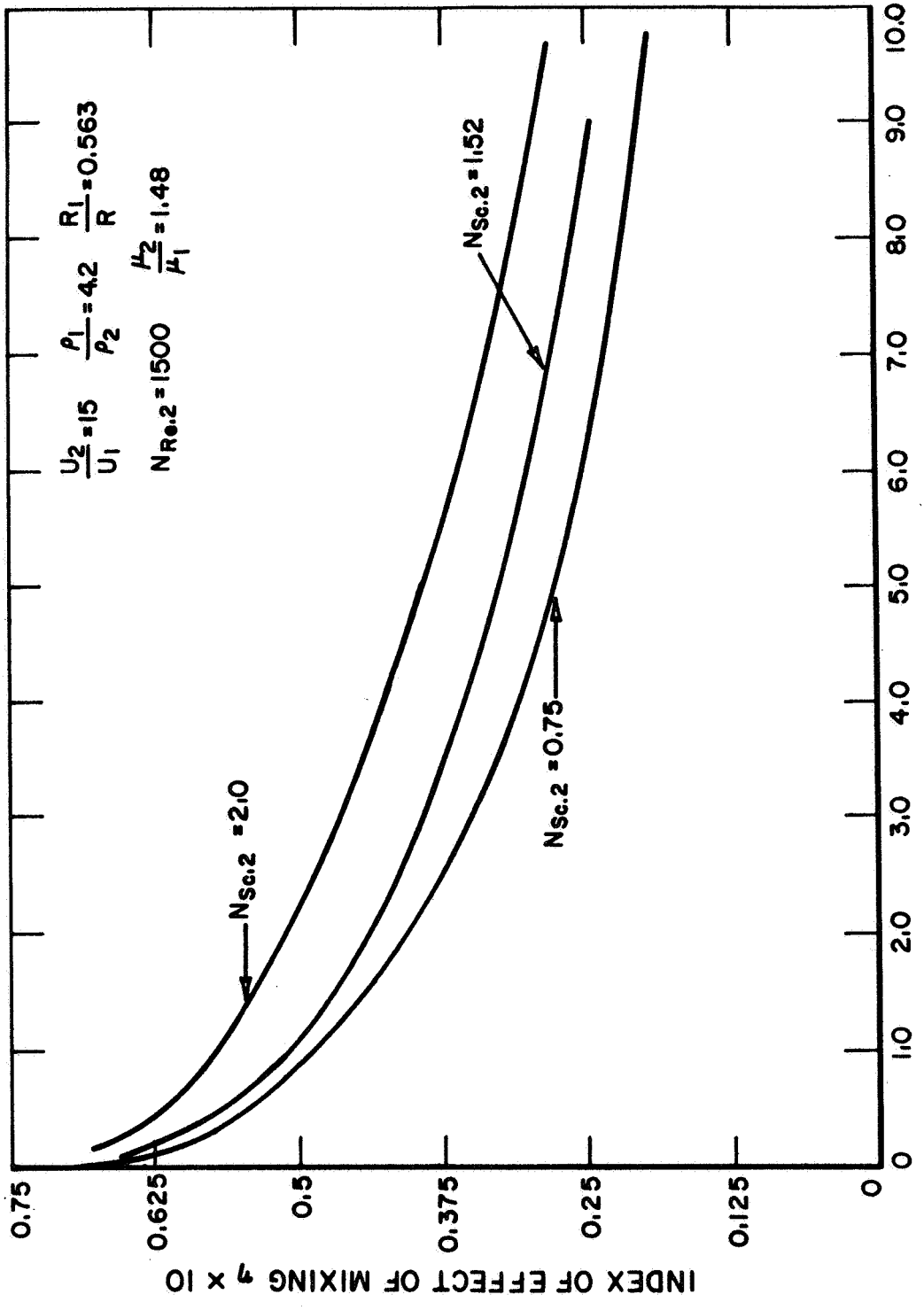

FIGURE 29. INDEX OF EFFECT OF MIXING VS. DOWNSTREAM DISTANCE

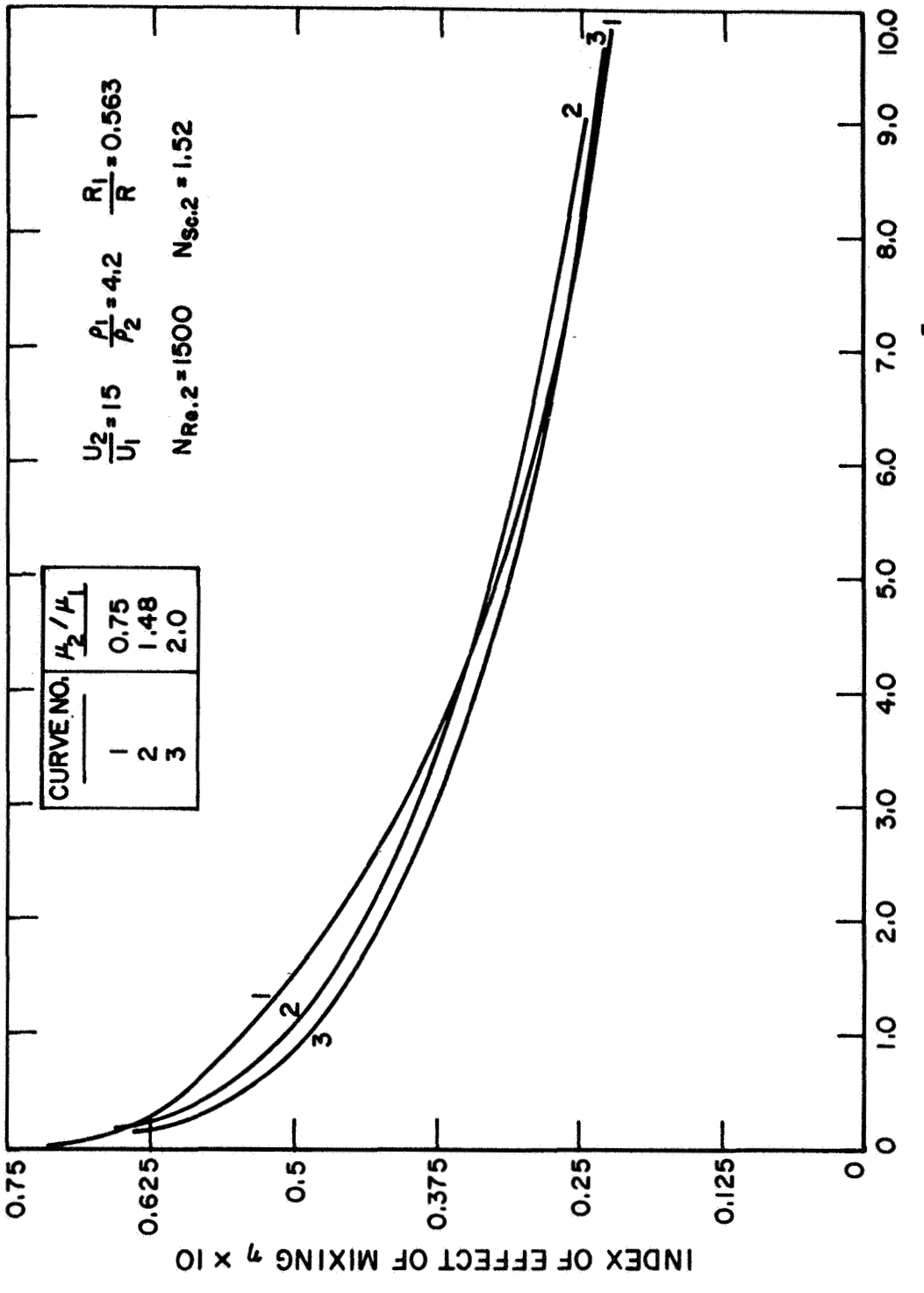

FIGURE 30. INDEX OF EFFECT OF MIXING VS. DOWNSTREAM DISTANCE

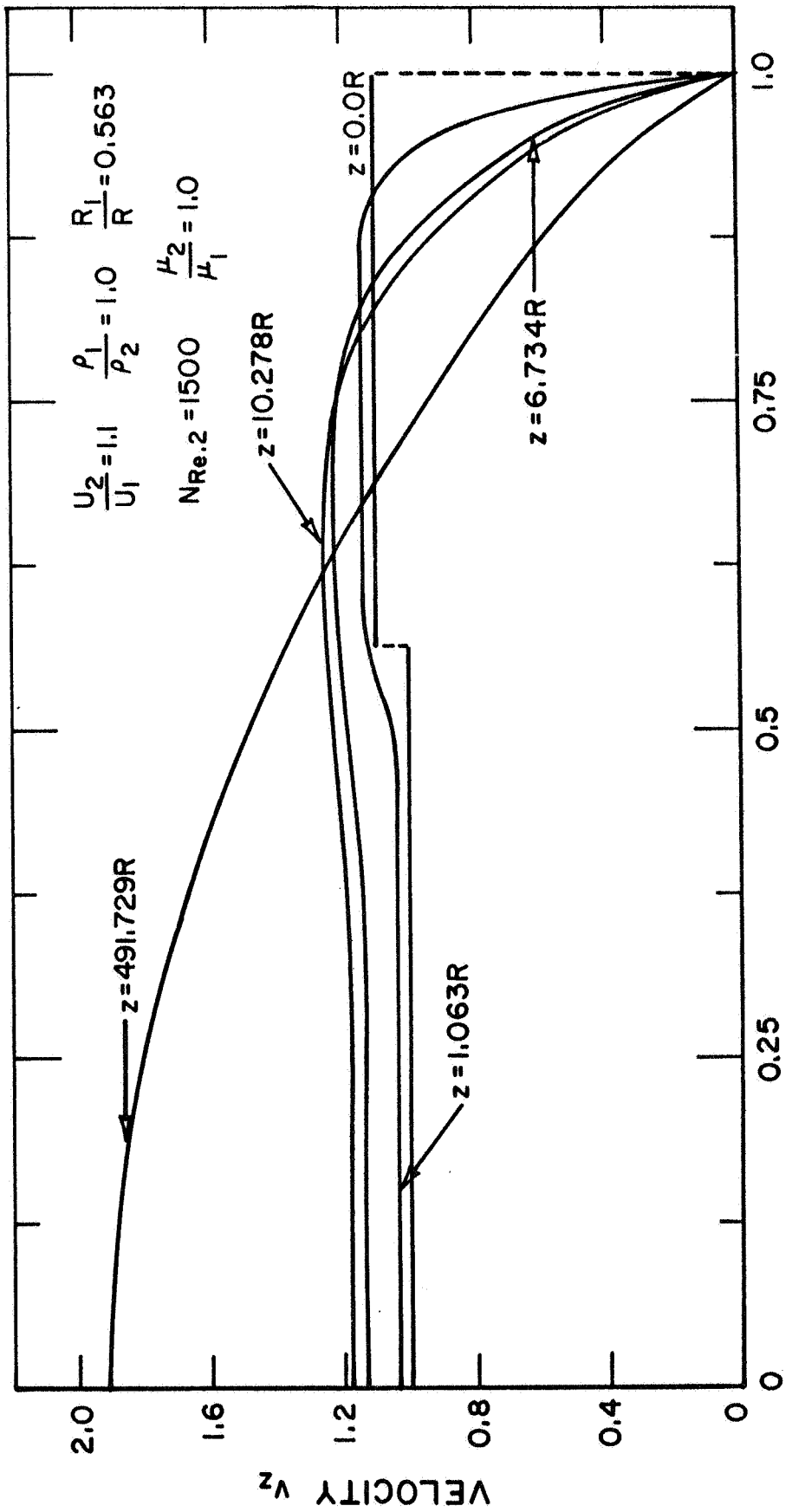

FIGURE 31. AXIAL VELOCITY PROFILES FOR RUN NO. 55.

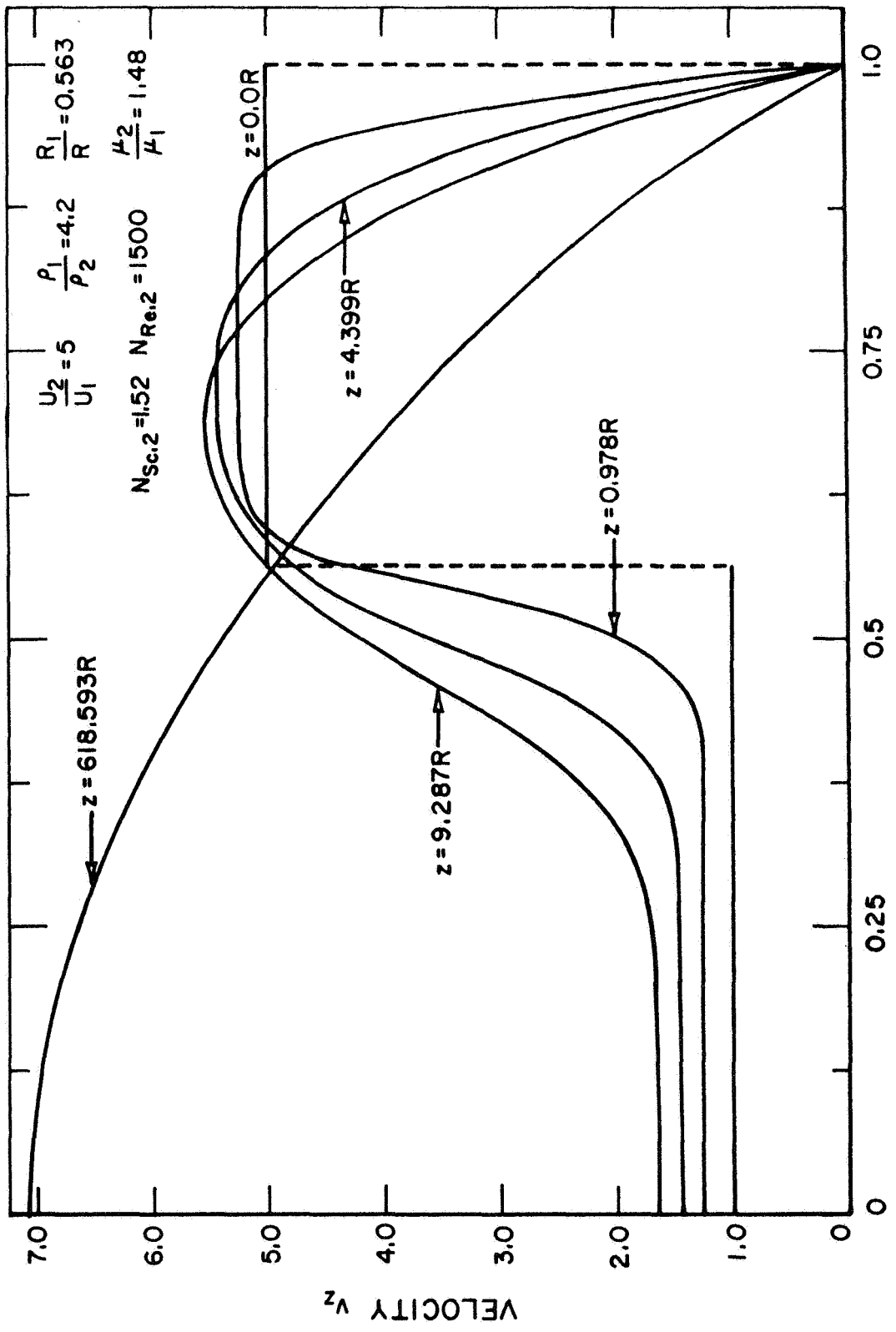

FIGURE 32. AXIAL VELOCITY PROFILES FOR RUN NO. 43.

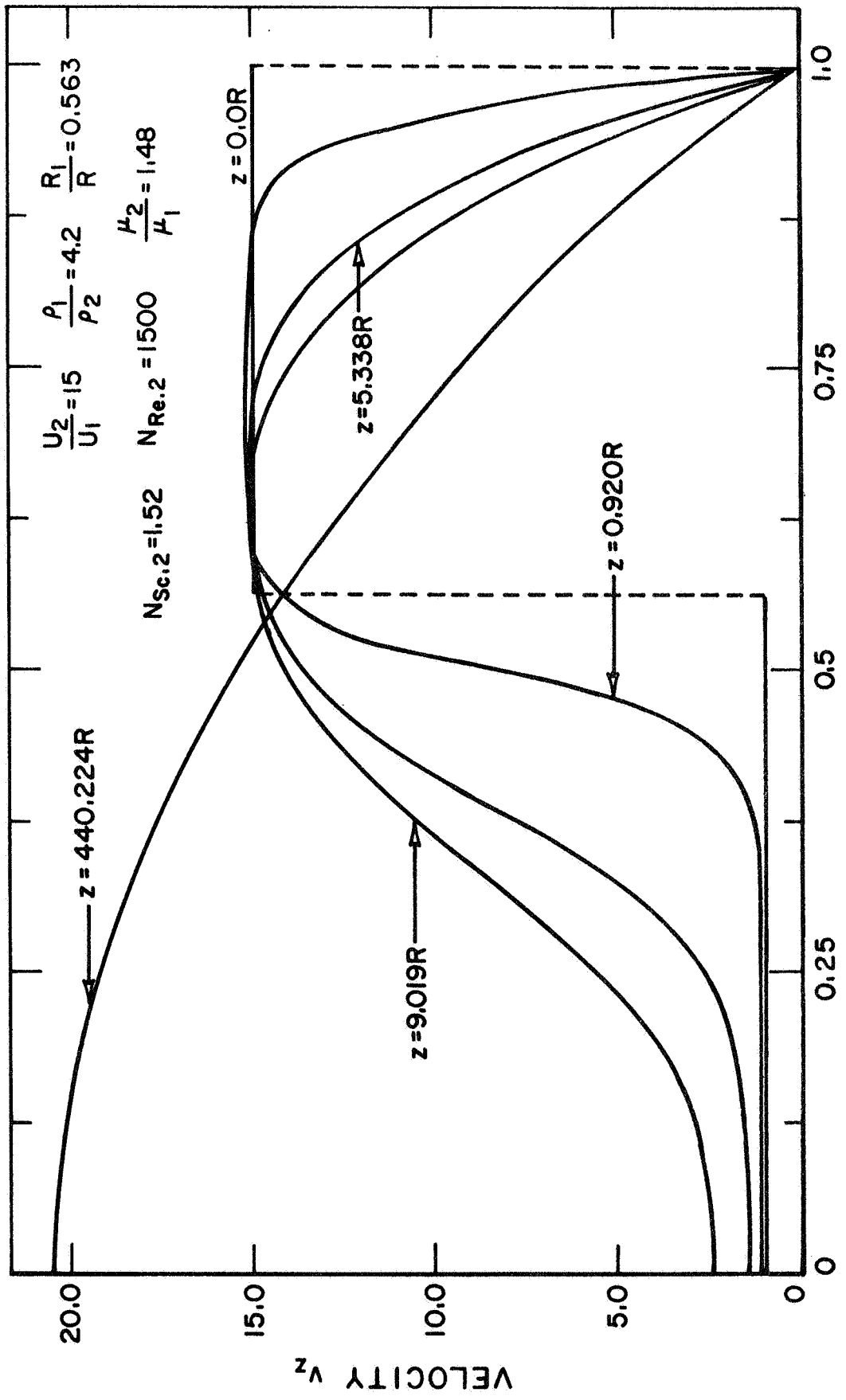

FIGURE 33. AXIAL VELOCITY PROFILES FOR RUN NO. 6.

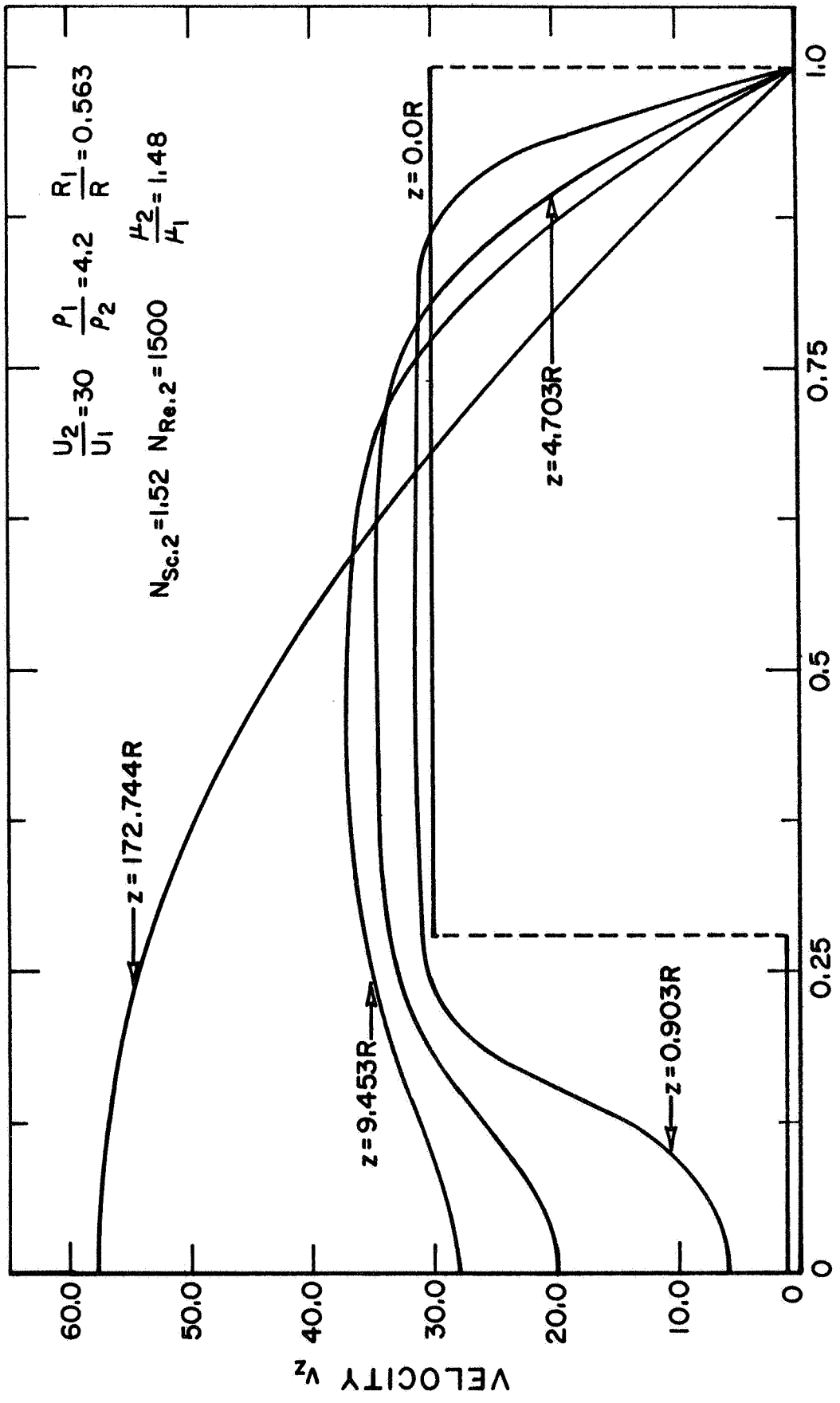

FIGURE 34. AXIAL VELOCITY PROFILES FOR RUN NO. 49.

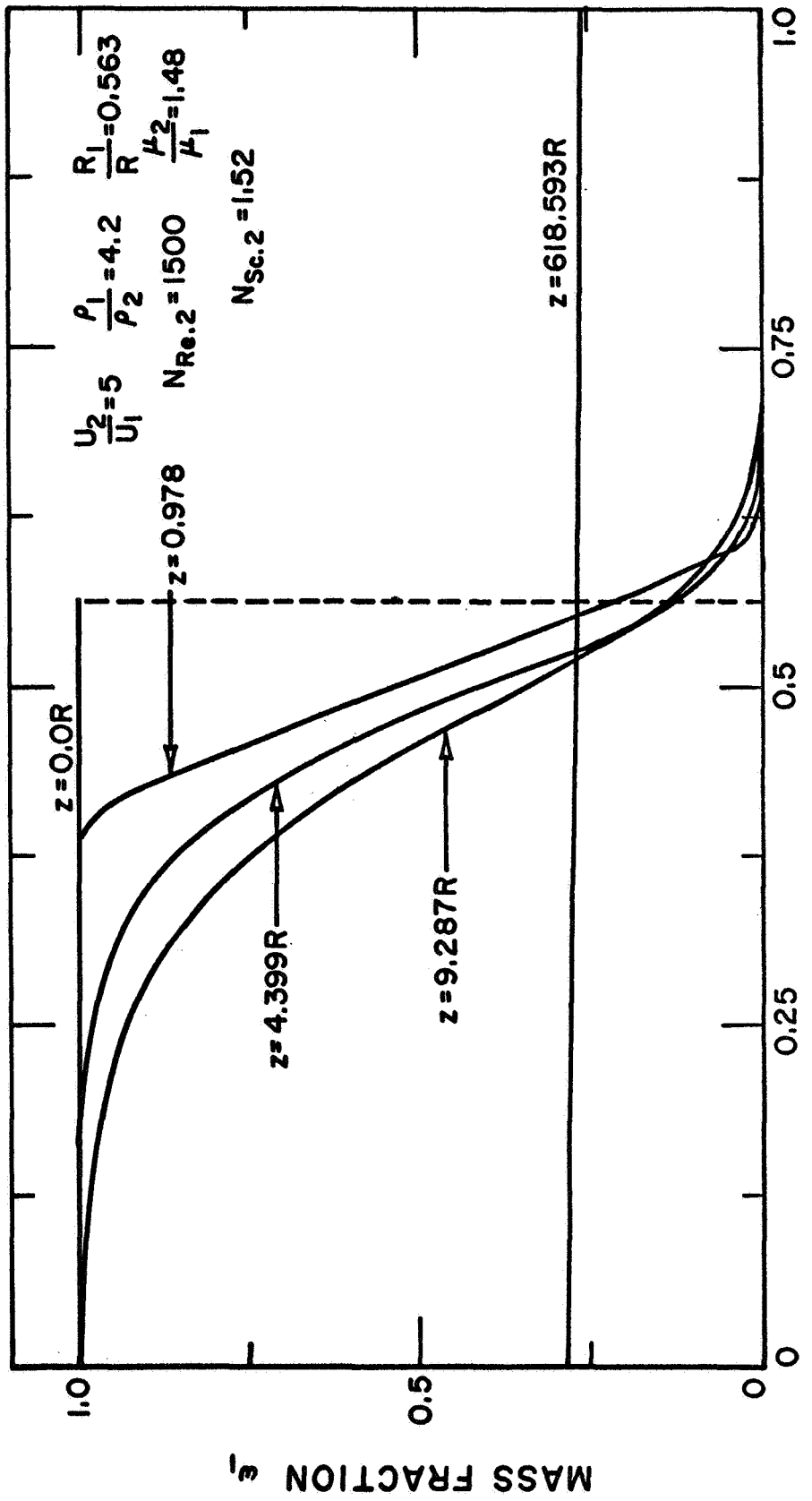

FIGURE 35. MASS FRACTION PROFILES FOR RUN NO. 43.

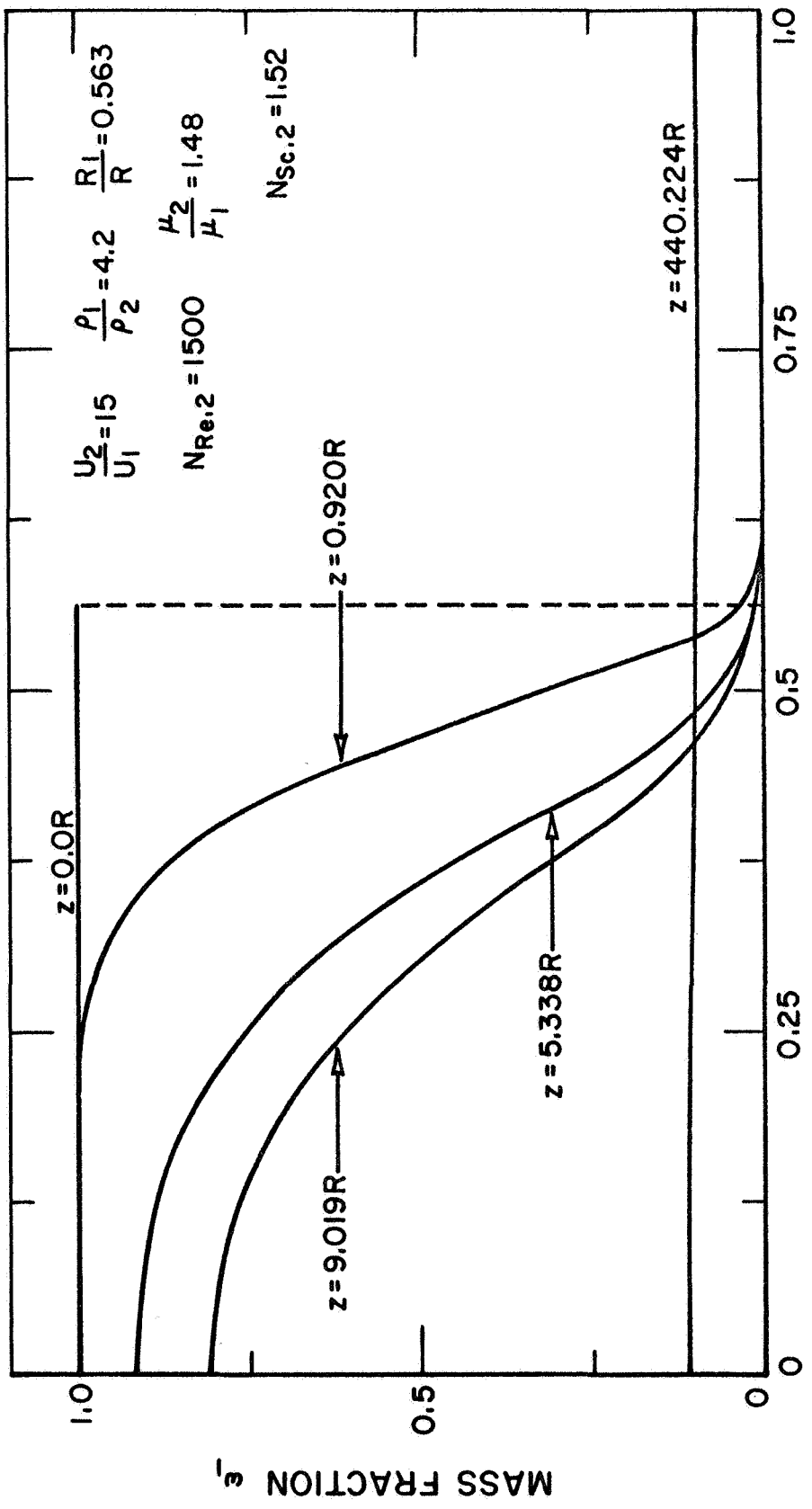

FIGURE 36. MASS FRACTION PROFILES FOR RUN NO. 6.

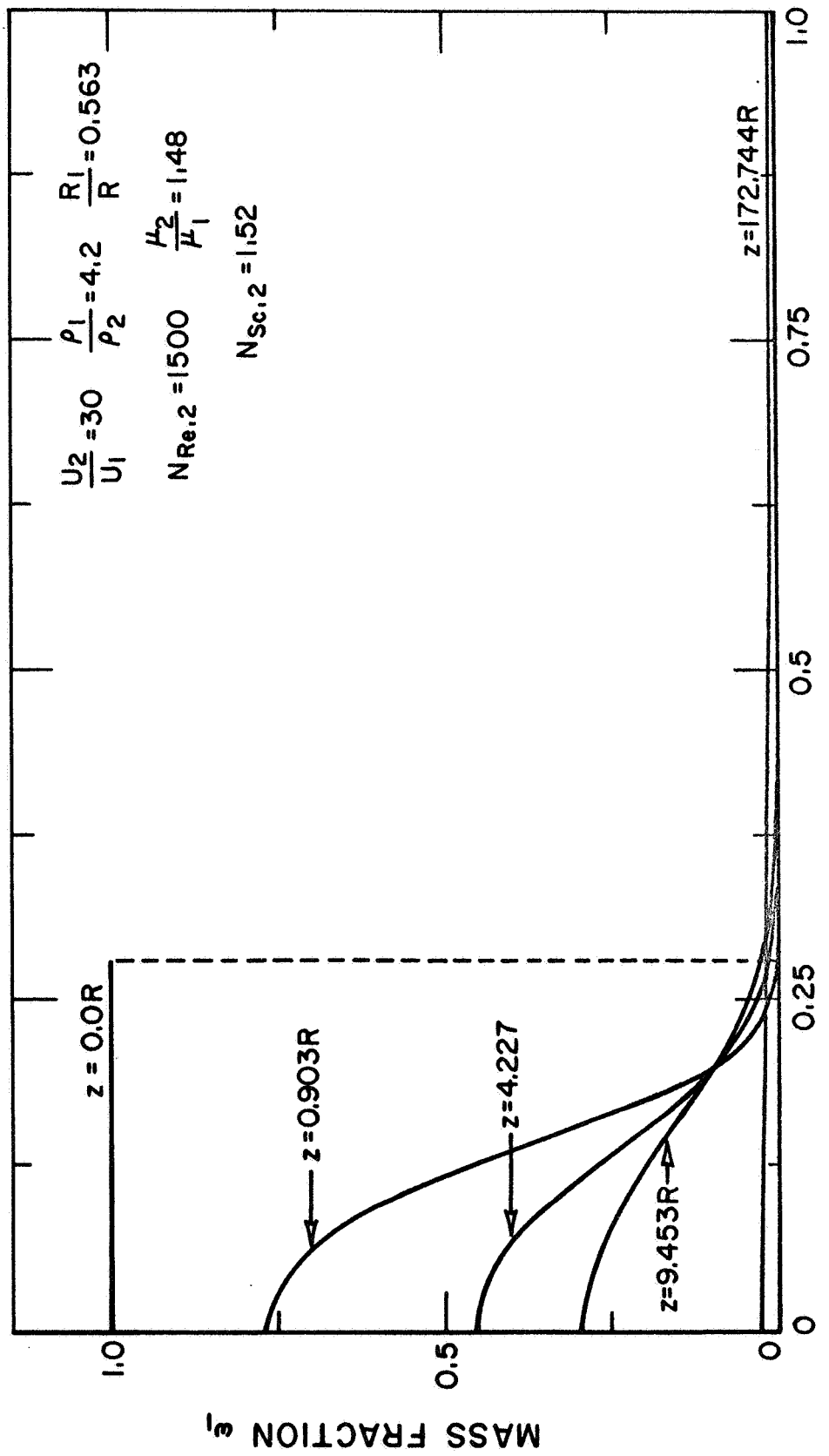

FIGURE 37. MASS FRACTION PROFILES FOR RUN NO. 49.

CHAPTER 5

CONCLUSION

The laminar heterogeneous mixing of coaxial axisymmetric confined jets has been investigated in order to provide a better understanding of the fluid mechanics of a coaxial flow gas-core nuclear reactor. The analysis is valid in the complete entrance region of the confining duct and permits wide variations of the inlet parameters. The flow field considered was isothermal and non-reacting. The low-velocity and high-density central gas stream mixes with a coflowing high-velocity low-density annular stream. The mathematical model of the problem was described by the boundary layer equations in the von Mises plane. These equations were solved by an explicit finite difference scheme. Numerical stability of the finite difference equations was ensured by satisfying Karplus' stability criterion. The von Neumann stability analysis was found to yield stability conditions similar to Karplus' conditions.

The results of the present analysis cannot be validated by direct comparison since neither experimental nor analytical results are available for such a flow problem. Hence, the numerical method

developed was verified by using it to solve the classical entrance flow problem. Also, as a partial check on the results of each case investigated, the fully developed values of the flow parameters were compared with the corresponding asymptotic values that were obtained independently from simple theoretical considerations. The agreement obtained in these comparisons establishes reliance in the numerical results.

The effects of the parameters $\frac{U_2}{U_1}$, $\frac{\rho_1}{\rho_2}$, $\frac{R_1}{R}$, $N_{Re,2}$, $N_{Sc,2}$, and $\frac{\mu_2}{\mu_1}$ were studied on L_{ω_1}, L_v, $v_{z,1}$, $\omega_{1,w}$ and η. A total of 57 flow cases, presented in Appendix D, was investigated. Typical running time for generating the results up to fully developed flow values was about ten minutes on the IBM 360/40 computer. The following conclusions may be drawn from the results of the parametric study.

The length of the mass fraction potential core, L_{ω_1}, decreases as $\frac{U_2}{U_1}$ increases, but L_{ω_1} increases as $\frac{\rho_1}{\rho_2}$ as well as $N_{Sc,2}$ increase. Also, L_{ω_1} increases with increase in $N_{Re,2}$; this variation remains similar when $\frac{R_1}{R}$ is reduced and $\frac{U_2}{U_1}$ is substantially increased.

The length L_v of the velocity potential core increases with increase in $\frac{U_2}{U_1}$ as well as with increase in $N_{Sc,2}$. An increase in $N_{Re,2}$ causes an increase in L_v and, at constant $N_{Re,2}$, an increase in $\frac{\rho_1}{\rho_2}$ increases L_v; similar behavior is also observed at lower $\frac{R_1}{R}$ and higher $\frac{U_2}{U_1}$. At low velocity ratios, increase in $\frac{\rho_1}{\rho_2}$ causes an increase in L_v, but at higher velocity ratios, higher $\frac{\rho_1}{\rho_2}$ results in smaller L_v. These conclusions must be substantiated with further results as L_v is very sensitive to pressure gradient.

For incompressible flow, the asymptotic centerline velocity depends only on the radius ratio and the entrance velocities, so that the effect of the other parameters is confined to the mixing region only. An increase in $\frac{\rho_1}{\rho_2}$ reduces the centerline velocity in the mixing region, while an increase in $\frac{R_1}{R}$ slows down the development of the flow. An increase of $N_{Re,2}$ decreases the centerline velocity for $\frac{U_2}{U_1} = 5$ and $\frac{R_1}{R} = 0.563$; this behavior remains unaltered when $\frac{U_2}{U_1}$ is increased to 30 and $\frac{R_1}{R}$ is reduced to 0.28. The centerline velocity decreases with increase in $N_{Sc,2}$; the flow develops faster for lower $N_{Sc,2}$.

An increase in $\frac{U_2}{U_1}$ or a decrease in $\frac{\rho_1}{\rho_2}$ or $\frac{R_1}{R}$, reduces the spreading of the jet. The asymptotic value of the mass fraction depends only on the ratios $\frac{U_2}{U_1}$, $\frac{\rho_1}{\rho_2}$ and $\frac{R_1}{R}$ for incompressible flow;

hence the effect of the other parameters is felt in the initial mixing region only. The wall mass fraction decreases as $N_{Re,2}$ increases for $\frac{U_2}{U_1} = 5$ and $\frac{R_1}{R} = 0.563$; this effect is similar when $\frac{U_2}{U_1}$ is increased to 30 and $\frac{R_1}{R}$ is reduced to 0.28, with the exception that mixing is considerably faster in the latter case. An increase in $N_{Sc,2}$ causes a marked decrease on the rate of mixing.

The effect of mixing is indicated by a mass ratio η^*. η decreases as $\frac{U_2}{U_1}$ increases and η increases as $\frac{\rho_1}{\rho_2}$ increases; η decreases as $\frac{R_1}{R}$ decreases, indicating a considerable reduction in the loss of mass of the jet. At $\frac{U_2}{U_1} = 5$, $\frac{R_1}{R} = 0.563$, increase of $N_{Re,2}$ increases η; this effect remains similar on increasing $\frac{U_2}{U_1}$ to 30 and reducing $\frac{R_1}{R}$ to 0.28, although in the latter case, mixing is very rapid. Increase of $N_{Sc,2}$ retards the mass diffusion process, resulting in an increase in η.

A reduction in the developing length results from an increase in $\frac{U_2}{U_1}$ or a decrease in $\frac{\rho_1}{\rho_2}$. An increase in $\frac{U_2}{U_1}$ leads to rapid

---

* As defined in 4.5.5

$$\eta = \frac{\left[\begin{array}{l}\text{mass of species 1 in a given volume (between the entrance} \\ \text{section and a section downstream) of the confining duct}\end{array}\right]}{\left[\begin{array}{l}\text{mass of species 1 in the same volume had there been} \\ \text{no mixing}\end{array}\right]}$$

change of the centerline values, i.e., rapid mixing and narrower jet.

For some combinations of the flow parameters, a positive pressure gradient or an oscillatory negative pressure gradient was observed in the initial region. These lead to rather inexact description of the initial region and a deterioration in the agreement of the end values, depending upon the extent of the affected initial region. This behavior is not completely understood as yet and further investigation may be necessary. Also, for the cases investigated, the effect of change in $\frac{\mu_2}{\mu_1}$ was small, so that no definite trend of this effect could be established.

In the course of the investigation, numerical instability was encountered for some combinations of the flow parameters. It is recommended that some grouping of these parameters be found in order to determine its range over which a stable numerical solution may be obtained. Also, the original aim of the von Mises transformation or of the φ-transformation was to obtain stable solutions for a wide range of the flow parameters. Experience with a similar jet mixing problem in the r-z plane revealed that the range in the ψ-z or the φ-z plane was not much wider; as such, it may be worth the

attempt to solve the present flow problem in the physical plane where non-uniform entrance profiles can also be studied more conveniently.

As mentioned in section 4.5, turbulent jet mixing is being experimentally investigated by Weinstein and his associates at the Illinois Institute of Technology. An investigation of confined coaxial turbulent mixing of heterogeneous jets has been recently completed by this group. The measured effects of $\frac{U_2}{U_1}$ and $\frac{\rho_1}{\rho_2}$ on the jet mixing agrees qualitatively with the prediction of the present report. Thus for laminar as well as turbulent mixing,

> The length of the mass fraction potential core L_{ω_1} decreases as $\frac{U_2}{U_1}$ increases and an increase in $\frac{\rho_1}{\rho_2}$ causes a decrease in the rate of mixing and hence increases the developing length.

Hence, the present study provides trends which are useful in understanding turbulent jet mixing.

APPENDIX A

DERIVATION OF EQUATIONS FOR ρ, $\frac{dp}{dz}$ AND v_r

A.1 Expression for Density

The two relations employed in the derivation of Equation (4), the expression for density of a binary system, can be found in Reference 27. These are

$$x_1 M_1 + x_2 M_2 = M \tag{A-1}$$

$$\frac{\omega_1}{M_1} + \frac{\omega_2}{M_2} = \frac{1}{M} \tag{A-2}$$

where

M molecular weight of mixture

M_i molecular weight of fluid component i; $i = 1,2$

x_i mole fraction of species i; $i = 1,2$

ω_i mass fraction species i; $i = 1,2$

From Equations (A-1) and (A-2), it can be shown that

$$x_1 = \frac{\frac{\omega_1}{M_1}}{\frac{\omega_1}{M_1} + \frac{\omega_2}{M_2}} \tag{A-3}$$

In the present analysis, density is assumed to be a function of composition only. Hence,

$$\rho = x_1 \rho_{p,1} + x_2 \rho_{p,2} \tag{A-4}$$

where

ρ	mass average density of mixture
$\rho_{p,i}$	density of pure component i; i = 1,2

Using the relation

$$x_1 + x_2 = 1 \tag{A-5}$$

Equation (A-4) becomes

$$\rho = x_1 \left[\rho_{p,1} - \rho_{p,2} \right] + \rho_{p,2} \tag{A-6}$$

Substituting Equation (A-3) into Equation (A-6) gives the required expression for density.

$$\rho = \frac{\frac{\omega_1}{M_1}}{\frac{\omega_1}{M_1} + \frac{\omega_2}{M_2}} \left[\rho_{p,1} - \rho_{p,2} \right] + \rho_{p,2} \qquad \text{(A-7)}$$

A.2 Equation of Constraint in the φ-z Plane

Details of the derivation of the Equation of Constraint, Equation (68), which is used to evaluate $\frac{dp}{dz}$, are given below.

The mass rate of flow across every section of the duct is given by Equation (11).

$$\int_0^R 2\pi r \rho v_z \, dr = \dot{m} \qquad \text{(A-8)}$$

Differentiating Equation (A-8) with respect to z and simplifying,

$$\int_0^R r \frac{\partial(\rho v_z)}{\partial z} \, dr = 0 \qquad \text{(A-9)}$$

This integral relation in the physical plane can be transformed to the von Mises plane by using the relation

$$\int_0^R F(r,z)\,dr = \int_0^\Psi F(\psi,z) \frac{1}{J} \, d\psi \qquad \text{(A-10)}$$

where J is the Jacobian of the transformation.

Using the relation (A-10), Equation (A-9) can be transformed to the von Mises plane as

$$\int_0^{\Psi} \left[-\rho v_r r \frac{\partial(\rho v_z)}{\partial \psi} + \frac{\partial(\rho v_z)}{\partial z} \right] \frac{d\psi}{\rho v_z} = 0 \qquad \text{(A-11)}$$

Transforming Equation (A-11) to the φ-z plane gives

$$\int_0^{\Phi} \left[-\rho v_r r \frac{d\varphi}{d\psi} \frac{\partial(\rho v_z)}{\partial \varphi} + \frac{\partial(\rho v_z)}{\partial z} \right] \frac{d\varphi}{\rho v_z \frac{d\varphi}{d\psi}} = 0 \qquad \text{(A-12)}$$

The momentum Equation (67) in the φ-z plane can be written, after rearranging, as

$$\frac{\partial(\rho v_z)}{\partial z} = v_z \frac{\partial \rho}{\partial z} - \left[\frac{1}{v_z} \frac{dp}{dz} \right] + \rho \frac{d\varphi}{d\psi} \cdot \frac{\partial}{\partial \varphi} \left[\mu r^2 \rho v_z \frac{d\varphi}{d\psi} \frac{\partial v_z}{\partial \varphi} \right] \qquad \text{(A-13)}$$

Equation (A-13) is substituted into Equation (A-12) to give

$$\int_0^{\Phi} \left\{ - \rho v_r r \frac{d\varphi}{d\psi} \frac{\partial(\rho v_z)}{\partial\varphi} + v_z \frac{\partial\rho}{\partial z} - \frac{1}{v_z} \frac{dp}{dz} \right.$$

$$\left. + \rho \frac{d\varphi}{d\psi} \frac{\partial}{\partial\varphi} \left[\mu r^2 \rho v_z \frac{d\varphi}{d\psi} \frac{\partial v_z}{\partial\varphi} \right] \right\} \frac{d\varphi}{\rho v_z \frac{d\varphi}{d\psi}} = 0 \qquad \text{(A-14)}$$

Rearranging Equation (A-14) yields

$$\frac{dp}{dz} = \frac{1}{\int_0^{\Phi} \frac{d\varphi}{\rho v_z^2 \frac{d\varphi}{d\psi}}} \int_0^{\Phi} \left[\begin{array}{l} - \rho v_r r \frac{d\varphi}{d\psi} \frac{\partial(\rho v_z)}{\partial\varphi} + v_z \frac{\partial\rho}{\partial z} \\ \\ + \rho \frac{d\varphi}{d\psi} \frac{\partial}{\partial\varphi} \left[\mu r^2 \rho v_z \frac{d\varphi}{d\psi} \frac{\partial v_z}{\partial\varphi} \right] \end{array} \right] \frac{d\varphi}{\rho v_z \frac{d\varphi}{d\psi}}$$

(A-15)

In order to obtain Equation (68) from Equation (A-15), the term $\frac{\partial\rho}{\partial z}$ in Equation (A-15) must be replaced by the derivative of Equation (A-7). Differentiating Equation (A-7) with respect to z gives

$$\frac{\partial\rho}{\partial z} = \frac{\frac{\partial\omega_1}{\partial z}}{M_1 M_2 \left[\frac{\omega_1}{M_1} + \frac{\omega_2}{M_2} \right]^2} \left[\rho_{p,1} - \rho_{p,2} \right] \qquad \text{(A-16)}$$

and substitution of Equation (A-16) into Equation (A-15) yields

$$\frac{dp}{dz} = \frac{1}{\int_0^{\Phi} \frac{1}{\rho v_z^2} \frac{d\varphi}{d\psi} d\varphi} \int_0^{\Phi} \left[\begin{array}{l} - \rho v_r \, r \, \frac{d\varphi}{d\psi} \frac{\partial(\rho v_z)}{\partial \varphi} \\ \\ + \frac{v_z \frac{\partial \omega_1}{\partial z}}{M_1 M_2 \left[\frac{\omega_1}{M_1} + \frac{\omega_2}{M_2} \right]^2} \left[\rho_{p,1} - \rho_{p,2} \right] \\ \\ + \rho \frac{d\varphi}{d\psi} \frac{\partial}{\partial \varphi} \left[\mu r^2 \rho v_z \frac{d\varphi}{d\psi} \frac{\partial v_z}{\partial \varphi} \right] \end{array} \right] \frac{d\varphi}{\rho v_z \frac{d\varphi}{d\psi}} \tag{A-17}$$

This equation is the required equation of constraint.

A.3 Equation for Determining v_r

As mentioned earlier in Chapter 2, v_r is determined from a modified form of the continuity equation. This equation for v_r is derived here.

The continuity equation (1) in the physical plane

$$\frac{\partial}{\partial r} (\rho v_r r) + \frac{\partial}{\partial z} (\rho v_z r) = 0 \tag{A-18}$$

when integrated between r and $r + \Delta_1 r$, gives

$$\left[\rho v_r r\right]_r^{r+\Delta_1 r} = - \int_r^{r+\Delta_1 r} r \frac{\partial}{\partial z} (\rho v_z) dr \qquad \text{(A-19)}$$

Using the mean value theorem, Equation (A-19) can be written as

$$\left[\rho v_r r\right]_{r_1}^{r_2} = - \left[\frac{\partial}{\partial z} (\rho v_z)\right]_{mv} \int_{r_1}^{r_2} r \, dr \qquad \text{(A-20)}$$

where

$$r_1 = r \qquad \text{(A-21)}$$

$$r_2 = r + \Delta_1 r \qquad \text{(A-22)}$$

$$mv = \text{mean value}$$

Simplifying, Equation (A-20) becomes

$$\left[\rho v_r r\right]_{r_2} = \left[\rho v_r r\right]_{r_1} - \left[\frac{\partial}{\partial z} (\rho v_z)\right]_{mv} \left[\frac{r_2^2 - r_1^2}{2}\right] \qquad \text{(A-23)}$$

Equation (A-23) can be transformed to the φ-z plane as

$$\left[\rho v_r r\right]_{r_2} = \left[\rho v_r r\right]_{r_1} - \left[- \rho v_r r \frac{d\varphi}{d\psi} \frac{\partial(\rho v_z)}{\partial \varphi} + \frac{\partial(\rho v_z)}{\partial z}\right]_{mv} \left[\frac{r_2^2 - r_1^2}{2}\right] \qquad \text{(A-24)}$$

or

$$\left[\rho v_r r\right]_{r_2} = \left[\rho v_r r\right]_{r_1} + \frac{1}{2} r_{2,1} \left[\begin{array}{l} \left\{ \left[\rho^2 v_r r \frac{d\varphi}{d\psi}\right]_{r_1} + \left[\rho^2 v_r r \frac{d\varphi}{d\psi}\right]_{r_2} \right\} \left[\frac{\partial v_z}{\partial \varphi}\right]_{mv} \\ + \left\{ \left[\rho v_r r v_z \frac{d\varphi}{d\psi}\right]_{r_1} + \left[\rho v_r r v_z \frac{d\varphi}{d\psi}\right]_{r_2} \right\} \left[\frac{\partial \rho}{\partial \varphi}\right]_{mv} \\ - \left\{ \left[\frac{\partial(\rho v_z)}{\partial z}\right]_{r_1} + \left[\frac{\partial(\rho v_z)}{\partial z}\right]_{r_2} \right\} \end{array} \right] \tag{A-25a}$$

where

$$r_{2,1} = \frac{r_2^2 - r_1^2}{2} \tag{A-25b}$$

Solving explicitly for $v_{r_{r_2}}$, Equation (A-25) gives the following equation which is used for the evaluation of v_r.

$$\left[v_r\right]_{r_2} = \frac{\left[\rho v_r r\right]_{r_1} + \frac{1}{2}\left[P_1 + P_2\right]\left[\frac{r_2^2 - r_1^2}{2}\right]}{\left[\rho r\right]_{r_2}\left\{1 - P_3\left[\frac{r_2^2 - r_1^2}{2}\right]\right\}} \tag{A-26}$$

where

$$P_1 = \left[\rho^2 v_r r \frac{d\varphi}{d\psi}\right]_{r_1} \left[\frac{\partial v_z}{\partial \varphi}\right]_{mv} + \left[\rho v_r r v_z \frac{d\varphi}{d\psi}\right]_{r_1} \left[\frac{\partial \rho}{\partial \varphi}\right]_{mv} \tag{A-27}$$

$$P_2 = -\left[\frac{\partial(\rho v_z)}{\partial z}\right]_{r_1} - \left[\frac{\partial(\rho v_z)}{\partial z}\right]_{r_2} \tag{A-28}$$

$$P_3 = \frac{1}{2}\left[\rho \frac{d\varphi}{d\psi}\right]_{r_2} \left[\frac{\partial v_z}{\partial \varphi}\right]_{mv} + \frac{1}{2}\left[v_z \frac{d\varphi}{d\psi}\right]_{r_2} \left[\frac{\partial \rho}{\partial \varphi}\right]_{mv} \tag{A-29}$$

APPENDIX B

FINITE DIFFERENCES AND THEIR PRESENT APPLICATION

Finite difference techniques play an important role in obtaining solutions of coupled non-linear PDEs not solvable at present by analytical methods. A brief review of the various finite difference forms, the basic definitions of terms used in the stability analysis and the selection of the finite difference scheme for the present study are presented here.

B.1 Approximation of Derivatives by Finite Differences

Taylor's series expansion is the basic principle used in establishing a finite difference approximation (FDA) to the derivative of a variable at a point. Assuming that a sufficient number of higher derivatives exists, three basic forms are available for FDAs of continuous derivatives, namely, forward, backward and central differences. Using the discretized rectangular grid shown in Figure 2, these may be written as

Forward Difference

$$\left[\frac{\partial F}{\partial r}\right]_{m,n} = \frac{F(m+1,n) - F(m,n)}{\Delta r} - O(\Delta r) \qquad \text{(B-1)}$$

Backward Difference

$$\left[\frac{\partial F}{\partial r}\right]_{m,n} = \frac{F(m-1,n) - F(m,n)}{\Delta r} + O(\Delta r) \qquad (B\text{-}2)$$

Central Difference

$$\left[\frac{\partial F}{\partial r}\right]_{m,n} = \frac{F(m+1,n) - F(m-1,n)}{2\Delta r} - O(\Delta r)^2 \qquad (B\text{-}3)$$

Similarly, a second derivative can be given by

$$\left[\frac{\partial^2 F}{\partial r^2}\right]_{m,n} = \frac{F(m+1,n) - 2F(m,n) + F(m-1,n)}{\Delta r^2} + O(\Delta r)^2 \qquad (B\text{-}4)$$

Forms similar to the above FDAs may be derived for $\frac{\partial F}{\partial z}$ and $\frac{\partial^2 F}{\partial z^2}$.

The difference between a derivative and the FDA used to represent it is known as the truncation error. The central difference approximation given by Equation (B-3) has a truncation error of order $(\Delta r)^2$ and, hence, its use is desired so far as possible. Also, the FDAs having truncation errors of order higher than $(\Delta r)^2$ could be obtained by introducing additional points in the neighborhood of (m,n), such as (m,n+2) and (m,n-2), etc. However, with these forms, special

equations are needed for treating the points adjacent to the boundaries; also the computations at each grid point require increased computer time. Reference 34 has a comprehensive table for the various finite difference representations of continuous derivatives.

B.2 Numerical Stability, Consistency and Convergence

In order that the obtained solution of the finite difference equations (FDEs) be meaningful, it is necessary to ensure consistency, stability and convergence of the numerical computation scheme used. Von Neumann's[23] definitions of these terms, as interpreted by Agarwal and Torda,[18] are included here for the sake of completeness.

An FDE is consistent with its corresponding PDE if the truncation error in the difference equation goes to zero as the grid steps approach zero.

An FDE is stable if its numerical solution remains bounded at given values of the independent coordinates as the step sizes tend to zero. In general, stability is a function of only the difference equations, and has no direct connection with the differential problem.

The exact solution of an FDE converges to the exact solution of its corresponding PDE if the truncation error of the solution goes to zero as the grid steps approach zero.

Consistency and stability, considered individually, are only necessary, not sufficient for convergence. For a properly posed linear boundary value problem, consistency and stability together constitute

the necessary as well as sufficient conditions for convergence. Thus, it is sufficient to ensure consistency and numerical stability of the difference equations. Convergence will then be implied. For a non-linear boundary value problem, convergence can be proved by a method due to Strang.[25]

The consistency requirement mentioned above is satisfied for all the FDAs given in the previous section. A certain amount of caution, however, must be observed in a few rather exceptional cases. Richtmyer[35] quotes the DuFort and Frankel[36] approximation to the simple partial differential equation $u_{xx} = u_t$ and demonstrates that the consistency of the method depends on the way in which Δx and Δt are allowed to approach zero. In the present work, stability is ensured by satisfying the conditions obtained by Karplus'[22] and von Neumann's[23] methods.

B.3 Selection of Finite Difference Scheme

For a given partial differential equation there are several FDAs each having its own stability limits. Sherman and Grey[14] gave a detailed discussion of the presently known finite difference schemes for the solution of parabolic partial differential equations. Two of the widely known and used schemes are the explicit and the implicit methods. In both of these methods, the original non-linear PDEs are reduced to a set of linear algebraic equations. However, there is one basic difference. In the explicit scheme, the FDEs at

a grid point can be solved independently of each other, whereas, in the implicit schemes, the FDEs at a new line of integration must be solved simultaneously.

Implicit methods have gained wide favor because they are unconditionally stable for a wide class of problems compared to simple explicit methods which are often limited by stability consideration to the use of a small step size. Unfortunately, for many complex problems including the present study, implicit methods are more complex since in addition to the main dependent variables, there are subsidiary dependent variables and the task of solving the resultant simultaneous equations is difficult. Also, though the number of grid points at which computations are needed is reduced, the number of computations at each grid point increases, hence in general the total time required by the problem is still considerable. Although stability may not restrict the step sizes, other physical considerations like accuracy and desired resolution may often do so.

From the above paragraph, it is clear that the more complex a problem becomes in terms of non-linearities, number of subsidiary dependent variables or other complexities, the more necessary it becomes to use the most simple scheme. Additional factors are ease of programming and ease of checking the program. Based on these considerations, an all-explicit numerical method is used for the present study.

APPENDIX C

NUMERICAL STABILITY ANALYSES OF THE FINITE DIFFERENCE EQUATIONS

The two criteria used in the present analysis for testing difference equations for stability are those due to Karplus[22] and von Neumann. The latter method was first given by O'Brien, Hyman and Kaplan.[23] The methods as well as the derivations of the stability conditions are presented here.

C.1 Karplus' Method

C.1.1 Criterion for Stability

Karplus developed a criterion for the stability of finite difference equations using an analogy with Kirchoff's laws in electric circuit theory. The general application of this circuit theory approach to finite difference stability may be given as follows.

The FDE, whose stability at the point (m,n) is to be considered, represents an approximation to a PDE, and in general, it can be arranged as

$$a\left[F(m+1,n) - F(m,n)\right] + b\left[F(m-1,n) - F(m,n)\right]$$

$$+ c\left[F(m,n+1) - F(m,n)\right] + d\left[F(m,n-1) - F(m,n)\right] = 0 \qquad \text{(C-1)}$$

where F is the dependent variable, and a, b, c, d are the coefficients of the difference terms. Also, the coefficient a is positive and m refers to a bounded space coordinate.

Then the FDE is stable

1. if all the coefficients are positive (C-2)

or

2. if, when all the coefficients are not positive, the sum of all the coefficients is negative. (C-3)

The criterion is also applicable to equations in several independent variables and to equations in which the coefficients are not constant. Because of its simplicity, Karplus' method is presently finding wide applications.

C.1.2 Determination of Stability Conditions

The numerical stability conditions of the finite difference equations used in determining the values of the flow parameters are derived by the Karplus method.

Momentum Equation

Equation (88) is the finite difference form of the momentum equation. To obtain the stability conditions for this equation, it is rearranged in the form of Equation (C-1) to give

$$\left[2\mu r^2 \rho v_z \left[\frac{d\varphi}{d\psi}\right]^2 + 2\mu \frac{d\varphi}{d\psi} \Delta\varphi + \mu r^2 \rho v_z \frac{d^2\varphi}{d\psi^2} \Delta\varphi + r^2 \left[\frac{d\varphi}{d\psi}\right]^2 F_M \Delta\varphi \right]_{m,n} \left[\frac{v_z(m+1,n) - v_z(m,n)}{2\Delta\varphi^2} \right]$$

$$- \left[- 2\mu r^2 \rho v_z \left[\frac{d\varphi}{d\psi}\right]^2 + 2\mu \frac{d\varphi}{d\psi} \Delta\varphi + \mu r^2 \rho v_z \frac{d^2\varphi}{d\psi^2} \Delta\varphi + r^2 \left[\frac{d\varphi}{d\psi}\right]^2 F_M \Delta\varphi \right]_{m,n} \left[\frac{v_z(m-1,n) - v_z(m,n)}{2\Delta\varphi^2} \right]$$

$$- \left[\frac{v_z(m,n+1) - v_z(m,n)}{\Delta z} \right] - \left[\frac{1}{\rho v_z} \frac{dp}{dz} \right]_{m,n} = 0 \qquad \text{(C-4)}$$

where

$$F_M = \mu\rho \frac{\partial v_z}{\partial\varphi} + \mu v_z \frac{\partial\rho}{\partial\varphi} + \rho v_z \frac{\partial\mu}{\partial\varphi} \qquad \text{(C-5)}$$

To apply the Karplus criterion, it is necessary to determine the sign of the coefficient of the first term in Equation (C-4), i.e., the sign of the quantity

$$2\mu r^2 \rho v_z \left[\frac{d\varphi}{d\psi}\right]^2 + 2\mu \frac{d\varphi}{d\psi} \Delta\varphi + \mu r^2 \rho v_z \frac{d^2\varphi}{d\psi^2} \Delta\varphi + r^2 \left[\frac{d\varphi}{d\psi}\right]^2 F_M \Delta\varphi \qquad \text{(C-6)}$$

From an order of magnitude analysis and numerical experimentation, it is found that expression (C-6) is positive, i.e.,

$$\left[2\mu r^2 \rho v_z \left[\frac{d\varphi}{d\psi}\right]^2 + 2\mu \frac{d\varphi}{d\psi} \Delta\varphi + \mu r^2 \rho v_z \frac{d^2\varphi}{d\psi^2} \Delta\varphi + r^2 \left[\frac{d\varphi}{d\psi}\right]^2 F_M \Delta\varphi \right] > 0 \tag{C-7}$$

or

$$\Delta\varphi > - \frac{2\mu r^2 \rho v_z \left[\frac{d\varphi}{d\psi}\right]^2}{2\mu \frac{d\varphi}{d\psi} + \mu r^2 \rho v_z \frac{d^2\varphi}{d\psi^2} + r^2 \left[\frac{d\varphi}{d\psi}\right]^2 F_M} \tag{C-8}$$

Examining the inequality (C-8) shows that

$$2\mu r^2 \rho v_z \left[\frac{d\varphi}{d\psi}\right]^2 > 0 \tag{C-9}$$

and though $\frac{d^2\varphi}{d\psi^2} < 0$ for the present transformation, the expression

$$2\mu \frac{d\varphi}{d\psi} + \mu r^2 \rho v_z \frac{d^2\varphi}{d\psi^2} + r^2 \left[\frac{d\varphi}{d\psi}\right]^2 F_M > 0 \tag{C-10}$$

Thus, condition (C-8) becomes

$$\Delta\varphi > - \text{ positive quantity} \tag{C-11}$$

i.e.,

$\Delta\varphi$ has no limitation from stability consideration.

It is seen in Equation (C-4) that the coefficients are not all of the same sign. Thus, applying Karplus' condition (C-3), Equation (C-4) yields

$$\left[4\mu r^2 \rho v_z \left[\frac{d\varphi}{d\psi}\right]^2 \right]_{m,n} \frac{1}{2\Delta\varphi^2} - \frac{1}{\Delta z} < 0 \qquad \text{(C-12)}$$

i.e.,

$$\Delta z < \left[\frac{1}{2\mu} \cdot \frac{1}{r^2 \rho v_z} \frac{1}{\left[\frac{d\varphi}{d\psi}\right]^2} \right]_{m,n} \Delta\varphi^2 \qquad \text{(C-13)}$$

Thus, the stability conditions for Equation (88) are

1. $\Delta\varphi$ has no restriction (C-14)

2. $$\Delta z < \left[\frac{1}{2\nu} \frac{1}{r^2 \rho^2 v_z} \frac{1}{\left[\frac{d\varphi}{d\psi}\right]^2} \right]_{m,n} \Delta\varphi^2 \qquad \text{(C-15)}$$

Centerline Momentum Equation

At the centerline, the finite difference form of the momentum equation is given by Equation (91). Arranging it in the form corresponding to Equation (C-1) results in the equation

$$2\mu_{m,n} \left[\frac{v_z(m+1,n) - v_z(m,n)}{\Delta\varphi^2} \right] - \left[\frac{v_z(m,n+1) - v_z(m,n)}{\Delta z} \right]$$

$$- \left[\frac{1}{\rho v_z} \frac{dp}{dz} \right]_{m,n} = 0 \qquad \text{(C-16)}$$

Multiplying Equation (C-16) by $\Delta\varphi^3$ and rewriting,

$$2\mu_{m,n}\Delta\varphi\left[v_z(m+1,n) - v_z(m,n)\right] - \Delta\varphi^3\left[\frac{v_z(m,n+1) - v_z(m,n)}{\Delta z}\right]$$

$$- \Delta\varphi^3\left[\frac{1}{\rho v_z}\frac{dp}{dz}\right]_{m,n} = 0 \qquad \text{(C-17)}$$

Examination of the coefficient of the first term reveals that

$$2\mu_{m,n}\Delta\varphi > 0 \qquad \text{(C-18)}$$

i.e.,

$$\Delta\varphi > 0 \qquad \text{(C-19)}$$

Hence $\Delta\varphi$ has no stability restriction.

All the coefficients of Equation (C-16) are not of the same sign, hence, using condition (C-3), Equation (C-16) yields

$$\frac{2\mu_{m,n}}{\Delta\varphi^2} - \frac{1}{\Delta z} < 0 \qquad \text{(C-20)}$$

i.e.,

$$\Delta z < \frac{1}{2\mu_{m,n}}\Delta\varphi^2 \qquad \text{(C-21)}$$

Summarizing, the stability conditions for Equation (91) are

1. $\Delta\varphi$ has no restriction (C-22)

2. $$\Delta z < \frac{1}{2\mu_{m,n}} \Delta\varphi^2 \qquad \text{(C-23)}$$

Diffusion Equation

In order to determine the stability conditions of the finite difference form of the diffusion equation, Equation (94) is rearranged in the form of Equation (C-1) to give

$$\left[2r^2\rho^2 D_{12} v_z \left[\frac{d\varphi}{d\psi}\right]^2 + r^2\rho^2 D_{12} v_z \frac{d^2\varphi}{d\psi^2} \Delta\varphi + 2\rho D_{12} \frac{d\varphi}{d\psi} \Delta\varphi + r^2 F_D \left[\frac{d\varphi}{d\psi}\right]^2 \Delta\varphi \right]_{m,n} \left[\frac{\omega_1(m+1,n) - \omega_1(m,n)}{2\Delta\varphi^2} \right]$$

$$- \left[- 2r^2\rho^2 D_{12} v_z \left[\frac{d\varphi}{d\psi}\right]^2 + r^2\rho^2 D_{12} v_z \frac{d^2\varphi}{d\psi^2} \Delta\varphi + 2\rho D_{12} \frac{d\varphi}{d\psi} \Delta\varphi + r^2 F_D \left[\frac{d\varphi}{d\psi}\right]^2 \Delta\varphi \right]_{m,n} \left[\frac{\omega_1(m-1,n) - \omega_1(m,n)}{2\Delta\varphi^2} \right]$$

$$- \left[\frac{\omega_1(m,n+1) - \omega_1(m,n)}{\Delta z} \right] = 0 \qquad \text{(C-24)}$$

where

$$F_D = \rho^2 D_{12} \frac{\partial v_z}{\partial\varphi} + 2\rho D_{12} \frac{\partial\rho}{\partial\varphi} + \rho^2 v_z \frac{\partial D_{12}}{\partial\varphi} \qquad \text{(C-25)}$$

To apply Karplus' criterion, it is necessary to determine the sign of the following expression

$$\left\{ 2r^2\rho^2 D_{12} v_z \left[\frac{d\varphi}{d\psi}\right]^2 + r^2\rho^2 D_{12} v_z \frac{d^2\varphi}{d\psi^2} \Delta\varphi + 2\rho D_{12} \frac{d\varphi}{d\psi} \Delta\varphi + r^2 F_D \left[\frac{d\varphi}{d\psi}\right]^2 \Delta\varphi \right\} \tag{C-26}$$

From an order of magnitude analysis and some numerical experimentation, it was found that expression (C-26) is positive, i.e.,

$$\left\{ 2r^2\rho^2 D_{12} v_z \left[\frac{d\varphi}{d\psi}\right]^2 + r^2\rho^2 D_{12} v_z \frac{d^2\varphi}{d\psi^2} \Delta\varphi + 2\rho D_{12} \frac{d\varphi}{d\psi} \Delta\varphi + r^2 F_D \left[\frac{d\varphi}{d\psi}\right]^2 \Delta\varphi \right\} > 0 \tag{C-27}$$

i.e.,

$$\Delta\varphi > \frac{-2r^2\rho^2 D_{12} v_z \left[\frac{d\varphi}{d\psi}\right]^2}{2\rho D_{12} \frac{d\varphi}{d\psi} + r^2\rho^2 D_{12} v_z \frac{d^2\varphi}{d\psi^2} + r^2 F_D \left[\frac{d\varphi}{d\psi}\right]^2} \tag{C-28}$$

Examining the right hand member of the above inequality

$$2r^2\rho^2 D_{12} v_z \left[\frac{d\varphi}{d\psi}\right]^2 > 0 \tag{C-29}$$

Also, though $\frac{d^2\varphi}{d\psi^2} < 0$ for the present transformation, the expression in the denominator of the right hand member is positive, i.e.,

$$\left[2\rho D_{12} \frac{d\varphi}{d\psi} + r^2\rho^2 D_{12} v_z \frac{d^2\varphi}{d\psi^2} + r^2 F_D \left[\frac{d\varphi}{d\psi}\right]^2 \right] > 0 \qquad \text{(C-30)}$$

Thus,

$$\Delta\varphi > -\left[\text{positive quantity}\right] \qquad \text{(C-31)}$$

i.e.,

$\Delta\varphi$ has no stability limitations.

The coefficients in Equation (C-24) are not all of the same sign. Therefore, using Karplus' condition (C-3), Equation (C-24) yields

$$\left[4r^2\rho^2 D_{12} v_z \left[\frac{d\varphi}{d\psi}\right]^2 \right]_{m,n} \frac{1}{2\Delta\varphi^2} - \frac{1}{\Delta z} < 0 \qquad \text{(C-32)}$$

i.e.,

$$\Delta z < \left[\frac{1}{2D_{12}} \quad \frac{1}{r^2\rho^2 v_z} \quad \frac{1}{\left[\frac{d\varphi}{d\psi}\right]^2} \right]_{m,n} \Delta\varphi^2 \qquad \text{(C-33)}$$

Thus the stability conditions for the Equation (94) are

1. $\Delta\varphi$ has no restriction (C-34)

2. $$\Delta z < \left[\frac{N_{Sc}}{2\nu} \quad \frac{1}{r^2\rho^2 v_z} \quad \frac{1}{\left[\frac{d\varphi}{d\psi}\right]^2} \right]_{m,n} \Delta\varphi^2 \qquad \text{(C-35)}$$

Centerline Diffusion Equation

At the centerline, the finite difference form of the diffusion equation is given by Equation (97). Arranging it in the form corresponding to Equation (C-1) results in the equation

$$2\rho D_{12}\left[\frac{\omega_1(m+1,n) - \omega_1(m,n)}{\Delta\varphi^2}\right] - \left[\frac{\omega_1(m,n+1) - \omega_1(m,n)}{\Delta z}\right] = 0 \qquad (C\text{-}36)$$

Multiplying Equation (C-36) by $\Delta\varphi^3$ and rewriting

$$2\rho D_{12}\Delta\varphi\left[\omega_1(m+1,n) - \omega_1(m,n)\right] - \Delta\varphi^3\left[\frac{\omega_1(m,n+1) - \omega_1(m,n)}{\Delta z}\right] = 0 \qquad (C\text{-}37)$$

Examining the coefficient of the first term reveals that

$$\left[2\rho D_{12}\right]_{m,n}\Delta\varphi > 0 \qquad (C\text{-}38)$$

i.e.,

$$\Delta\varphi > 0 \qquad (C\text{-}39)$$

Hence, $\Delta\varphi$ has no restriction from stability consideration.

Both the coefficients in Equation (C-36) are not of the same sign. Hence, applying Karplus' condition (C-3) to Equation (C-35) yields

$$\frac{\left[2\rho D_{12}\right]_{m,n}}{\Delta\varphi^2} - \frac{1}{\Delta z} < 0 \qquad (C\text{-}40)$$

i.e.,

$$\Delta z < \frac{1}{\left[2\rho D_{12} \right]_{m,n}} \Delta\varphi^2 \qquad \text{(C-41)}$$

Summarizing, the stability conditions for Equation (97) are

1. $\Delta\varphi$ has no restriction (C-42)

2. $$\Delta z < \frac{1}{\left[2\rho D_{12} \right]_{m,n}} \Delta\varphi^2 \qquad \text{(C-43)}$$

C.2 Von Neumann's Method

C.2.1 Criterion for Stability

The von Neumann stability analysis reported by O'Brien, Hyman and Kaplan[23] was later extended by Lax and Richtmyer[35] who have shown various circumstances under which the von Neumann condition is a sufficient as well as a necessary condition for convergence. The Lax-Richtmyer analysis of stability is presented in detail by Richtmyer[35] and the following is a summary of the same analysis presented here for the sake of completeness.

The difference equations are assumed to be linear and two spatial variables m and n are used, with n denoting the axial direction. Thus, the following system of linear difference equations with constant coefficients is analyzed for stability.

$$\sum_{N_1(\bar{\beta})} B^{1}_{\bar{\beta}}\, \bar{u}^{n+1}\,(\varphi_1 + \beta_1\Delta\varphi_1, \ldots, \varphi_d + \beta_d\Delta\varphi_d)$$

$$+ \sum_{N_o(\bar{\beta})} B^{o}_{\bar{\beta}}\, \bar{u}^{n}\,(\varphi_1 + \beta_1\Delta\varphi_1, \ldots, \varphi_d + \beta_d\Delta\varphi_d) = 0 \qquad \text{(C-44)}$$

where

$\bar{u}^{n+1}$ the solution function of the difference equation at the new line, i.e., vector whose components are the values of the dependent variables at a point of the new line.

$\bar{u}^{n}$ the solution function at a point of the previous line.

$\bar{\beta}$ the vector whose components are $\beta_1, \ldots, \beta_d$, the value of which indicates the point of the new line.

$B^{1}_{\bar{\beta}}$ a p x p matrix, where p is the number of dependent variables. The elements of the matrix are the coefficients of the terms of the equations. The superscript indicates the line, the subscript the point on the line. (Similar definition holds for $B^{o}_{\bar{\beta}}$).

$\sum_{N_i}$ Summation over the points of the new line.

$\sum_{N_o}$ Summation over the previous line.

$\varphi_1, \ldots, \varphi_d$ Denotes the coordinates of a lattice point.

The stability criterion for the above difference equations is that the absolute values of the eigenvalues of the amplification matrix $G(\Delta z, \bar{k})$ obey the inequality

$$\left| \lambda^i \right| \leq 1 + O(\Delta z) \qquad \text{for } 0 < \Delta z < z, \quad i = 1, \ldots, p \tag{C-45}$$

where

$$G = -\left[H_1 \right]^{-1} \left[H_0 \right] \tag{C-46}$$

$$H_1 = \sum_{N_1(\bar{\beta})} B^1_{\bar{\beta}} \exp\left[i \left[k_1 \beta_1 \Delta\varphi_1 + \ldots + k_d \beta_d \Delta\varphi_d \right] \right] \tag{C-47}$$

and

$$H_0 = \sum_{N_0(\bar{\beta})} B^1_{\bar{\beta}} \exp\left[i \left[k_1 \beta_1 \Delta\varphi_1 + \ldots + k_d \beta_d \Delta\varphi_d \right] \right] \tag{C-48}$$

Equation (C-45) is the von Neumann necessary condition for stability. In the present study, $\bar{\varphi}$ is a scalar and hence Equations (C-47) and (C-48) reduce to:

$$H_1 = \sum_{N_1(\bar{\beta})} B^1_{\bar{\beta}} e^{ik\Delta\varphi} \tag{C-49}$$

$$H_0 = \sum_{N_0(\bar{\beta})} B^0_{\bar{\beta}} e^{ik\Delta\varphi} \tag{C-50}$$

Determination of the Stability Conditions

The numerical stability conditions of the finite difference Equations (88) and (94) used in determining the values of the flow parameters are derived by von Neumann's method. As required by this method, Equations (88) and (94) are first linearized. The notations of Richtmyer[35] are used in this section.

Momentum Equation

The difference Equation (88) is rewritten, retaining only the linear terms.

$$\frac{(v_z)_m^{n+1} - (v_z)_m^n}{\Delta z} = -\left[\frac{1}{\rho v_z}\frac{dp}{dz}\right]_m^n + \left[\mu\rho v_z r^2\left[\frac{d\varphi}{d\psi}\right]^2\right]_m^n \left[\frac{(v_z)_{m+1}^n - 2(v_z)_m^n + (v_z)_{m-1}^n}{2\Delta\varphi}\right] + \left[\mu\rho v_z r^2\frac{d^2\varphi}{d\psi^2} + 2\mu\frac{d\varphi}{d\psi}\right]_m^n \left[\frac{(v_z)_{m+1}^n - (v_z)_{m-1}^n}{2\Delta\varphi}\right] \quad \text{(C-51)}$$

Rearranging Equation (C-51) and substituting

$$\sigma = \frac{\Delta z}{\Delta\varphi^2} \quad \text{(C-52)}$$

leads to the following equation

$$\left[v_z \right]_m^{n+1} - \left[\mu\rho v_z r^2 \sigma \left[\frac{d\varphi}{d\psi}\right]^2 + \mu\sigma \frac{d\varphi}{d\psi} \Delta\varphi + \frac{1}{2} \mu\rho v_z r^2 \frac{d^2\varphi}{d\psi^2} \sigma\Delta\varphi \right]_m^n$$

$$\left[v_z \right]_{m+1}^{n} + \left[-\mu\rho v_z r^2 \sigma \left[\frac{d\varphi}{d\psi}\right]^2 + \mu\sigma \frac{d\varphi}{d\psi} \Delta\varphi + \frac{1}{2} \mu\rho v_z r^2 \frac{d^2\varphi}{d\psi^2} \sigma\Delta\varphi \right]_m^n$$

$$\left[v_z \right]_{m-1}^{n} - \left[1 - 2\mu\rho v_z r^2 \sigma \left[\frac{d\varphi}{d\psi}\right]^2 \right]_m^n \left[v_z \right]_m^n + \left[\frac{1}{\rho v_z} \frac{dp}{dz} \right]_m^n = 0 \qquad \text{(C-53)}$$

The matrices H_o and H_1 can now be calculated on substituting the Fourier series for the dependent variable. It is to be noted that superscripts n and n+1 replace the superscripts 0 and 1.

$$B_m^n = \left[-1 + 2\mu\rho v_z r^2 \sigma \left[\frac{d\varphi}{d\psi}\right]^2 \right]_m^n \qquad \text{(C-54)}$$

$$B_{m+1}^n = \left[-\mu\rho v_z r^2 \sigma \left[\frac{d\varphi}{d\psi}\right]^2 - \mu\sigma \frac{d\varphi}{d\psi} \Delta\varphi - \frac{\mu}{2} \rho v_z r^2 \frac{d^2\varphi}{d\psi^2} \sigma\Delta\varphi \right]_m^n \qquad \text{(C-55)}$$

$$B_{m-1}^n = \left[-\mu\rho v_z r^2 \sigma \left[\frac{d\varphi}{d\psi}\right]^2 + \mu\sigma \frac{d\varphi}{d\psi} \Delta\varphi + \frac{\mu}{2} \rho v_z r^2 \frac{d^2\varphi}{d\psi^2} \sigma\Delta\varphi \right]_m^n \qquad \text{(C-56)}$$

$$B_m^{n+1} = 1 \tag{C-57}$$

Now

$$H_n = B_m^n \, e^{ikm\Delta\varphi} + B_{m+1}^n \, e^{ik(m+1)\Delta\varphi} + B_{m-1}^n \, e^{ik(m-1)\Delta\varphi} \tag{C-58}$$

Substituting Equations (C-54) through (C-57) into Equation (C-58) yields

$$\begin{aligned} H_n = & \left[-1 + 2\mu\rho v_z r^2 \left[\frac{d\varphi}{d\psi}\right]^2 \right]_m^n e^{ikm\Delta\varphi} \\ & + \left[-\mu\rho v_z r^2 \sigma \left[\frac{d\varphi}{d\psi}\right]^2 - \mu\sigma \frac{d\varphi}{d\psi}\Delta\varphi - \frac{\mu}{2}\rho v_z r^2 \frac{d^2\varphi}{d\psi^2}\sigma\Delta\varphi \right]_m^n e^{ik(m+1)\Delta\varphi} \\ & + \left[-\mu\rho v_z r^2 \sigma \left[\frac{d\varphi}{d\psi}\right]^2 + \mu \frac{d\varphi}{d\psi}\sigma\Delta\varphi + \frac{\mu}{2}\rho v_z r^2 \frac{d^2\varphi}{d\psi^2}\sigma\Delta\varphi \right]_m^n e^{ik(m-1)\Delta\varphi} \end{aligned} \tag{C-59}$$

On simplifying, Equation (C-59) gives

$$H_n = e^{ikm\Delta\varphi} \left[\begin{array}{l} -1 + 2\mu\rho v_z r^2 \sigma \left[\frac{d\varphi}{d\psi}\right]^2 \\ -\mu\rho v_z r^2 \left[\frac{d\varphi}{d\psi}\right]^2 \sigma \left[e^{ik\Delta\varphi} + e^{-ik\Delta\varphi} \right] \\ -\mu\sigma \frac{d\varphi}{d\psi}\Delta\varphi \left[e^{ik\Delta\varphi} - e^{-ik\Delta\varphi} \right] \\ -\frac{\mu}{2}\rho v_z r^2 \frac{d^2\varphi}{d\psi^2}\sigma\Delta\varphi \left[e^{ik\Delta\varphi} - e^{-ik\Delta\varphi} \right] \end{array} \right] \tag{C-60}$$

Using the following identities

$$\cos k\Delta\varphi \equiv \frac{e^{ik\Delta\varphi} + e^{-ik\Delta\varphi}}{2} \tag{C-61}$$

$$\sin k\Delta\varphi \equiv \frac{e^{ik\Delta\varphi} - e^{-ik\Delta\varphi}}{2i} \tag{C-62}$$

$$\cos \frac{2k\Delta\varphi}{2} \equiv 1 - 2 \sin^2 k\frac{\Delta\varphi}{2} \tag{C-63}$$

and simplifying, Equation (C-60) gives

$$H_n = e^{-ikm\Delta\varphi}\left\{ - 1 + 2\mu\rho v_z r^2 \sigma\left[\frac{d\varphi}{d\psi}\right]^2 \left[1 - \cos k\Delta\varphi \right]\right.$$

$$\left. - \left[2 \frac{d\varphi}{d\psi} + \frac{\rho}{2} v_z r^2 \frac{d^2\varphi}{d\psi^2} \right] (i\mu\sigma\Delta\varphi) \sin k\Delta\varphi \right\} \tag{C-64}$$

Similarly, using Equation (C-56), H_1 can be written as

$$H_{n+1} = e^{ikm\Delta\varphi} \left[1 \right] \tag{C-65}$$

The amplification matrix G can be obtained by substituting Equations (C-60) and (C-65) into Equation (C-46) and simplifying

$$G = \left\{ 1 - 4\mu\rho v_z r^2 \sigma \left[\frac{d\varphi}{d\psi}\right]^2 \sin^2 k\frac{\Delta\varphi}{2} + i\left[\frac{2d\varphi}{d\psi} + \frac{\rho}{2} v_z r^2 \frac{d^2\varphi}{d\psi^2}\right] \mu\sigma\Delta\varphi \sin k\Delta\varphi \right\} \tag{C-66}$$

or

$$|G| = \left[\left[1 - 4\mu\rho v_z r^2 \sigma \left[\frac{d\varphi}{d\psi}\right]^2 \sin^2 k\frac{\Delta\varphi}{2}\right]^2 + \left[2\frac{d\varphi}{d\psi} + \frac{\rho}{2} v_z r^2 \frac{d^2\varphi}{d\psi^2}\right]^2 \mu^2\sigma^2 \Delta\varphi^2 \sin^2 k\Delta\varphi \right]^{\frac{1}{2}} \tag{C-67}$$

Using the von Neumann condition (C-45), Equation (C-67) yields, after simplification,

$$\left\{ \left[1 - 4\mu\rho v_z r^2 \sigma \left[\frac{d\varphi}{d\psi}\right]^2 \sin^2 k\frac{\Delta\varphi}{2}\right]^2 + \left[2\frac{d\varphi}{d\psi} + \frac{\rho}{2} v_z r^2 \frac{d^2\varphi}{d\psi^2}\right]^2 \mu^2\sigma O(\Delta z) \sin^2 k\Delta\varphi \right\} \leq 1 \tag{C-68}$$

The second term on the left hand side is of order (Δz) and is neglected, in comparison with the first term. Simplifying, the above inequality becomes

$$\pm \left[1 - 4\mu\rho v_z r^2 \sigma \left[\frac{d\varphi}{d\psi}\right]^2 \sin^2 k\frac{\Delta\varphi}{2}\right] \leq 1 \tag{C-69}$$

Using the positive sign,

$$\sigma \geq 0 \tag{C-70}$$

Using the negative sign,

$$-1 + 4\mu\rho v_z r^2 \sigma \left[\frac{d\varphi}{d\psi}\right]^2 \sin^2 k\frac{\Delta\varphi}{2} \leq 1 \qquad \text{(C-71)}$$

Therefore

$$\sigma \leq \frac{1}{2\mu}\frac{1}{\rho v_z r^2}\frac{1}{\left[\frac{d\varphi}{d\psi}\right]^2}\frac{1}{\sin^2\frac{k\Delta\varphi}{2}} \qquad \text{(C-72)}$$

The minimum value of σ is obtained when $\sin^2\frac{k\Delta\varphi}{2} = 1$ and is given by

$$\sigma \leq \frac{1}{2\mu}\frac{1}{\rho v_z r^2}\frac{1}{\left[\frac{d\varphi}{d\psi}\right]^2} \qquad \text{(C-73)}$$

Thus, substituting Equation (C-52) into Equations (C-70) and (C-73) gives

$$0 \leq \Delta z \leq \frac{1}{2\mu}\frac{1}{r^2\rho v_z}\frac{1}{\left[\frac{d\varphi}{d\psi}\right]^2}\Delta\varphi^2 \qquad \text{(C-74)}$$

i.e.,

$$\Delta z < \left[\frac{1}{2\nu}\frac{1}{r^2\rho^2 v_z}\frac{1}{\left[\frac{d\varphi}{d\psi}\right]^2}\right]_m^n \Delta\varphi^2 \qquad \text{(C-75)}$$

Diffusion Equation

The difference Equation (94) is rewritten retaining only the linear terms.

$$\frac{(\omega_1)_m^{n+1} - (\omega_1)_m^n}{\Delta z} = \left[r^2\rho^2 D_{12} v_z \left[\frac{d\varphi}{d\psi}\right]^2\right]_m^n \left[\frac{(\omega_1)_{m+1}^n - (2\omega_1)_m^n + (\omega_1)_{m-1}^n}{\Delta\varphi^2}\right]$$

$$+\left[r^2\rho^2 D_{12} v_z \frac{d^2\varphi}{d\psi^2} + 2\rho D_{12} \frac{d\varphi}{d\psi}\right]_m^n \left[\frac{(\omega_1)_{m+1}^n - (\omega_1)_{m-1}^n}{2\Delta\varphi}\right] \qquad \text{(C-76)}$$

Using the procedure as discussed in the derivation of the stability condition for the momentum equation and using the von Neumann conditions (C-45), Equation (C-76) gives

$$-1 + 4r^2\rho^2 D_{12} v_z \sigma \left[\frac{d\varphi}{d\psi}\right]^2 \sin^2 \frac{k\Delta\varphi}{2} \leq 1 \qquad \text{(C-77)}$$

After simplification Equation (C-77) becomes

$$\Delta z < \left[\frac{N_{Sc}}{2\nu} \frac{1}{r^2\rho^2 v_z} \frac{1}{\left(\frac{d\varphi}{d\psi}\right)^2}\right]_m^n \Delta\varphi^2 \qquad \text{(C-78)}$$

The von Neumann conditions (C-75) and (C-78) for the momentum and diffusion equations are identical to the Karplus conditions (C-15) and (C-35) for the same equations.

Thus, the present stability analysis leads to the observation that Karplus' criterion is simpler to apply as compared to the von Neumann criterion.

APPENDIX D

INITIAL DATA FOR FLOW CASES INVESTIGATED

A total of 57 flow cases was investigated for the parametric study of the confined jet mixing problem. Detailed results of all these cases are available but are presented here for only some selected cases. In all these cases, the confining duct radius R, the outer stream density ρ_2, and the outer stream viscosity μ_2 had the following constant values.

1. $R = 0.0833$ ft.

2. $\rho_2 = 0.075 \frac{\text{lbm.}}{\text{cu.ft.}}$

3. $\mu_2 = 0.124 \times 10^{-4} \frac{\text{lbm.}}{\text{ft.sec.}}$

The values of the flow parameters at the initial section are presented here in tabular form.

$$U_1 = 0.227 \frac{ft}{sec}, \quad \frac{U_2}{U_1} = 15, \quad \frac{R_1}{R} = 0.563, \quad \frac{\rho_1}{\rho_2} = 4.223, \quad N_{Re,2} = 1500$$

Run No.	$\frac{\mu_2}{\mu_1}$	$N_{Sc,2}$	$N_{Re,1}$
1	0.750	0.750	410
2	0.750	1.519	410
3	0.750	2.000	410
4	1.000	1.519	544
5	1.475	0.750	803
6	1.475	1.519	803
7	1.475	2.000	803
8	1.750	1.519	953
9	2.000	0.750	1090
10	2.000	1.519	1090
11	2.000	2.000	1090

$$U_1 = 0.227 \frac{ft}{sec}, \quad \frac{U_2}{U_1} = 15, \quad \frac{R_1}{R} = 0.563, \quad \frac{\rho_1}{\rho_2} = 8.333, \quad N_{Re,2} = 1500$$

Run No.	$\frac{\mu_2}{\mu_1}$	$N_{Sc,2}$	$N_{Re,1}$
12	0.750	0.750	772
13	0.750	1.519	772
14	0.750	2.000	772
15	1.000	1.519	1073
16	1.475	0.750	1520
17	1.475	1.519	1520
18	1.475	2.000	1520
19	1.750	1.519	1878
20	2.000	0.750	2065
21	2.000	1.519	2065
22	2.000	2.000	2065

$$U_1 = 0.138 \frac{ft}{sec}, \quad \frac{U_2}{U_1} = 15, \quad \frac{R_1}{R} = 0.280, \quad \frac{\rho_1}{\rho_2} = 4.223, \quad N_{Re,2} = 1500$$

Run No.	$\frac{\mu_2}{\mu_1}$	$N_{Sc,2}$	$N_{Re,1}$
23	0.750	0.750	123
24	0.750	1.519	123
25	0.750	2.000	123
26	1.475	0.750	243
27	1.475	1.519	243
28	1.475	2.000	243
29	2.000	0.750	330
30	2.000	1.519	330
31	2.000	2.000	330

$$U_1 = 0.138 \frac{ft}{sec}, \quad \frac{U_2}{U_1} = 15, \quad \frac{R_1}{R} = 0.280, \quad \frac{\rho_1}{\rho 2} = 8.333, \quad N_{Re,2} = 1500$$

Run No.	$\frac{\mu_2}{\mu_1}$	$N_{Sc,2}$	$N_{Re,1}$
32	0.750	0.750	234
33	0.750	1.519	234
34	0.750	2.000	234
35	1.475	0.750	460
36	1.475	1.519	460
37	1.475	2.000	460
38	2.000	0.750	625
39	2.000	1.519	625
40	2.000	2.000	625

$$\frac{R_1}{R} = 0.563 \ , \quad \frac{U_2}{U_1} = 5 \ , \quad \frac{\mu_2}{\mu_1} = 1.475 \ , \quad N_{Sc,2} = 1.519$$

Run No.	U_1 $\frac{ft}{sec}$	$\frac{\rho_1}{\rho_2}$	$N_{Re,1}$	$N_{Re,2}$
41	0.454	4.223	1607	1000
42	0.454	8.333	3040	1000
43	0.681	4.223	2411	1500
44	0.681	8.333	4570	1500
45	0.908	4.223	3215	2000
46	0.908	8.333	6090	2000

$$\frac{R_1}{R} = 0.28 \ , \quad \frac{U_2}{U_1} = 30 \ , \quad \frac{\mu_2}{\mu_1} = 1.475 \ , \quad N_{Sc,2} = 1.519$$

Run No.	U_1 $\frac{ft}{sec}$	$\frac{\rho_1}{\rho_2}$	$N_{Re,1}$	$N_{Re,2}$
47	0.046	4.223	80	1000
48	0.046	8.333	153	1000
49	0.069	4.223	121	1500
50	0.069	8.333	230	1500
51	0.092	4.223	162	2000
52	0.092	8.333	306	2000

$$N_{Re,2} = 1500, \quad \frac{R_1}{R} = 0.563$$

Run No.	U_1 $\frac{ft}{sec}$	$\frac{U_2}{U_1}$	$\frac{\rho_1}{\rho_2}$	$\frac{\mu_2}{\mu_1}$	$N_{Re,1}$	$N_{Sc,2}$
53	0.341	10	4.223	1.475	1205	1.519
54	0.341	10	8.333	1.475	2377	1.519
55	3.096	1.1	1.000	1.000	1756	-
56	3.406	1.0	4.223	1.475	12056	1.519
57	0.852	4.0	1.000	1.000	483	-

REFERENCES

1. Ragsdale, R. G., and Rom, F. E., "Gas-Core Reactor Work at NASA/Lewis," NASA TM X-52309, 1967.

2. Ragsdale, R. G., and Weinstein, H., "On the Hydrodynamics of a Coaxial Flow Gaseous Reactor," Proceedings ARS/ANS/IAS Nuclear Propulsion Conference, Aug. 1962, TID 7653, Part 1, pp. 82-88.

3. Weinstein, H., and Ragsdale, R. G., "A Coaxial Flow Reactor - A Gaseous Nuclear Rocket Concept," Preprint 1518-60, American Rocket Society, Inc., 1960.

4. Schlichting, H., "Laminar Strahlausbreitung," ZAMM, Bd. 13, 1933.

5. Andrade, E. N., da C., and Tsien, L. C., "Velocity Distribution in a Liquid to Liquid Jet," Proceedings, Physical Society, Vol. 49, 1937, pp. 381-391.

6. Squire, H. B., "The Round Laminar Jet," Quarterly Journal of Mechanics and Applied Mathematics, Vol. 4, Part 3, Sept. 1951, pp. 321-329.

7. Pai, S. I., "Two-Dimensional Jet Mixing of a Compressible Fluid," Journal of Aeronautical Sciences, Vol. 16, No. 8, August 1949, pp. 463-469.

8. Pai, S. I., "Axially Symmetrical Jet Mixing of a Compressible Fluid," Quarterly of Applied Mathematics, Vol. 10, No. 2, July 1952.

9. Torda, T. P., "Wake of a Flat Plate in Laminar Flow," Proceedings of the Third Mid-Western Conference on Fluid Mechanics, Edwards Brothers, Ann Arbor, Michigan, 1953.

10. Torda, T. P., Thompson, W. J., and Genetti, B. K., "Mixing of Axially Symmetric and Two-Dimensional Jets," Proceedings of the Second U.S. National Congress on Applied Mechanics (1954), ASME, N.Y., 1955.

11. Torda, T. P., and Stillwell, H. S., "Analytical and Experimental Investigations of Incompressible and Compressible Mixing of Streams and Jets," Wright Air Development Center, TR-55-347, March 1956.

References (Cont'd)

12. Kleinstein, G., "An Approximate Solution for the Axisymmetric Jet of a Laminar Compressible Fluid," Quarterly of Applied Mathematics, Vol. 20, No. 1, April 1962, pp. 49-54.

13. Weinstein, H., and Todd, C. A., "A Numerical Solution of the Problem of Mixing of Laminar Coaxial Streams of Greatly Different Densities - Isothermal Case," NASA TN D-1534, 1963.

14. Sherman, M. P., and Grey, J., "Interaction between a Partly Ionized Laminar Subsonic Jet and a Cool Stagnant Gas," Aeronautical Engineering Laboratory Report No. 707, Princeton University, Princeton, New Jersey (1964).

15. Wood, B., Diffusion in a Laminar Confined Jet, D.Sc.Thesis, Massachusetts Institute of Technology, (1964).

16. Burke, S. P., and Schumann, T. E. W., "Diffusion Flames," Industrial and Engineering Chemistry, Vol. 20, 1928, p. 998.

17. Savage, L. D., "The Enclosed Laminar Diffusion Flame," Combustion and Flame, Vol. 6, 1962, p. 77.

18. Seider, W. D., Confined Jet Mixing in the Entrance Region of a Tubular Reactor, Ph.D. Thesis, University of Michigan, 1966.

19. Fejer, A. A., Torda, T. P., Boehman, L. I., Ghia, K. N., and Hermann, W. G., "Research on Mixing of Coaxial Streams," ARL 67-0058, 1967.

20. Agarwal, U., and Torda, T. P., "Numerical Investigation of Unsteady Laminar Incompressible Coaxial Boundary Layer Flows," NASA CR-908.

21. Mehta, U., and Lavan, Z., Private Communications. Illinois Institute of Technology, Chicago, Illinois.

22. Karplus, W. J., "An Electric Circuit Theory Approach to Finite Difference Stability," Transactions AIEE, Vol. 77, Part 1, 1958.

23. O'Brien, G. O., Hyman, M. A., and Kaplan, S., "A Study of the Numerical Solution of Partial Difference Equations," Journal of Mathematical Physics, Vol. 29, 1957, p. 223.

References (Cont'd)

24. Lax, P. D., "Difference Approximation to Solution of Linear Differential Equations - An Operator Theoretic Approach," Lecture Series of the Symposium on Partial Differential Equations, University of Kansas Press, Lawrence, Kansas, 1957.

25. Strang, W. G., "Accurate Partial Difference Methods II: Non-Linear Problems," Numerische Mathematik, Vol. 6, 1964, p. 37.

26. Stoddard, F., "Finite-Difference Methods for Computing Viscous Flow with Arbitrary Chemistry," Boeing Document, D2-22426, March 1963.

27. Bird, R. B., Stewart, W. E., and Lightfoot, E. N., Transport Phenomena, John Wiley, New York, (1960).

28. Wilke, C. R., "A Viscosity Equation for Gas Mixtures," Journal of Chemical Physics, Vol. 18, No. 4, April 1950.

29. Wilke, C. R., and Lee, C. Y., "Estimation of Diffusion Coefficients for Gases and Vapors," Industrial and Engineering Chemistry, Vol. 47, No. 6, June 1955.

30. Hornbeck, R. W., "Laminar Flow in the Entrance Region of a Pipe," Applied Scientific Research, Section A, Vol. 13, 1964, p. 224.

31. Wu, J. C., "The Solution of Laminar Boundary Layer Equations by the Finite Difference Method," Douglas Report, SM-37484, April 1960.

32. Schuyler, F. L., and Torda, T. P., "An Aerothermochemical Analysis of Solid Propellant Combustion," AIAA Journal, Vol. 4, No. 12, December 1966.

33. Lavan, Z., and Fejer, A. A., "Investigation of Swirling Flows in Ducts," ARL 66-0083, May 1966.

34. McCormick, J. M., and Salvadori, M. G., Numerical Methods in Fortran, Prentice-Hall, Inc., New Jersey, 1965.

35. Richtmyer, R. D., Difference Methods for Initial-Value Problems, Interscience Publishers, Inc., New York, 1957.

36. DuFort, E. C., and Frankel, S. P., "Stability Conditions in the Numerical Treatment of Parabolic Differential Equations," Mathematical Tables and Other Aids to Computation, Vol. 7, 1953, p. 135.